NPL
National Physical Laboratory

Good Practice Guide No. 151

Mechanical Characterisation of 3D Fibre-Reinforced Plastic (FRP) Composites

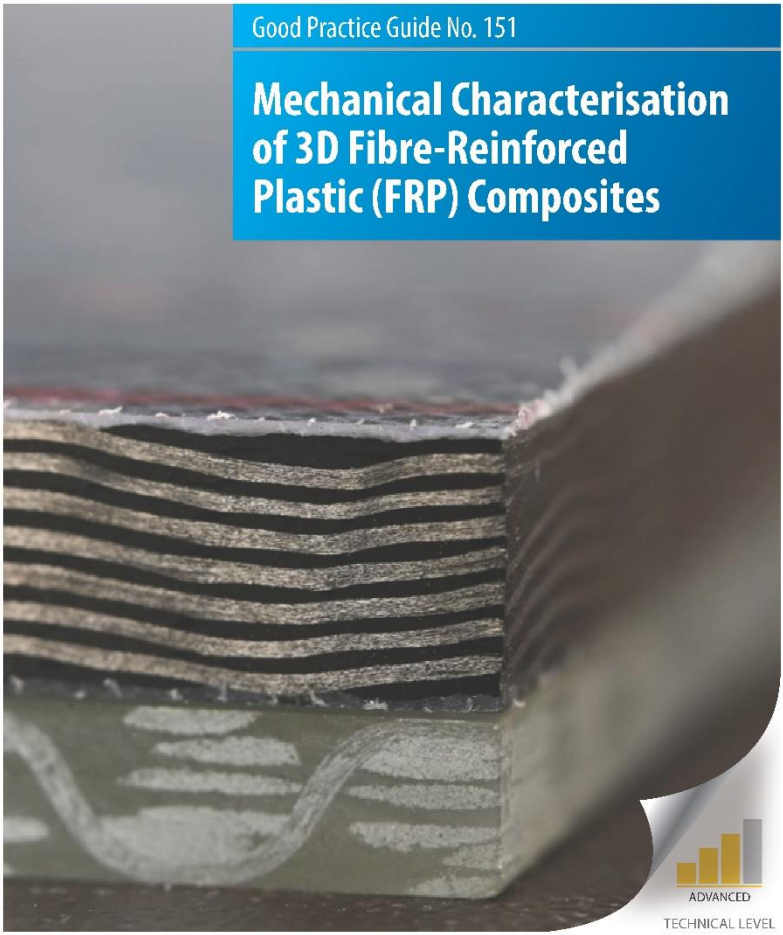

ADVANCED
TECHNICAL LEVEL

Department for Business, Energy & Industrial Strategy

FUNDED BY BEIS

The National Physical Laboratory (NPL)

NPL is the UK's National Measurement Institute, and is a world-leading centre of excellence in developing and applying the most accurate measurement standards, science and technology available.

NPL's mission is to provide the measurement capability that underpins the UK's prosperity and quality of life.

Version 1.0

ISSN: 1368-6550

https://doi.org/10.47120/npl.mgpg151

NPL Authors and Contributors

Matt Poole
Michael Gower

Find out more about NPL measurement training at **www.npl.co.uk/training** or our e-learning Training Programme at **www.npl.co.uk/e-learning**

National Physical Laboratory
Hampton Road
Teddington
Middlesex
TW11 0LW
United Kingdom

Telephone: +44 (0)20 8977 3222
e-mail: training@npl.co.uk
www.npl.co.uk

Abstract

This Guide details good practice for the mechanical characterisation of 3D fibre-reinforced polymer (FRP) composite materials. Good practice guidance has been proposed after a thorough assessment of the applicability of existing mechanical test standards covering tension, compression, flexure, shear, fracture toughness and impact/post-impact loading. For test method assessments undertaken, two 3D woven composite architectures, a glass fibre-reinforced epoxy orthogonal and a carbon fibre-reinforced epoxy layer-to-layer, have been studied. Due to the relatively large unit cell sizes found in 3D composite formats, testing was conducted using both standard and non-standard test specimen dimensions where possible. From the evaluation of the chosen test methods, the Guide aims to provide an understanding of the mechanical performance of 3D composite materials, as well as good practice recommendations not included in existing standards.

Chapter 1 details the scope of this Guide and an introduction to 3D FRP composites. Common 3D composite formats, i.e. z-pinning, stitching, tufting, and 3D weaving are discussed, alongside descriptions of the two material formats that have been used to assess the applicability of current test standards.

Chapters 2 and 3 address tensile and compressive testing, in both notched and unnotched forms, while Chapter 4 focuses on flexural testing. Each of these chapters examine current international test standards for each loading condition and provide recommendations for testing when using 3D composite formats. For these loading cases, many of the test standards are very similar in methods of loading, making choice of test method reasonably arbitrary. Therefore, examination of the general principles of loading are undertaken through the guise of a singular test method.

Chapter 5 provides an assessment of shear testing, the test methods for which are significantly different from each other. For example, in-plane shear test methods include ±45° tension, V-notch beam, V-notch rail shear, and plate twist. For interlaminar shear testing, test methods include short beam shear, double beam shear and double notch shear. This chapter examines the key features of each test method and an assessment with regards to their applicability to 3D composites is presented.

In Chapter 6, mode I and mode II fracture toughness tests are examined. Finally, in Chapter 7, post-impact behaviour in the form of compression-after-impact is investigated. The limitation of damage via drop-weight impact to a localised region, because of the through-thickness reinforcement is observed. Compression testing using standard test specimen dimensions is assessed for the two 3D composite formats tested, with widely contrasting results.

Acknowledgements

This Good Practice Guide has been produced within NPL's NMS programme which is funded by BEIS. Support and input from colleagues within the mechanical testing team of the Advanced Engineering Materials (AEM) group at NPL is recognised and was greatly appreciated throughout the project's lifetime. Thanks also goes to members of the Breakthrough Aerospace Materials (BAM) Project who let NPL attend project meetings as an observer.

Contents

Chapter 1

Introduction

- Scope
- What are 3D fibre-reinforced polymer (FRP) composites?
- Materials used for the evaluation of mechanical test standards

Scope

Over recent decades, fibre-reinforced plastic (FRP) composite materials have found increasing use in a variety of industrial applications. The excellent mechanical properties, low weight, fatigue and corrosion resistance of this class of materials gives them considerable advantages compared to more traditional materials. However, FRP composites are not without their shortcomings. Depending on the application, layers of fibres and matrix (plies) are stacked and orientated to tailor or optimise the material stiffness and strength to the required application, which can result in composites with highly orthotropic properties. An example of this orthotropy is the through-thickness stiffness and strength for laminated composites in which the fibre reinforcement is in-plane (i.e. the 1 and/or 2 directions), see Figure 1; these properties are typically low, of the order of the matrix. Due to the low through-thickness strength, composite laminates are prone to layer separation, or delamination, when loaded under conditions such as impact, bending and even in-plane loading. This type of damage can severely reduce the load carrying capability of a component, particularly under in-plane compressive load. As such, many composite components are over-designed to mitigate this type of failure and consequently the composite material is not utilised effectively.

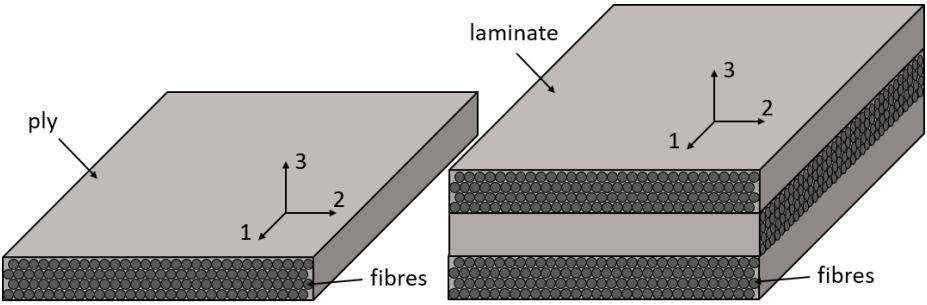

Figure 1. *Illustration of a composite ply and laminate*

A plethora of methods for improving through-thickness and interlaminar properties have been proposed and are the subject of continuing research. These methods include but are not limited to: (i) toughening of the matrix by dissolving or dispersing elastomeric and/or thermoplastic particulates; (ii) ply-level interleaving; and (iii) the use of through-thickness reinforcements. This Guide focuses specifically on FRP composites utilising various forms of through-thickness reinforcement. The inclusion of through-thickness reinforcement leads to these materials being referred to as 3D composites, with fibre reinforcement generally orientated along all three principal material directions.

When designing and manufacturing composite components it is essential to characterise and/or predict the mechanical behaviour of the material and component under a range of loading conditions. Numerical and analytical models are commonly developed and used to predict material behaviour and aid component design. However, to do this effectively, accurate characterisation of the properties of the material is required, and this is generally performed using a range of experimental measurement methods. Many of these methods are covered by national and international standards with associated precision data generated from interlaboratory comparison exercises to evidence suitable levels of repeatability and reproducibility. Due to the complexity of composite materials, test standards often only cater for certain types of material format, i.e. unidirectional, multidirectional, woven fabrics etc, with, in some cases, several standards available for measuring nominally the same property. This complexity increases further when composites with through-thickness reinforcements are considered. Material properties measured using test specimens should be representative of the bulk material, however, with the addition of through-thickness reinforcement, the volume considered representative of the bulk material can become large. While the test standards do not explicitly state that they cannot be used for 3D composites, it is not known whether many of the test standards, which were developed for composites with in-plane reinforcement, are suitable for characterising the mechanical properties of 3D composites.

The aim of this document is to provide guidance on the suitability of current international material test standards for determining the mechanical properties of 3D composites. The guidance has been developed from a programme of work in which two woven 3D composite material formats (glass fibre-reinforced epoxy orthogonal and carbon fibre-reinforced epoxy layer-to-layer) have been tested using a range of international composite mechanical test standards. Although the work was limited to 3D woven materials, it should be noted that many of the observations will be relevant to other 3D reinforcement formats e.g. stitched, tufted etc.

An introduction to 3D FRP composites

This section provides an outline of various formats of 3D FRP composites, their method of manufacture and mechanical property characteristics observed in the literature. Through-thickness reinforcements can be incorporated into material architectures in a variety of different ways and are often chosen depending on both component design and application requirements. Typical methods that can be used for through-thickness reinforcement include, but are not limited to, z-pinning, stitching, tufting and 3D weaving. Each of these methods are discussed in the following sections.

Z-pinning

In the automotive and aerospace industry sectors, it has become commonplace to find components manufactured from composite fabrics pre-impregnated with a resin, typically

epoxy. These pre-impregnated, or “prepreg”, plies are cut from rolls that contain consistent fibre/resin volume fractions and reinforcement architecture along their length. Like dry fabric preforms, prepreg plies are stacked and if processed correctly can lead to the production of high-quality laminated composites. However, for laminated composites, regardless of the way they are manufactured, they tend to have low through-thickness strengths (compared to in-plane values) and are susceptible to failure via damage such as delamination. For prepreg layups, a common method of increasing the through-thickness properties is to insert pins of 1 mm in diameter or less, often metallic or composite, in an array at various locations across the uncured laminate. The process of adding these pins through the thickness of the material is known as z-pinning. Z-pinning can be performed on both dry fabric and prepreg preforms, but the latter has the most prevalent usage. It is also worth noting that according to Mouritz [1], other through-thickness reinforcement techniques have been attempted with prepreg preforms; however, they were found to induce unacceptable levels of fibre damage, resulting in a noticeable degradation in the in-plane mechanical properties.

In the manufacture of z-pinned composites any layup can be used as long as its thickness does not exceed the length of the pins to be inserted [1]. The z-pins are initially inserted into a soft foam carrier, typically in a square array, to provide uniform spacing and support to the pins during insertion into the composite component. The foam carrier is then placed on top of the uncured prepreg panel, and using an ultrasonic horn, the pins are driven into the material. The ultrasonic horn works by emitting a high frequency compressive wave which, when passed over the foam carrier, causes it to collapse under pressure forcing the z-pins down toward the underlying prepreg. Z-pins are usually chamfered at the end facing the prepreg to help part fibres allowing the pin to penetrate the material. Additionally, the ultrasonic horn provides some heating to the prepreg that softens the matrix allowing for easier insertion of the pins. The ultrasonic horn is repeatedly passed over the prepreg until all the z-pins protrude from the underside of prepreg by some distance, often less than 0.5 mm. At this point, the remaining length of z-pin protruding above the top surface of the prepreg is sheared off using a sharp blade. Once full penetration of the z-pins has been achieved, the prepreg can be cured. After curing, any remaining lengths of pin are carefully abraded away using fine polishing paper. The z-pin insertion process is detailed schematically in Figure 2.

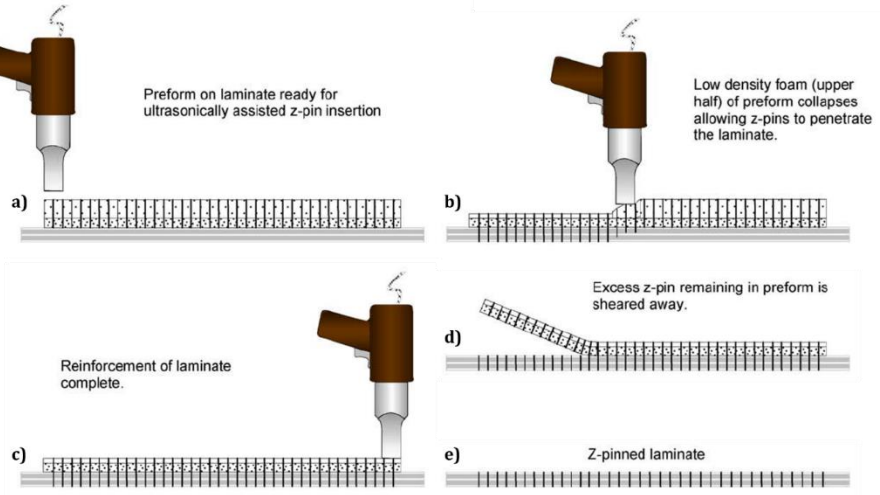

***Figure 2**. Steps involved in the z-pinning of a prepreg laminate (a-e) [1]*

Insertion of z-pins into prepreg laminates is not without its difficulties [2]. For instance, when shearing off the excess length of pin from the top surface of the prepreg, it has been noted that the pins can become off-set from the through-thickness direction (Figure 3a) and this off-set can become further exaggerated during curing. Off-set angles are typically found to be between 10° and 20° from the vertical, with each pin angled in the direction of the shear force. Along with an off-set angle of alignment, z-pins have also been found to create perturbations to the microstructure of the material. To accommodate the addition of a z-pin into the composite, fibres must be spread apart or misaligned from their intended angle of orientation. The misalignment of fibres creates 'eyelet' shaped resin-rich regions, as can be seen in Figure 3b. These resin-rich regions occur in each layer of the laminate and are orientated along the fibre direction. Both the angle of misalignment and size of the resin-rich regions increase with increasing pin diameter. However, when the z-pin density is increased, the resin-rich regions can coalesce into a resin channel, whilst the degree of fibre misalignment is reduced (Figure 3c). As well as in-plane fibre misalignment, the insertion of pins into a prepreg produces out-of-plane crimp, which is confined to a localised region surrounding the z-pins (Figure 3a). It is also possible for fibres to be broken local to the z-pins on insertion. The movement of fibres in the microstructure as a result of z-pin insertion causes prepreg laminates to swell in order to accommodate the pins. In a non-constrained layup this can result in lateral spreading of fibres, whilst in a confined mould, or frame, this typically results in an increase in the thickness of the laminate. Compared with an unpinned laminate, swelling can cause a slight reduction in the in-plane fibre volume fraction. Finally, cracks have been observed to form at the interface between the z-pin and the surrounding laminate (Figure 3d). This is the result of a mismatch in elastic

moduli between the z-pins and the laminate causing high tensile strains to be generated which in turn causes debonding of the z-pin from the laminate.

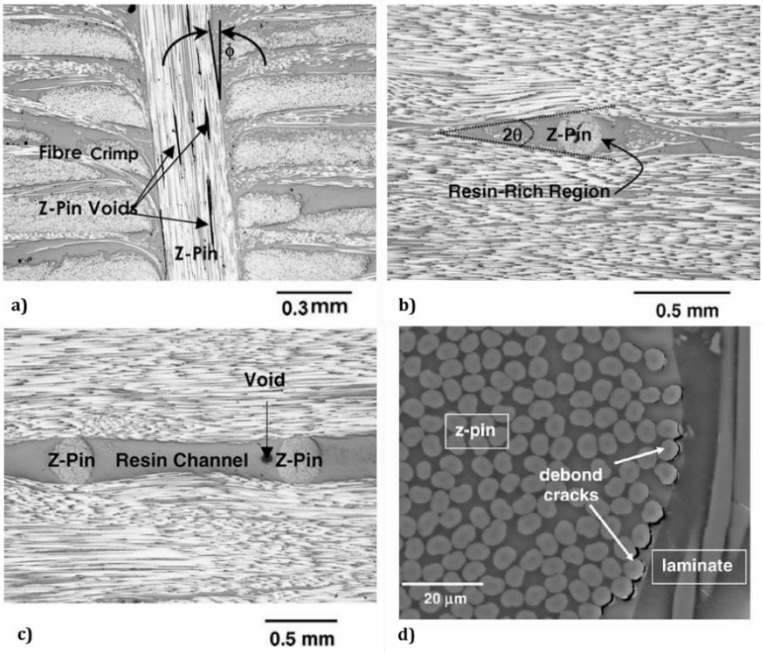

***Figure 3**. Typical changes to the microstructure as a result of z-pinning: a) z-pin offset and fibre crimp, b) fibre misalignment and resin-rich regions, c) fibre misalignment and resin channels [2], d) debonding of z-pin from surrounding material [3]*

For z-pinned composites it is commonplace in the literature for the effects of z-pin volume content, diameter, and length to be evaluated and compared to those of the unpinned material. Using these metrics for comparison, it has been observed that both the impact resistance [4, 5] and fracture toughness (resistance to delamination growth) [6, 7, 8, 9, 10, 11, 12] of various layups improve compared to unpinned counterparts. In both cases the z-pins develop a bridging zone that produces traction forces, which reduce interlaminar stresses acting on the crack front. This can slow and ultimately halt the growth of a delamination crack front by distributing the energy needed for crack growth along the z-pin/laminate interfaces.

In contrast, the addition of z-pins has been observed to be detrimental to both static and fatigue in-plane properties. Tensile [2, 3], compressive [5, 13] and flexural [14] in-plane properties generally reduce with both increasing z-pin volume content and z-pin diameter. The measured loss in performance is also sensitive to the preform layup, with 0° unidirectional (UD) and ±45°

laminates often showing the largest and smallest reduction in properties, respectively. These losses are generally attributed to the changes in microstructure that occur from z-pinning. For instance, in compressive loading 0° fibres are highly sensitive to fibre waviness as it can induce micro-buckling failures, whereas ±45° fibres are much less sensitive to changes in out-of-plane perturbations such as waviness [13].

Stitching

Stitching is a technique used to bind multiple layers of fibres together with the aim of improving the through-thickness strength and thus improving the delamination resistance. Stitching uses a similar principle and methodology to conventional sewing of textile fabrics, and typically uses any of three stitching styles: (i) lock-stitch, (ii) modified lock-stitch and (iii) chain-stitch (Figure 4 [15]). The lock-stitch requires two threads, one along each surface of the preform, that are interlocked within the fabric structure. In composites, thread cross-over toward the centre of the structure can cause unwanted stress concentrations and distortion of the in-plane fibres [16]. This can be mitigated to some extent through the use of a modified lock-stitch where thread interlocking remains along one surface of the composite, as indicated in Figure 4b. In contrast to lock-stitching, chain-stitching only uses a single thread, but requires the linking of loops on one side producing a chain (Figure 4c). Of the three stitching methods, the modified lock-stitch is preferred since it is the most secure and alters the in-plane structure least; if the chain-stitch is too loose, the entire stitch can come apart.

Localised damage in the form of fibre breakage and fibre misalignment, both in-plane and out-of-plane, can occur from the stitching process because of the needle and thread penetrating the material. It is generally noted that there is less damage imparted on dry preforms since the needle tip can more easily push aside many fibres, whereas in prepreg material the uncured resin can impede the needle action. While stitching can be used on prepreg material, it is mostly used on dry fabric preforms. Stitching threads typically consist of glass, carbon, or aramid fibre yarns.

As expected, the fracture toughness and through-thickness properties are found to be improved by stitching. In contrast, many studies have provided conflicting results when testing in-plane properties. Both the composite structure and the stitching yarn parameters appear to play a significant role in determining whether a property will be improved, degraded or produce no change in properties when compared to their unstitched counterpart. Generally, increasing the size of the stitching thread and stitching density appears to reduce the overall in-plane strength. Loss of strength most noticeably occurs in tensile and compressive loading, where these factors influence the degree of fibre misalignment. Small changes in fibre alignment with respect to the loading direction can drastically reduce the overall load bearing capabilities of composites. Additionally, stitching has also been shown to affect the failure modes. For instance, under

compressive loading, failure occurs as a combination of matrix cracking and Euler buckling since delamination damage is suppressed by the through-thickness reinforcement.

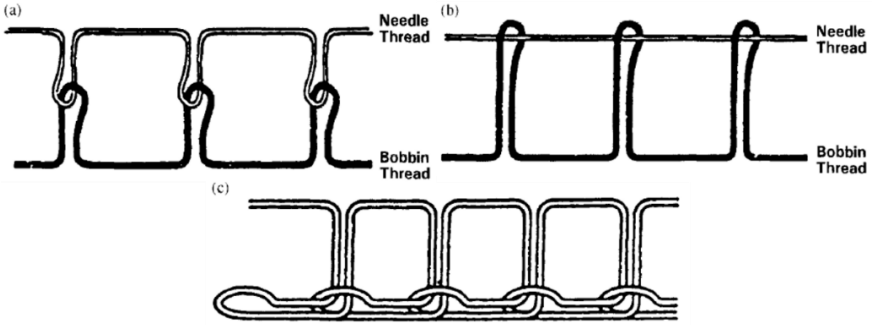

***Figure 4**. Commonly used types of stitching: a) lock-stitch; b) modified lock-stitch; c) chain-stitch*

Tufting

Compared with other through-thickness reinforcement methods for composite materials, tufting is a relatively new technique. It has many similarities to stitching, using similar threads, used on dry preforms, and can be automated via the use of robotic arms [17]. However, unlike stitching it only requires access to one side of the preform, uses a single needle and does not require locking of the thread. The lack of locking threads means that the tension in the tufting thread can remain low, enabling effects on in-plane properties, such as crimp, to be reduced.

The tufting process works by insertion of a hollow needle carrying the tufting thread, which upon retraction leaves the thread held in place by friction. As shown in Figure 5a this process occurs in three stages: 1) the presser foot and needle move to the required location, 2) penetration of the needle and thread into the preform, and 3) retraction of the needle through the fabric where a thread loop remains at one end of the preform and the thread is held in place by surrounding material [18]. Directly under the preform during tufting is a nylon sheet followed by support material. When the needle fully penetrates the preform it will pierce the support material, which in turn will hold the thread loops produced, similar to the way z-pins are held after insertion. The support material is typically a silicone-based material, or a solid closed cell foam such as PVC, the choice of which can depend on parameters such as preform shape and/or choice of thread. The tufting head, which contains the needle, can provide variability in stitch length i.e. length between tufts, insertion angle, and length of loops [17]. From the tufting head, the thread can be partially or fully inserted through-the-thickness of the preform depending on the desired result. According to Dell'Anno et al. [19], the needle must penetrate through the preform/support 12-14 mm further than the intended loop end position. This is due to a combination of distance between needle tip and eye, as well as some partial pull-out of threads

during insertion of subsequent tufts. Therefore, it is suggested that any partial reinforcement should be used on thick (>15 mm) preforms and/or preforms with a tight fibre structure to ensure that partial reinforcement can be achieved. Additionally, pre-compression is applied to the material by a foot on the tufting head to reduce bulk factor and stop tufts becoming kinked during curing, especially in a resin transfer moulding (RTM) tool [20].

It has been noted that tufting works well on many woven fabric and non-crimp fabric preforms, especially those with a loose structure as the needle can easily displace the in-plane fibres. While non-crimp fabrics (NCF) also work very well with tufting, those containing non-structural stitches have been observed to restrict movement of fibres during needle penetration resulting in in-plane fibre damage [19, 21].

Improvements in both the delamination resistance, mode I and mode II fracture toughness [18, 20, 21, 22, 23, 24], and impact resistance [25, 26, 27, 28] have been observed through the addition of tufts to layups. The size of the improvement and energy absorption capacity are a function of the layup, the size and material of the tufting thread and the tuft density. In a study by Martins et al. [28] it was noted that there was a smaller knockdown of residual compressive strength post-impact in the tufted materials compared to untufted. Tufts suppress delamination growth and restrict crack propagation to higher loads, thus reducing potential knockdown from impact. However, in-plane properties such as tension and compression of tufted layups are generally found to decrease when compared to their untufted counterpart [18, 21, 29, 30, 31]. In both cases the size of the knockdown is dependent on the fibre orientation, with composites containing a higher proportion of 0° fibres displaying a greater loss of strength. As mentioned above, to accommodate tufting threads, regions of in-plane fibres must move and become misaligned from their intended orientation. Misalignment of fibres has the greatest influence on loading when fibres are oriented toward the loading direction, i.e. 0°, and decreases as the fibre orientation increases away from the loading direction; at 45° the effect of misalignment tends to be minimal. In compression, the suppression of delamination growth due to tufting promotes failure by kinking and shear-based failures.

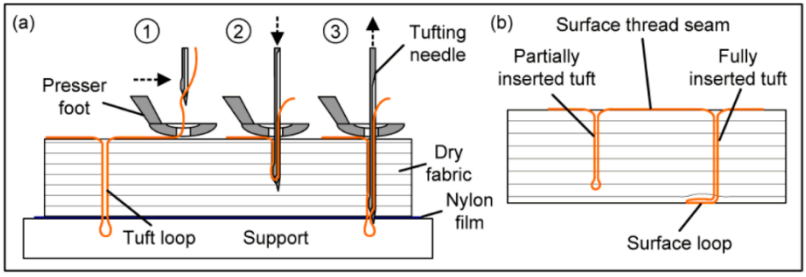

***Figure 5**. Tufting process [18]*

3D weaving

3D weaving is the creation of a single-ply fabric preform with a fully integrated through-thickness reinforcement. 3D fabrics tend to be woven using either modified 2D weaving machines, such as a Jacquard loom, or on purpose-built 3D weaving machines. It is possible to manufacture using a traditional 2D weaving machine without any modification but there is a limit to the thickness of the material that can be woven. The restriction of thickness is removed when weaving using a modified 2D weaving machine, whereby 3D woven preforms with thicknesses greater than 50 mm can be achieved [32]. The three most common 3D woven architectures are orthogonal, layer-to-layer and angle-interlock; examples of each are shown in Figure 6. These architectures are based on the through-thickness path traversed by the z-binder tows; bespoke z-binder paths can be produced to suit application and structural design. In-plane fibre orientations in 3D woven preforms are generally fixed to 0° (warp) and 90° (weft) with the through-thickness reinforcement following a variety of different paths. However, machines are being developed to reduce the restriction on in-plane fibre orientation, such that each layer can potentially have any chosen orientation [33]. Examples of 3D woven fabrics with 0°, 90° and 45° fibres are shown in Figure 7 with the z-binder running along the 0°, or warp, direction.

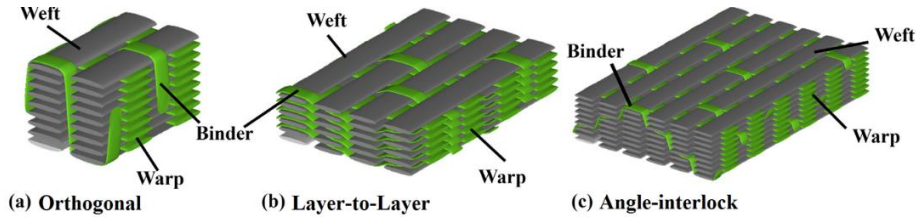

***Figure 6**. Examples of 3D woven composite fabric formats; a) Orthogonal; b) Layer-to-layer; c) Angle-interlock [34]*

As mentioned, 3D woven preforms are often manufactured using modified 2D weaving machines. This is the most commonly available method of manufacture for these materials. It is restricted to building up the fabric preform one weft layer at a time, which can limit the speed of manufacture [35]. As for traditional 2D weaving, all warp and z-binder tows are lifted during weaving to allow for weft tow insertion. Unfortunately, this can cause abrasion damage to the fibres which in turn can lead to fibre breakage. Some studies have found that the dry fibre tensile strength of individual warp tows and z-binders can drop by up to 30% [36] and 50% [37], respectively. However, in the fully woven and resin cured form the total degradation of tensile strength for the three most common structures, i.e. orthogonal, layer-to-layer, and angle-interlock, was approximately 10% from the expected strength with no damage [38, 39]. Using purpose-built 3D weaving machines can eliminate much of the fibre damage that can occur during weaving. In these machines only the z-binders are lifted while the warp tow layers remain

under a fixed tension. In addition, multiple weft tow layers can be inserted simultaneously, reducing the weaving time. By leaving the warp tows fixed under tension, and only weaving the z-binder, crimp along in-plane tows can be reduced [32, 40].

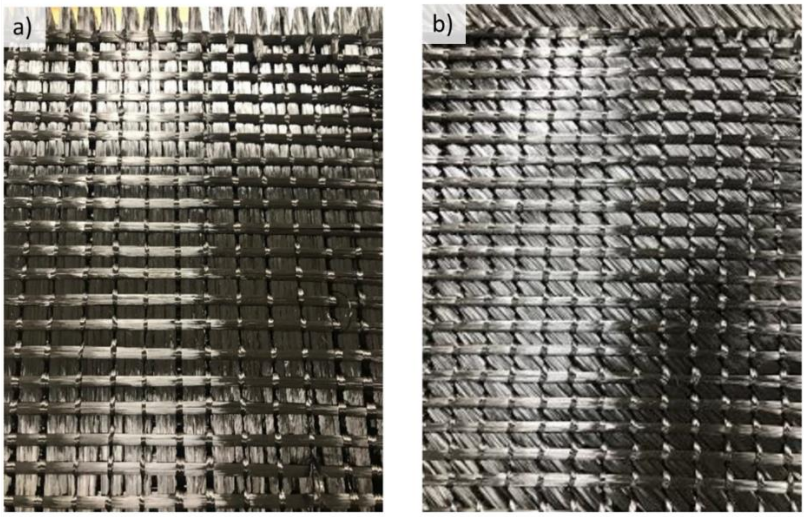

***Figure 7**. Two 3D woven composites with different in-plane fibre orientations; a) orthogonal [90/0/90/0/90]; b) off-axis [90/45/0/-45/90] [33]*

There are several advantages to 3D weaving compared to other layup and through-thickness reinforcement techniques. For instance, 3D woven preforms are manufactured as a single ply, which reduces manufacturing times as the preforms can be taken directly to the infusion stage without additional preparation. Weaving preforms in this way is not restricted to flat preforms but can be used to produce structural elements such as, but not limited to, I-, π- and T-sections, see Figure 8. The ability to directly weave 3D preforms reduces manufacturing time and cost [32].

Figure 8. *Examples of 3D woven structural elements pre-infusion. Image taken from Erginer Seramik [41]*

Other methods of through-thickness reinforcement take 2D layups and add a reinforcement. As such, it is possible to perform direct comparisons between the 2D layup and the through-thickness reinforced version to assess the influence on the material properties. For 3D woven composites, this type of comparison is not as easy to perform, though some studies have attempted to compare against 2D fabric weaves such as a plain weave by normalising to a specific fibre volume fraction [42]. Most studies tend to compare different types of 3D woven structures when looking at the influence on in-plane properties, where the main difference is the z-binder path and size of unit cell areas [43, 44]. For properties such as fracture toughness and impact resistance, it is a little easier to make a comparison against materials without a through-thickness reinforcement [45, 46]. Under out-of-plane loading, most 2D composites tend to have similarly low through-thickness properties and the inclusion of any through-thickness reinforcement creates noticeable improvements to the out-of-plane performance of these materials [47, 48].

Materials used for the evaluation of mechanical test standards

The suitability and applicability of current international material test standards for determining the mechanical properties of 3D composites have been assessed using two 3D woven FRP composite materials; a glass fibre-reinforced epoxy (GFRE) orthogonal (ORT) material, and a carbon fibre-reinforced epoxy (CFRE) layer-to-layer (LTL) woven material. Details of these materials are given in Table 1. For both materials, composite panels were produced by BAMD Ltd. The method of composite manufacture used was a laminating process rather than infusion.

Layers of MTC510 epoxy resin film were placed on both surfaces of the dry fabric preforms, which were then sandwiched between aluminium caul plates to produce two smooth material surfaces. The laminate stack was then vacuum bagged and placed within an autoclave to cure. The cure cycle used was four hours at 100°C at a pressure of 5 bar. This process was used for both materials, however the CFRE LTL used a supported resin film material resulting in there being a polyester mesh and a clear resin-rich layer on the surface of each panel.

***Table 1**. Details of the GFRE 3D orthogonal and CFRE 3D layer-to-layer woven materials*

Details	GFRE orthogonal (ORT)	CFRE layer-to-layer (LTL)
Weaver	Axis Composites	Sigmatex
Z-binder structure	Orthogonal	Layer-to-layer
No. of warp layers (per ply)	5	7
No. of weft layers (per ply)	6	8
Tow type	Hybon 2002 E-glass	Toray T700SC 12k 50C
Tex of tows (g/km)	1200	800
Areal density (gsm)	3330	5300
Warp unit cell length (mm)	8	10
Weft unit cell length (mm)	10	17
Approx. composite thickness (mm)	3	5
Resin	MTC510 epoxy	
Fibre volume fraction, V_f (%)	37.3 ± 1.5	65.2 ± 0.6
Void volume fraction, V_v (%)	0.01 ± 0.27	0.8 ± 0.06
Panel manufacturer	BAMD	

Glass fibre-reinforced epoxy (GFRE) orthogonal (ORT) material

The GFRE orthogonal fabric was manufactured by Axis Composites Ltd. using 1200 Tex Hybon 2002 E-glass fibre. It consists of five warp and six weft tow layers with a through-thickness z-binder that holds all the layers together. The z-binder is positioned between each column of warp tows and runs in the same direction. As shown in Figure 9a and 9b, the z-binder traverses the entire thickness of the material and crosses over a single surface weft tow before returning through-the-thickness. It can be seen in Figure 9a and 9c that the path of each z-binder is opposite to its neighbours ensuring adequate binding of all the layers across the material. The

unit cell length in the weft-direction is ~10 mm, whilst in the warp-direction it is ~8 mm. The difference in unit cell length between the two directions is a combination of the size and spacing of the fibre tows. The spacing between warp tows is restricted to some extent by the width of the z-binders, whilst the weft tow spacing is restricted by the thickness of the z-binder.

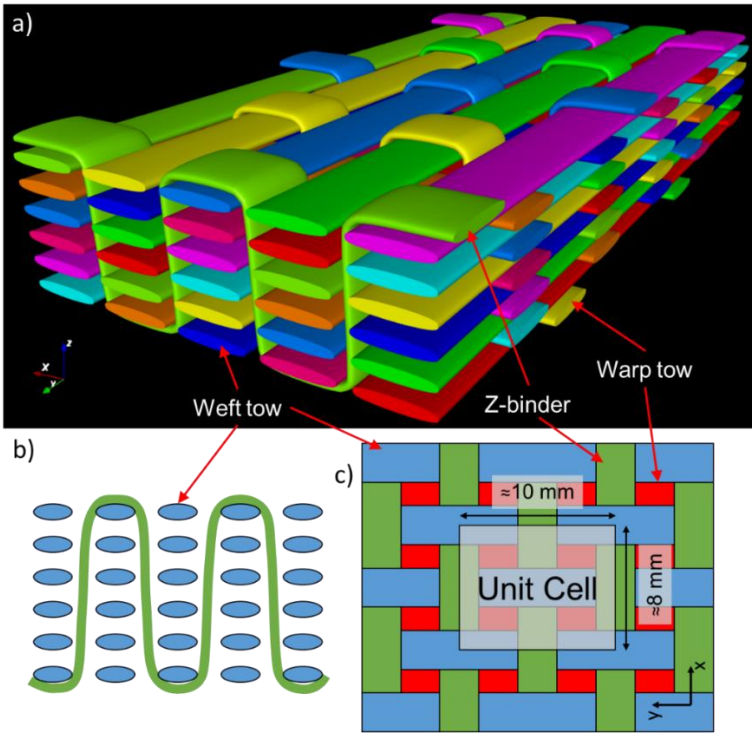

Figure 9. *GFRE 3D orthogonal woven structure: a) 3D representation; b) through-thickness z-binder cross-section; c) top-down schematic of the woven structure indicating the size of the unit cell*

Carbon fibre-reinforced epoxy (CFRE) layer-to-layer (LTL) material

The carbon-fibre LTL fabric was manufactured by Sigmatex Ltd. on a modified Jacquard loom using Toray T700SC 12K fibre tows. It has 7 warp tow and 8 weft tow layers, with multiple stacked z-binders running in the warp-direction. The through-thickness path of the z-binder consists of it traversing two weft tow layers through-the-thickness and across five weft tow columns, interlacing between each weft tow layer as shown in Figure 10a and 10b. There are an equal number of z-binders as warp tow layers, each following the same pattern. This pattern leaves four weft tows, three along the surface and one below the surface, unbound by z-binders. It can be seen in Figure 10c that across the surface, and along the length of a weft tow, the

position of the z-binder crown, i.e. the crossover section of z-binder, repeats every four z-binders.

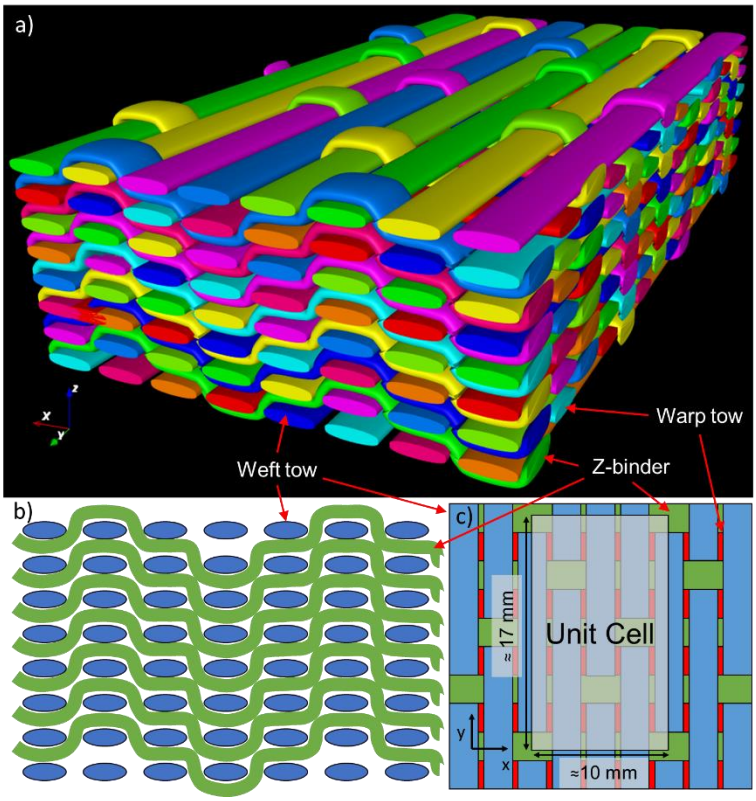

Figure 10. *CFRE 3D layer-to-layer woven structure: a) 3D representation; b) through-thickness z-binder cross-section; c) top-down schematic of the woven structure indicating the size of the unit cell*

The combination of the through-thickness path and surface pattern results in long sections of weft tow that remain unbounded at each surface of the material. As for the orthogonal weave, the spacing between warp tows and weft tows is restricted by the dimensions of the z-binder, i.e. width and thickness. The weft tow spacing is much smaller than the warp tow spacing, causing the warp-direction unit cell length to be shorter than the weft-direction unit cell, ~10 and 17 mm, respectively, despite the long run of a single z-binder repeat across multiple weft tow columns. In addition, due to the combination of multiple z-binders through-the-thickness and close spacing of the weft tows, the resin-rich regions are quite small.

Chapter 2

Tension

- Standard test methods for determining tensile properties
- Tensile testing of 3D composites in the literature
- Tension and open-hole tension testing
- Conclusions and recommendations

Introduction

Tensile testing is one of the most common methods for testing materials due to its relatively simple test setup and ability to measure several fundamental material properties such as tensile strength, modulus, elongation at failure and Poisson's ratio. The general premise is to apply a controlled pulling force to a material until either failure occurs or a predefined load is reached. Alongside the measurement of properties, this test method is useful for determining a material's response to loading, which can be of equal importance to its failure load. Using the material response, further analysis can be undertaken to discern the means by which failure initiates and develops. Unlike homogeneous and isotropic materials such as metals, initial failures in composites can develop at relatively low stresses/strains in the form of cracks and/or delamination damage. The development of these damage modes may not be immediately noticeable, potentially leading to catastrophic failure of an in-service component should an understanding of the material response to loading not be well understood.

Standard test methods for determining tensile properties

Unnotched Tension

For FRP composite materials there are several test standards available for tensile testing, which differ mostly with regards to the material formats they cater for and test specimen geometries. Tensile test standards include ASTM D638 [49], ASTM D5083 [50], ASTM 3039 [51], and ISO 527 [52]. ASTM D638 is a plastics standard that can be used for testing both reinforced and unreinforced plastics with a tensile modulus less than 20 GPa and is commonly used for thermoplastic composites. As for ASTM D638, ASTM D5038 is for use with low tensile modulus materials (<20 GPa) but only covers thermoset matrix composites. The final two test standards mentioned, i.e. ASTM D3039 and ISO 527, tend to be more popular choices for testing FRP composites as there is less restriction on the types of materials that can be tested. While ASTM D3039 tends to be used for high modulus fibre-based composites, ISO 527 can be used for a variety of reinforced and unreinforced plastic materials and contains many of the elements described within both ASTM D638 and D5083. For the remainder of this Chapter, only ASTM D3039 and ISO 527 will be considered.

Test Method	Key features
ASTM D638	• Limited to materials with a modulus ≤ 20 GPa • Dog-bone specimen geometry • Restrictive specimen dimensions

ASTM D5083	• Limited to materials with a modulus ≤ 20 GPa • Thermoset reinforced plastics only • Straight-sided specimens • Restrictive specimen dimensions
ASTM D3039	• Straight-sided specimens • Flexible specimen dimensions – representative of the bulk material • Strain measured using strain gauges or extensometer • Suggests using end tabs with a 7-10° taper at one end
BS EN ISO 527	• Suitable for a variety of unreinforced and reinforced plastics – parts 4/ 5 more specifically for fibre-reinforced plastic composites • Various specimen geometries depending on composite format • Restrictive specimen dimensions • Allows contact and non-contact strain measurement techniques

Features of tensile test standards

Tensile test specimens are typically of the order of 200-250 mm long. The use of a relatively long gauge-section is designed to avoid the effects created by stress concentrations near to the ends of the grips used to transfer tensile load into the specimen. ASTM D3039 recommends that the minimum length between the grips (free length) should be determined by the length over which the strain is measured with an extensometer, i.e. the gauge-length, plus twice the width of the specimen. Here the general recommendation for specimen width is 15 mm for 0° unidirectional specimens, and 25 mm for 90° and multidirectional balanced and symmetric specimens. While 25 mm is a suggested width for multidirectional materials, ASTM D3039 does recognise that the choice of specimen width, and thickness, should be made with consideration to a statistical representation of the bulk material. As such any width and thickness can be used if it fulfils this criterion. For woven fabric composites, the width should be selected based on consideration of the size of the unit cell. Additionally, edge effects need to be considered when choosing the specimen width as multidirectional materials can develop through-thickness stresses along free edges, which may become severe enough to lead to the development of damage such as delaminations. The specimen width should be appropriately proportioned such that the region influenced by edge effects is only a small proportion of the width [53]. A width of 25 mm is usually sufficient for most 2D composite formats.

ISO 527 is a five-part test standard used to determine the tensile properties of plastics and fibre-reinforced plastic composites. Part 1 details the general principles related to all aspects of testing and data analysis; the remaining four parts provide information on specific test conditions and specimen geometries for testing different formats of polymer-based materials.

Of most relevance and interest here, other than Part 1, is Part 4 which covers isotropic and orthotropic fibre-reinforced polymer composites [54]. It is in this document that the details of test specimen geometries and dimensions for composites with multidirectional and woven formats are recommended. There are essentially two types of test specimen; the Type 1B specimen is dog-bone in shape i.e. narrow gauge-section compared to the width of the gripped regions, whilst Type 2 and 3 specimens are straight-sided. For the Type 1B specimen, the width of the gauge-section is limited to 10 mm and it is suggested that this specimen is suitable for thermoplastic composites, especially those with a lower fibre volume content. This specimen geometry is not recommended for multidirectional continuous-fibre composites since it produces a region of discontinuous fibres that, due to the low shear strength of many composites and the high shear stresses around the grip, can lead to axial splitting and premature failure [53, 55]. As such, for many composite material formats, straight-sided specimens are recommended. For Type 2 and 3 specimens, the width is recommended to be 25 mm as per ASTM D3039. Unlike ASTM D3039, ISO 527-4 is more restrictive on the allowable specimen width, although a width of 50 mm can be used if the tensile strength is reasonably low. While the recommended specimen geometry in ISO 527-4 is the same as that recommended by ASTM D3039, it is generally limited to these dimensions. In addition, the standard only allows specimens of thickness 2-10 mm to be used.

For measurement of strain, both standards require the longitudinal strain to be measured on both surfaces to determine the degree of bending that might develop during loading. ASTM D3039 states that bending of 3-5% is permissible, whereas ISO 527-4 states that bending should not exceed 3%. Both standards allow the use of extensometers or strain gauges for the measurement of strain. If extensometers are used, a gauge-length of 50 mm is recommended, whereas for strain gauges ASTM D3039 suggests that an active grid-length of no less than 3 mm should be used, with 6 mm being adequate for most composites. When testing woven fabric composites, it is recommended that the length of the strain gauge should be at least that of a unit cell, however, there are currently no maximum dimensions cited for a unit cell. In contrast, ISO 527 does not provide any recommendations for strain gauge size. It is worth noting that ISO 527 does allow the use of non-contact strain measurements so long as they meet the accuracy requirements; this is not permitted by ASTM D3039. The use of non-contact strain measurement techniques is useful for the measurement of strain for woven fabric-based composites with large unit cells.

Failure should occur within the gauge-length of the specimen. However, it is not uncommon for failure to occur at, or near to, the grips; failures at these locations are considered invalid. Should multiple instances of grip, or near grip, failure occur the test setup may need to be re-examined. In ASTM D3039, a failure is considered valid if it occurs at a distance greater than one specimen width away from the tabs or grips. Figure 11 (ASTM D3039) shows example failure modes along with associated notation that can be used to describe the type of failure and its location. Failure

modes in the top row are generally considered invalid, while those in the bottom row are acceptable.

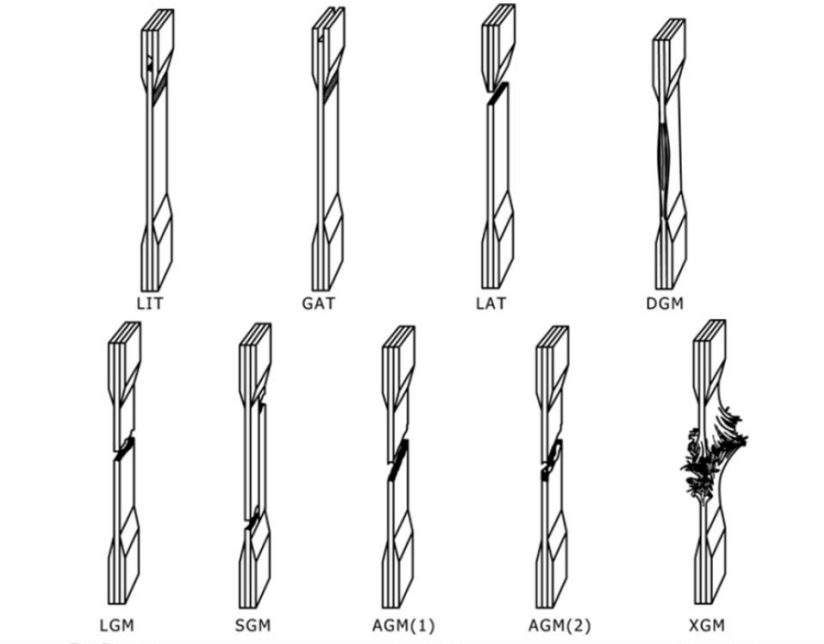

First Character

Failure Type	Code
Angled	A
edge Delamination	D
Grip/tab	G
Lateral	L
Multi-mode	M(xyz)
long. Splitting	S
eXplosive	X
Other	O

Second Character

Failure Area	Code
Inside grip/tab	I
At grip/tab	A
<1W from grip/tab	W
Gage	G
Multiple areas	M
Various	V
Unknown	U

Third Character

Failure Location	Code
Bottom	B
Top	T
Left	L
Right	R
Middle	M
Various	V
Unknown	U

***Figure 11**. Examples of different tensile failure modes as per ASTM D3039 [51]*

Open-hole (Notched) tension (OHT)

ASTM D5766 is the only international standard available for tensile testing of polymer composites with an open hole. It is essentially a supplementary standard to ASTM D3039, in that it is for use with multidirectional high strength/modulus composites with a balanced and symmetric structure. The main differences here are related to specimen dimensions. Specimens are recommended to be between 200 and 300 mm in length, with a thickness of 2-4 mm, a nominal width of 36 mm and a centrally located hole 6 mm in diameter i.e. a width-to-hole

diameter ratio of 6. Additionally, it is not necessary to use end tabs because of the stress concentration that develops around the hole.

While the presence of a hole dominates the specimen response and strength, the use of long specimens is to ensure that a uniform strain is achieved in the specimen away from the region of influence of the hole. Whilst ASTM D5766 does not explicitly state that other widths may not be used, it is recommended that a width-to-hole diameter ratio of 6 is maintained unless the influence of hole size is to be investigated. Since the hole dominates the specimen response, it is important to make sure that holes are drilled in a consistent manner, without causing damage to the specimen. Hole damage, such as matrix cracking and delamination, can result in the reduction of the stress concentration around the hole, potentially causing the test specimen to fail at higher loads than would be expected. It is recommended in NPL Good Practice Guide No. 38 [56] that Klenk drill bits are used for machining of composite materials; these bits have a sickle-shaped drill head and are most suitable for minimising damage around holes. Failure is only considered acceptable if it occurs across the hole; examples of acceptable failures are shown in Figure 12.

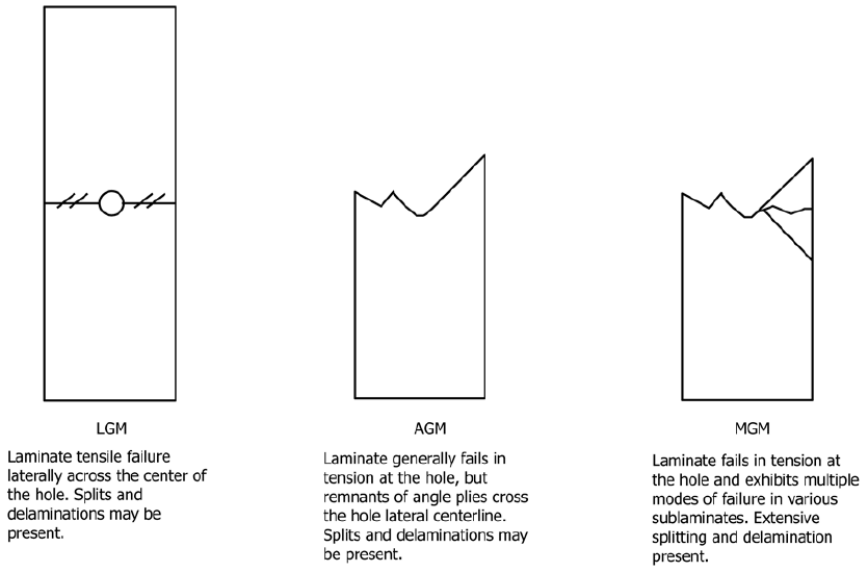

***Figure 12**. Examples of acceptable open-hole tension failures per ASTM D5766 [57]*

Tensile testing of 3D composites in the literature

It was mentioned in the previous section that both ASTM D3039 and ISO 527 are commonly used for tensile testing of polymer composites. However, in the literature regarding 3D woven composites, ASTM D3039 tends to be cited more often. While many of the citations of ASTM D3039 use the recommended test specimen dimensions, i.e. 250 mm long, 25 mm wide, with a free length of 150 mm [34, 43, 44, 58, 59, 60, 61], there are a few that use non-standard dimensions [62, 63, 64]. Although ASTM D3039 does not prohibit the use of other specimen dimensions, the reason for using non-standard dimensions was not justified within the referenced studies. Additionally, many studies do not cite any test standards [42, 65, 66, 67, 68, 69, 70], with a large variation in the specimen dimensions being noted. While there is likely a reason for the specific choice of specimen dimensions, only two [67, 68] make reference to the unit cell sizes of their 3D woven preforms and how this is related to the chosen dimensions. For 3D woven composites, consideration of test specimen dimensions in relation to the unit cell size is important to ensure that measurements representative of the bulk material are made.

From the literature it has been observed that digital image correlation (DIC) tends to be the preferred strain measurement technique for tensile testing of 3D composites [34, 42, 43, 58, 60, 61, 62, 63, 64, 71]. Many of the uses of extensometers and strain gauges in the literature tend to be from older studies where DIC was not as readily available [44, 66, 67, 68, 70]; other studies couple them with DIC for verification of strain measurements [58, 72]. The use of non-contact strain measurement is currently only permitted within ISO 527 and whilst the International Digital Image Correlation Society (iDICs) have produced a Good Practice Guide for the use of DIC [73], there are currently no standards available for DIC. Due to the complexity of 3D composite structures, the use of DIC is very useful for understanding the effect of loading on the material structure. In addition, with large unit cell sizes, the area over which strain measurements should be made needs to be appropriately proportioned such that measurements of the averaged strain response can be made. The use of strain gauges for strain measurement of 3D composites may not be the most suitable technique due to the limited grid sizes available. Non-contact measurements such as DIC have the advantage that the area over which the strain can be averaged can be varied after the test has been completed.

Several 3D woven composite studies have, using DIC, observed high localised strains occurring around resin-rich regions when loading in the warp-direction [43, 60, 70]. The resin-rich regions correspond to where the z-binder enters the fabric as indicated in Figure 13 by the recurrence of high strains at fixed distances corresponding to the pattern of the z-binder [74]. It has been suggested that the initiation of transverse cracking damage typically observed at low bulk strain measurements is linked to these high strain regions. Other studies suggest that the sections of z-binders in these regions are stress concentrators that can induce damage [42, 69]. Often z-binders pinch the tows that they cross over as a result of their path length. By increasing the z-

binder path length and alleviating the pinching effects it has been observed that the strength can increase [67]. A similar effect was also observed by increasing the harness of the z-binder [74]; here a harness refers to the total number of tows crossed over and under before a pattern repeats. In both cases this causes an increase in the percentage of z-binder that aligns with the loading direction and contributes to load bearing. The improvements in strength and stiffness are generally greater along the warp-direction than weft-direction and are related to a reduction in both pinching and crimping that is caused by the z-binder crossover.

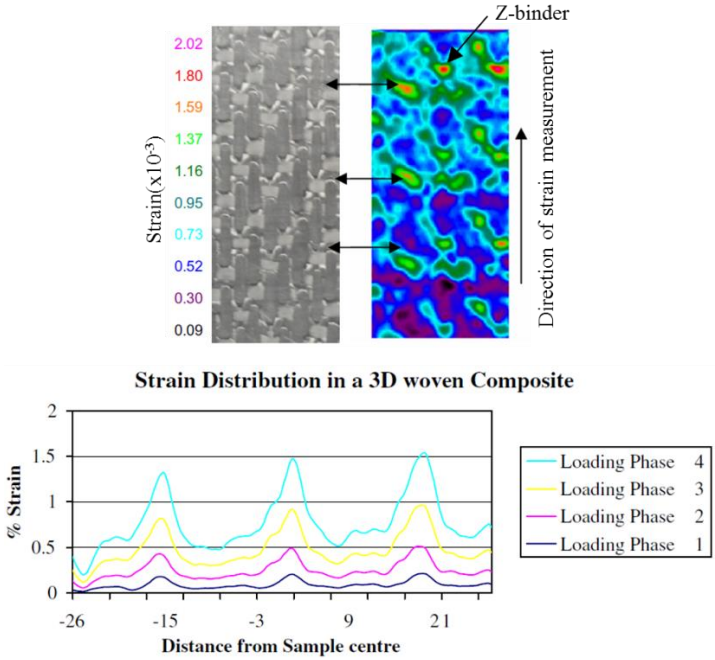

Figure 13. *Example of DIC strain map of a 4-harness 3D orthogonal woven composite and line profile across a z-binder at different loading stages [74]*

It is quite common for comparisons to be made between different 3D woven structures as there are not really any 2D equivalents without a through-thickness reinforcement. Materials used for these comparisons tend to have the same general structure, i.e. number of warp tow and weft tow layers, but the z-binder path is different [43, 60]. From these studies it was observed that both the z-binder path and pattern across multiple z-binders can influence the tensile strength and stiffness. Some patterns create a greater amount of crimp and misalignment in various load bearing tows that can lead to greater strains-at-failure but lower strengths and stiffnesses. In addition, the structures can also influence the notched behaviour. For instance, a study by Dai

et al. found that there was a greater knockdown in tensile strength for an orthogonal weave than an angle-interlock weave [71]. With a 4.1 mm diameter hole the orthogonal weave had a 15% reduction in strength, whilst the strength of the angle-interlock was only reduced by 2%. Increasing the hole size to 12.5 mm in diameter and the reduction in strength increased slightly to 20% and 7% for the orthogonal and angle-interlock, respectively. It was noted that the angle-interlock had smaller resin-rich regions and an overall more uniform strain distribution, suggesting that the size of these regions directly influences the strength. In both materials, longitudinal splits at the notch edge develop, relieving stresses and reducing notch sensitivity. It is generally proposed that 3D woven composites tend toward being notch insensitive [58, 66, 71].

Tension and open-hole tension testing

Test methods

Tension

ISO 527-4 was chosen for the tensile testing of the 3D composite materials tested reported in this Guide.

When testing coarse, woven materials with large unit cell sizes, it is important to consider the size of the test specimen. Testing methods like tensile testing are generally undertaken to either obtain fundamental material properties, such as strength, stiffness, and Poisson's ratio, or for quality control purposes. In both cases, but especially in the case of the former, it is preferred that the measurement is representative of the bulk material response. This can be achieved by making sure that there is at least one representative volume element present within the test area of the specimen. Unfortunately, many test standards are limited in the size of specimens that can be tested, requiring modification for use of non-standard test dimensions. As mentioned previously, for tensile testing the standard specimen width is 25 mm. For the 3D woven composites evaluated within this Guide, this width accommodates more than one-unit cell of each material direction across the width as indicated in Table 2. Comparative testing using non-standard dimensions can be useful for determining if the measured properties are representative of the bulk material. Here, tests were conducted using 25 mm and 35 mm wide specimens, with the average dimensions of tested specimens shown in Table 3

Table 2. *Number of unit cells present across fixed widths for the GFRE ORT and CFRE LTL materials*

Material	Width (mm)	No. of unit cells	
		Warp	Weft
GFRE ORT	25	~3	~2.5
	35	~4.5	~3.5
CFRE LTL	25	~1.5	~2.5
	35	~2	~3.5

Table 3. *Average dimensions (mean ± std. dev.) of tensile test specimens for both GFRE ORT and CFRE LTL materials. Five specimens tested per loading direction, width and material.*

Loading direction	Length (mm)	Free length (mm)	Gauge-length (mm)	Width (mm)	Thickness (mm)
GFRE ORT					
Warp	250	150	50	24.86 ± 0.07	3.09 ± 0.03
				34.99 ± 0.05	3.13 ± 0.05
Weft				24.89 ± 0.07	3.06 ± 0.02
				34.98 ± 0.14	3.07 ± 0.04
CFRE LTL					
Warp	250	150	50	25.12 ± 0.14	4.98 ± 0.03
				35.02 ± 0.02	4.98 ± 0.01
Weft				25.02 ± 0.04	4.99 ± 0.03
				35.02 ± 0.02	4.98 ± 0.01

Specimen preparation

FRP test specimens are typically machined from panels using a diamond saw; both manually adjusted, and computer automated versions are available. While a minimum of five test specimens per material loading direction are required by most test standards, it is recommended that at least seven are manufactured. The extra specimens are available for use should invalid or unusual test responses be observed. For the GFRE ORT and CFRE LTL materials discussed in this Guide the specimen dimensions are detailed in Table 3. Five specimens per loading direction, specimen width and material were tested.

End tabs were used on all specimens. Here, 2 mm thick Tufnol® 10G/40 with a ±45° fibre orientation and 3M™ Scotch-Weld™ Structural Paste Adhesive EC-9323-2 B/A were used successfully. It is important to ensure that there is a good bond strength between the end tabs and test specimen. This can be achieved through a roughening of the surface of both the end tab and the ends of the test specimen. Grit blasting prior to the attachment of end tabs is suggested as it provides an even and uniform level of surface roughening.

Further details on good machining practices for the preparation of FRP composite test specimens can be found in NPL Good Practice Guide No. 38 [56].

Test set-up

Whilst it is important to ensure that a sufficient number of representative unit cells of material are encompassed within a test specimen, it is also equally important to ensure that the capacity of the testing machine will enable loading to failure. The large difference in loading capacity of the two 3D woven materials reported in this Guide highlights this issue where the GFRE ORT required the use of a 200 kN load cell and 100 kN rated grips, whereas the CFRE LTL required a 500 kN load cell and 250 kN rated grips. Both materials were tested on Instron static test machines using mechanical wedge action grips. Alignment of the upper and lower mechanical wedge grips was achieved using a ground flat steel bar. Central alignment of the test specimens within the grips was achieved using strips of material cut to specific widths depending on the size of the grip faces used. Figure 14 shows an example of the test setup for a 25 mm wide GFRE ORT specimen.

Strain can be measured using either bonded strain gauges, extensometers, or non-contact optical methods such as DIC. Extensometers are often a preferred method due to the length of gauge-section covered when compared to the grid size of a strain gauge, though DIC and other optical extensometer techniques are becoming more popular. Back-to-back strain measurements are recommended to check for the degree of bending within the test specimen.

Note 1: It is possible to measure bending in a specimen using stereo (3D) DIC on one surface of the material. With two cameras angled towards one surface of a test specimen, and calibrated to the same reference, out-of-plane displacements can be measured. The stereo angle between both cameras is typically 15-30°, with the larger angle providing better accuracy for measurement of out-of-plane deflection.

Strain was measured using back-to-back longitudinal extensometers with a 50 mm gauge-length and ±2.5 mm travel, and a transverse extensometer with a 25 mm gauge-length and ±0.5 mm travel; the transverse extensometer was only used with the 25 mm wide test specimens.

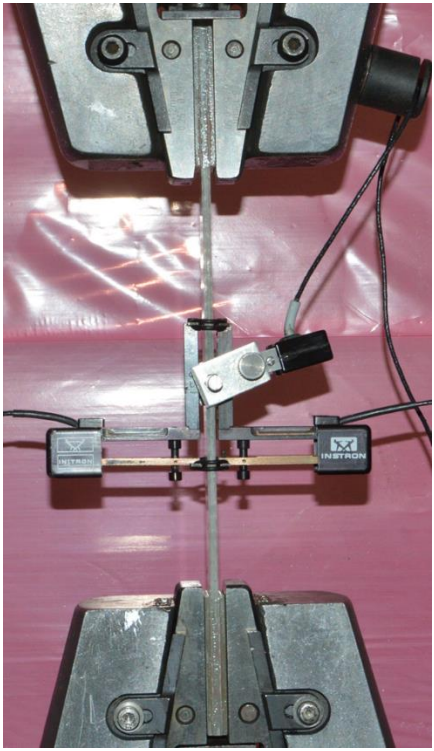

Figure 14. *Example of a tensile test setup using wedge grips, back-to-back longitudinal extensometers and a transverse extensometer*

The equations used for measurements of stress/strength, modulus and Poisson's ratio are shown in equations 1-4; where σ is stress/strength, F is the load, A is the cross-sectional area of the test specimen within the gauge-section, ε is strain, l_0 and Δl is the original length and change in length, respectively, E is the modulus, and ν is the Poisson's ratio. As per ISO 527, tensile modulus and Poisson's ratio were determined over the longitudinal strain range of 0.05%-0.25%.

$$\sigma_t = \frac{F}{A} \quad (1) \qquad \varepsilon = \frac{\Delta l}{l_0} \quad (2)$$

$$E_t = \frac{\Delta\sigma}{\Delta\varepsilon} = \frac{\sigma_2 - \sigma_1}{\varepsilon_2 - \varepsilon_1} \quad (3) \qquad \nu = -\frac{\varepsilon_{trans}}{\varepsilon_{long}} \quad (4)$$

Open-hole tension

Open-hole tension (OHT) testing was conducted in accordance with ASTM D5766. As for unnotched tensile testing, the use of non-standard test dimensions is required to ensure that measurements are representative of the bulk material. Dimensions of the test specimens for both materials used in this Guide can be seen in Table 4 and were chosen subject to the condition of maintaining a width-to-hole diameter ratio of 6. It is worth noting that the thickness of the CFRE LTL material is greater than the test standard recommendation and is therefore considered non-standard.

***Table 4**. Average dimensions (mean ± std. dev.) of OHT test specimens for both the GFRE ORT and CFRE LTL materials. Five specimens per loading direction, hole diameter and material were tested.*

Loading direction	Length (mm)	Distance between grips (mm)	Width (mm)	Thickness (mm)	Hole diameter (mm)
GFRE ORT					
Warp	250	150	23.99 ± 0.03	3.11 ± 0.03	4
			35.97 ± 0.10	3.18 ± 0.05	6
			47.99 ± 0.01	3.12 ± 0.05	8
Weft			24.02 ± 0.00	3.08 ± 0.05	4
			35.96 ± 0.04	3.19 ± 0.02	6
			47.99 ± 0.01	3.17 ± 0.05	8
CFRE LTL					
Warp	250	150	24.05 ± 0.04	5.05 ± 0.04	4
			36.03 ± 0.02	5.06 ± 0.02	6
			48.02 ± 0.01	5.03 ± 0.02	8
Weft			24.05 ± 0.02	4.85 ± 0.03	4
			36.04 ± 0.04	5.04 ± 0.05	6
			48.03 ± 0.01	5.03 ± 0.04	8

Specimen preparation and test set-up

Specimen preparation uses the same techniques as recommended for unnotched specimens, though the use of end tabs is not necessary. Hole drilling is performed using the set-up as shown

in Figure 15a. It is recommended that hole drilling is performed using sickle-shaped carbide drill bits (Figure 15b). A piece of scrap material should be placed under the test specimen to reduce damage as the drill bit exits the underside of the material. Testing of OHT specimens uses the same test set-up as for the plain tension testing.

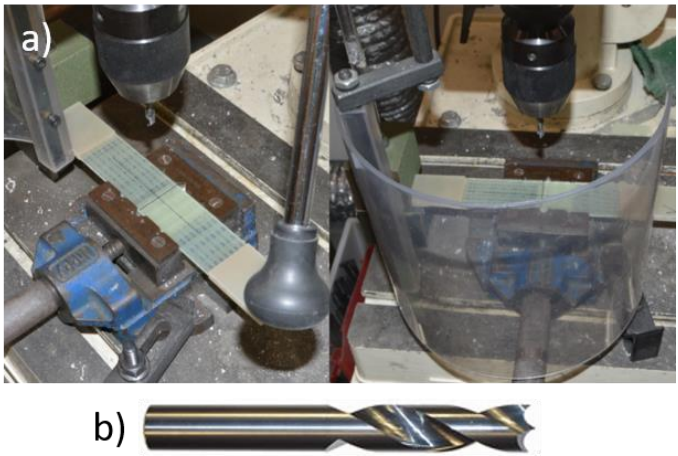

Figure 15. *Images showing; a) the setup used for drilling holes into specimens; b) Sickle-shaped carbide drill bit for hole drilling.*

Results and analysis

Tension

The GFRE ORT and CFRE LTL materials were tested using specimens of two different widths to investigate the effect on the measured tensile properties. Table 5 shows the average properties measured for each material, test direction, and width of test specimen, while the modulus and strength for each have been plotted against specimen width in Figure 16.

For the GFRE ORT material there are no significant changes in any of the measured properties for either loading direction when the width of the test specimen is increased. This tends to indicate that a specimen with a width of 25 mm already accommodates sufficient material to be considered representative of the bulk material. Considering the size of the unit cell along both the warp- and weft-direction this result seems reasonable and is perhaps not unexpected.

In contrast for the CFRE LTL more noticeable changes were observed in the tensile modulus and strength with increasing specimen width for both loading directions. Considering the unit cell size and width of the test specimens, both the 25 mm and 35 mm wide specimens contain more than one unit cell length. As such, it is reasonable to assume that there is sufficient

representation of the bulk material contained within the gauge area. However, the property measurements for the CFRE LTL material do not correspond with this observation. For the tensile strength, the increase in width causes a decrease in the warp-direction strength and an increase in the weft-direction strength, both equal to approximately 70 MPa. There are no clear differences between each specimen size to account for the observed changes in properties. Since the changes in strength are within 10% of each other, it is possible that these measurements are simply due to natural variation in the material and therefore are not significant. Further investigation may be required with even wider specimens, e.g. 50 mm and 100 mm in order to assess if there are indeed size effects for this particular material.

Table 5. *Tensile properties of GFRE ORT and CFRE LTL materials with measurements provided as mean ± std. dev.*

Loading direction	Width (mm)	Tensile modulus E (GPa)	Tensile strength σ (MPa)	Poisson's ratio
GFRE ORT				
Warp	25	18.2 ± 0.6	306 ± 18	0.17 ± 0.01
	35	18.4 ± 0.4	299 ± 16	-
Weft	25	19.8 ± 0.6	334. ± 14	0.16 ± 0.01
	35	20.6 ± 0.9	342 ± 29	-
CFRE LTL				
Warp	25	57.3 ± 1.0	954 ± 45	0.08 ± 0.01
	35	59.0 ± 0.3	885 ± 29	-
Weft	25	55.7 ± 0.9	902 ± 18	0.09 ± 0.01
	35	60.8 ± 0.8	967 ± 45	-

Recommendation 1: The dimensions of the test specimens should be chosen such that measurements made can be considered representative of the bulk material. Since the suggested free length of an ISO 527-4 and ASTM D3039 test specimen is already quite long, greater attention should be placed on determining a suitable specimen width. Ideally at least one unit cell length should be present across the width of the test specimen, though the greater the width the more representative it is of the bulk material. The 25 mm width suggested in both ISO 527-4 and ASTM D3039 should be considered a minimum for testing in tension and increased as necessary depending on the material format.

(Additional) It may be necessary to test at multiple specimen widths to determine the most suitable test specimen dimensions.

For the materials tested in this Guide, measurements of the tensile modulus and Poisson's ratio, regardless of loading direction and specimen width, produced low scatter. This suggests that the chosen extensometer gauge-lengths are appropriate for producing an adequate representation of the bulk strain for these materials. The biggest limitation with using extensometers is the need to remove them prior to failure. This is done to protect the extensometer from being damaged but prevents measurement of the full strain response. Whilst strain gauges can be used to measure the strain response to failure during loading, they can fail prior to ultimate load as a result of specimen damage and tend to measure a local rather than global strain response. The use of non-contact strain measurement techniques is recommended to measure the strain response to failure.

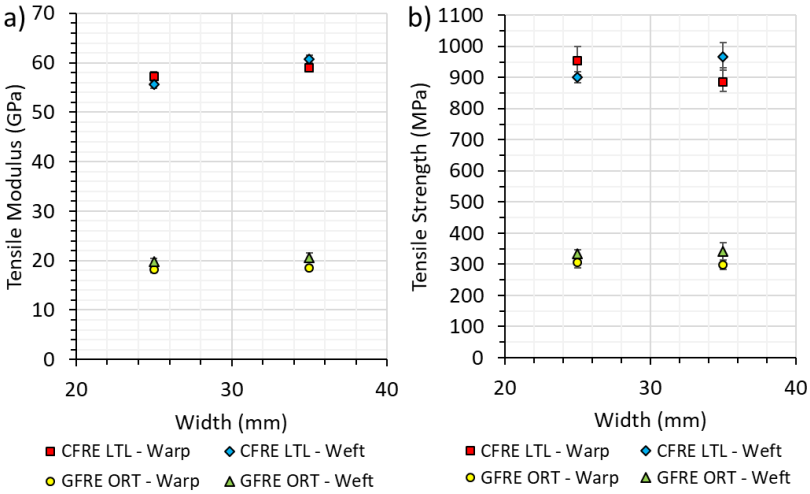

Figure 16. *Comparison of tensile properties with respect to specimen width for the GFRE ORT and CFRE LTL materials: a) modulus; b) strength*

Recommendation 2: Due to the relatively large unit cell sizes of 3D composites, strain should be measured using either an extensometer or non-contact strain measurement technique such as DIC; regardless of method they should cover a suitable gauge area to be considered representative of the bulk material. It is suggested that non-contact strain measurement techniques should be used if the strain to failure response is required.

(Additional) Regardless of whichever strain measurement technique is used, measurements of strain should be made on both faces of the test specimen.

Recommendation 3: Measurements of strain used for the determination of the tensile modulus should be made across at least one unit cell length along both the length and width of the test specimen. However, measuring across as many unit cells as possible, especially along the specimen length, will produce strain measurements more representative of the bulk material.

Open-hole tension (OHT)

Table 6 details the OHT strengths measured for both materials tested in the warp- and weft-material directions. Generally, the OHT strength of both materials decreases with increasing width and hole diameter regardless of material direction. The decreasing OHT strength suggests that these materials are notch sensitive. The average OHT (notched) strength data can be seen in Figure 17 plotted as a proportion of the plain, or unnotched, tensile strength; here, $^{W}/_{d}$ is the ratio of specimen width-to-hole diameter. For both materials and loading directions, except the CFRE LTL weft-direction, there is initially a 20% drop in strength with a specimen width of 24 mm and a hole diameter of 4 mm. The strength drops a further 20-30% when the width and hole diameter are increased to 48 mm and 8 mm, respectively. In comparison, the CFRE LTL weft-direction has a much smaller notch sensitivity but drops at least 30% regardless of test specimen dimensions. Previous studies have suggested that 3D woven composites are notch insensitive [58, 66, 71]. This does not match the measurements obtained here, which show that these materials become more notch sensitive with increasing hole diameter and specimen width.

Table 6. *OHT strengths for GFRE ORT and CFRE LTL materials tested with three different widths and open-hole diameters. Measurements provided as mean ± std. dev.*

Loading direction	Open-hole tensile (OHT) strength (MPa)		
	24 mm wide – Ø4 mm	36 mm wide – Ø6 mm	48 mm wide – Ø8 mm
GFRE ORT			
Warp	241 ± 22	228 ± 29	186 ± 8
Weft	265 ± 9	197 ± 10	176 ± 5
CFRE LTL			
Warp	707 ± 33	626 ± 26	526 ± 17
Weft	628 ± 37	664 ± 20	605 ± 28

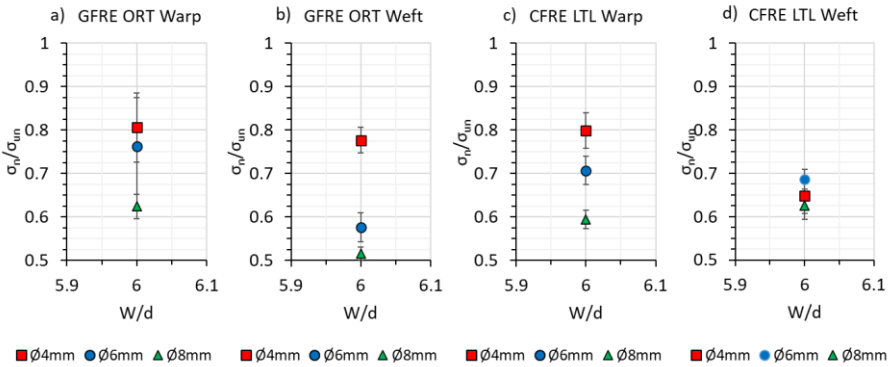

***Figure 17**. Ratio of notched (OH) to unnotched tensile strength against width-to-hole diameter (W/d) ratio for a) GFRE ORT warp-direction; b) GFRE ORT weft-direction; c) CFRE LTL warp-direction; d) CFRE LTL weft-direction*

The knockdown in strength, and associated scatter, for both materials can be explained by considering the location of the holes relative to the material structure. Figure 18 shows a plan-view schematic of the GFRE ORT (left) and CFRE LTL (right) structures including two different (with respect to the material structure) hole positions per hole diameter. It is worth noting that the schematic of the GFRE ORT material shown in Figure 18 is idealised as opposed to that seen in individual test specimens. As such, spacing between tows can vary from that shown in the schematic and will influence the scatter in measurements. Conversely, the CFRE LTL has a more uniform and regular structure, such that the schematic, although still idealised, is more representative of the actual material.

Hole diameter and position within the material structure appear to be directly related to the knockdown in strength observed in each material and loading direction. Using the GFRE ORT warp-direction loaded specimens as an example, it can be seen that depending on the exact hole position:

- a 4 mm hole can cut through either a single z-binder or at most the equivalent of one column of warp tows,
- a 6 mm hole could remove approximately half a column of warp tows or up to two columns of warp tows, and
- an 8 mm hole will always cut through at least one column of warp tows but can cut through up to two warp tow columns.

For this material, there is a large difference in the amount of load bearing material that can be removed depending on the position and size of the hole, which ultimately leads to a fair degree of scatter as clearly observed in Figure 17 for the 24 mm and 36 mm wide specimens. The much

smaller scatter of the 48 mm wide specimens tends to suggest that, regardless of the hole position, the presence of the 8 mm hole consistently removed a larger proportion of load bearing tows compared to other specimen width and hole size combinations.

The same comparisons between hole size, location and loss of strength can be made for both materials and loading directions and show good correlation. For instance, in the CFRE LTL weft-direction specimens the small spacing between weft tows allows each hole diameter to cut through comparable amounts of load bearing weft tows, producing a relatively similar knockdown in strength and overall less scatter.

The effect of hole size and its position relative to the material structure on the OHT strength clearly depends on the material format being tested. It is unlikely that all 3D composite materials will show the same degree of notch sensitivity. However, this can only be suitably evaluated by testing not only with standard test specimen dimensions. It is recommended to keep the width-to-hole ratio constant initially, with different width-to-hole ratios being considered for potential further analysis of the material performance. Furthermore, since the position of the hole influences the material performance, the number of tests conducted per specimen dimension should be increased beyond the five suggested within ASTM D5766 to allow for a much more random distribution of hole positions to be tested for. A Weibull statistical distribution could be conducted.

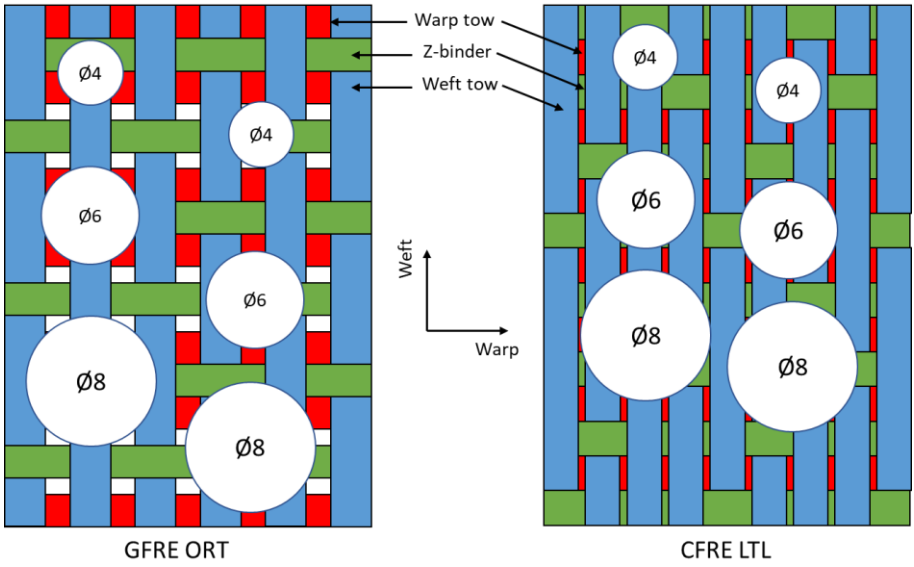

***Figure 18**. Plan-view schematics of the GFRE ORT (left) and CFRE LTL (right) material structures with different hole positions for different hole diameters.*

Recommendation 4: To better evaluate the tensile performance of 3D composites with an open-hole, it is recommended that tests be undertaken using a variety of test specimen dimensions while maintaining a width-to-hole diameter ratio of 6. A minimum of three different specimen dimensions should initially be adequate, though more will provide a fuller evaluation of the material performance.

(Optional) Conduct tests varying the width-to-hole diameter ratio.

Recommendation 5: Conduct more than five tests per specimen dimension to produce a better representation of the material performance.

Conclusions and recommendations

In this Chapter, plain tension and OHT testing was conducted according to ISO 527-4 and ASTM D5766, respectively. Tests were conducted using both standard and non-standard specimen dimensions to investigate the influence of unit cell size on strength and modulus measurements.

Plain tensile measurements undertaken indicate that the standard test dimensions recommended in both ISO 527-4 and ASTM D3039 are generally suitable for testing the 3D composite formats with the unit cell sizes studied in this Guide. It is important to consider the size of the unit cell in relation to the width of the test specimen. ***Ideally the width should encompass several unit cells of the material, though it is recommended that at least one unit cell is included***. A width of 25 mm should be viewed as a minimum for testing in tension, though non-standard widths should be used where necessary to ensure that there is adequate representation of bulk material.

For OHT the effect of hole size and location relative to the material structure suggests that insufficient testing has been done to characterise the materials used in this Guide. ASTM D5766 recommends that at least five tests should be undertaken using a single specimen width and hole size to characterise the OHT strength. However, the work in this Guide suggests that this may not be sufficient for 3D composites. ***It is recommended that a better evaluation of the material performance, and degree of notch sensitivity, can be achieved by testing with multiple specimen dimensions, while maintaining a width-to-hole diameter ratio of 6.*** For optional further analysis the width-to-hole diameter ratio could be varied. ***In addition to multiple test specimen dimensions, the number of test specimens per dimension should be increased to better evaluate the scatter in results due to the influence of hole position relative to the material structure.*** Depending on the material format it may be necessary to conduct a Weibull statistical distribution to evaluate the material performance better.

Chapter 3

Compression

- Standard test methods for determining compressive properties
- Compressive testing of 3D composites in the literature
- Compression and open-hole compression testing
- Conclusions and recommendations

Introduction

Compared to other methods of testing such as tension or flexure, compression is more challenging and can easily be performed incorrectly. Not only is there the question of the best method of introducing compressive load into a material, but effective testing is highly reliant on good alignment and a specimen gauge-length sufficiently short to avoid Euler buckling. Poor alignment and/or incorrectly proportioned specimen dimensions can result in Euler, or column, buckling; this is an instability in a material subjected to a compressive load whereby a small increase in load suddenly produces a large deformation, for instance bowing of a column. This type of failure is an unacceptable mode and should be avoided. A variety of different compression test methods have been developed, many of which have been standardised as shown in the following section. Generally, compression testing is conducted either through end-loading, shear-loading, or via a combination of both end- and shear-loading modes (Figure 19).

End-loading:	Compressive load applied only through the ends of the test specimen.
Shear-loading:	Compressive loads are applied via shear between the grip faces and end-tabbed regions of material
Combined:	Test specimens are gripped as for shear-loading whilst also having load applied directly through the ends of the specimen, creating a combination of end- and shear-loading.

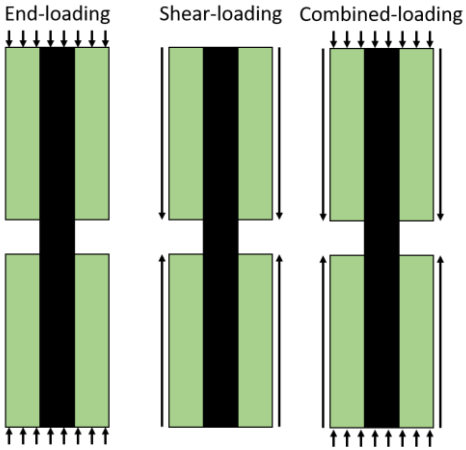

Figure 19. *Compression loading methods*

Each method of load introduction has specific advantages and disadvantages. For example, shear loading is not suitable for very thick laminates, because it causes strain distributions over the laminate thickness caused by shear strains and end tabs may shear off at high loads. End

loading is in many cases a sufficient and simple method for determination of compressive modulus but is very limited for ultimate strength determination. Combined loading overcomes several of these issues and can also be used for higher laminate thicknesses. The disadvantage is the need for supplementary machining of the specimen ends to ensure parallelism and squareness tolerances are met when using end-tabbed specimens.

Standard test methods for determining compressive properties

Unnotched compression

Due to the different ways of introducing a compressive load into specimens, there are several international standards available for compressive testing of composite materials. The table below shows a list of current compression test standards, indicating what type of loading is covered.

Test standard	End-loading	Shear-loading	Combined loading
ASTM D695	✓	×	×
ASTM D3410	×	✓	×
ASTM D6641	×	×	✓
ASTM D8066	×	✓	×
BS EN 2850	✓	×	×
BS EN ISO 14126	✓	✓	✓

The following is a brief review of each compression test standard, providing a general overview of the principles and features of each test method. A summary listing the advantages and disadvantages of each test method can be found at the end of this section.

ASTM D695 – Compressive Properties of Rigid Plastics

ASTM D695 can be used to determine the compressive properties of unreinforced and reinforced plastics via end-loading [75]. For reinforced plastics, the standard is limited to use on materials with a modulus up to 41.37 GPa. For compressive strength measurements, the test specimen geometry is either prismatic or dog-bone in form, depending on the thickness of the material. Prismatic specimens are short at 12.7 mm for specimens with a thickness of 3.2-6.4 mm, and 25.4 mm long for specimens with a thickness above 6.4 mm. The specimen lengths are short to reduce the possibility of buckling, but the standard allows the use of shorter length specimens should buckling be detected. Dog-bone specimens can also be used but are much

longer at 79.4 mm and are primarily suited for use on materials with a thickness of less than 3.2 mm. Modulus measurements can be made using prismatic specimens so long as the specimen length conforms to a slenderness ratio (length-to-thickness) within the range of 11-16:1. If the length of prismatic specimens is too short for strain measuring devices and/or failure occurs via delamination rather than a shear plane, then it is permissible to use the dog-bone specimens for both strength and modulus measurements. For both types of test specimen, the width of the gauge-section is fixed at 12.7 mm. Both types of specimen are tested in a sub-press containing compression platens that is placed within the frame of the testing machine as shown in Figure 20a and Figure 20b. Prismatic specimens are directly loaded into the sub-press and placed centrally between the platens. Due to the length of the dog-bone specimens, lateral supports like those shown in Figure 20c are used to prevent buckling. The specimen sits flush with one end of the support fixture and proud by 6.4 mm at the other end. The central section of the support fixture is slightly narrower than the test specimen so an extensometer/compressometer can be attached along the specimen's edge. The use of a dog-bone shape is used to minimise the potential for end crushing of the specimen and promote acceptable failures to occur within the gauge-section of the specimen.

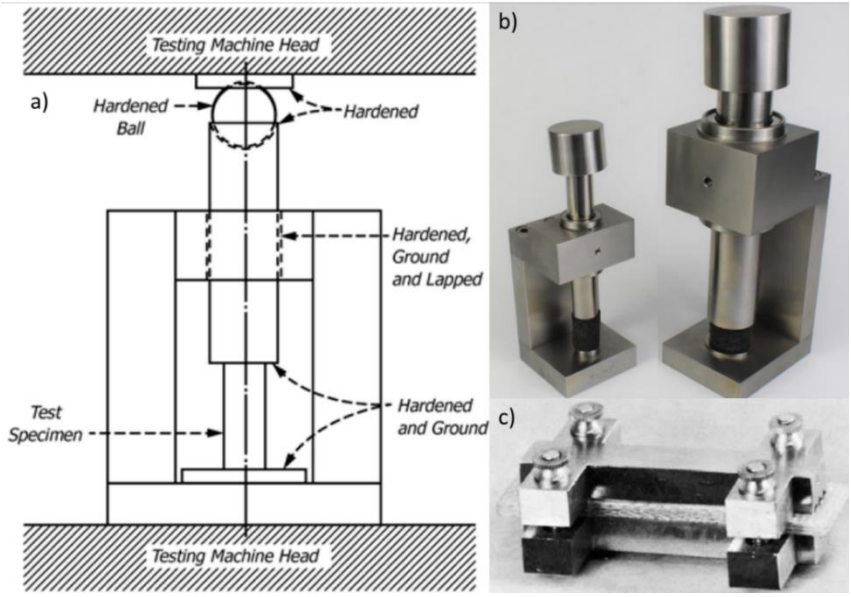

Figure 20. *Compression fixtures for use with ASTM D695: a) illustration of sub-press taken from test standard [75]; b) sub-presses produced by Wyoming Test Fixtures [76]; c) lateral supports suggested to be used on thin test specimens [75]*

A modified version of this test method, based on the Boeing standard BSS 7260 [77] and known as the modified D695, is often used for thin composites. The principal modification was to allow straight-sided specimens instead of dog-bones. Tabbed and un-tabbed specimens are recommended for measurement of strength and modulus, respectively. End tabs are used to reduce the potential brushing failure at the ends of the specimen, however the gauge-length between the end tabs is only 4.8 mm, making it difficult to make strain measurements. For modulus measurements, specimens are only loaded to a maximum strain of 0.3%. In addition to modifications to the test specimen geometry, a base was added to the support fixture to ensure the lateral supports remain vertical when placed between compression platens (Figure 21). For modulus measurements the grooves along the lateral support are relieved over a central 12.7 mm long section to provide the spacing needed for strain gauges. The modifications have never been adopted into ASTM D695, but were recently included within EN 2850 [78] for compression of unidirectional carbon fibre composites; however the specimen thickness is restricted to 2 mm ± 0.2 mm.

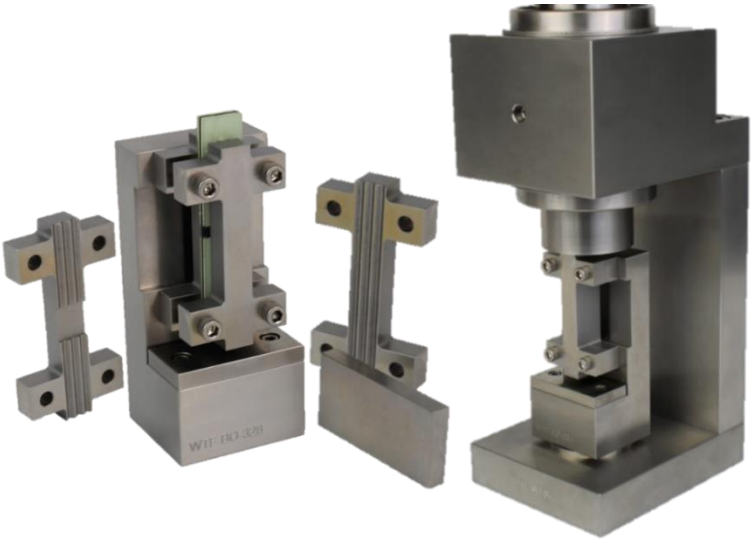

***Figure 21**. Lateral support test fixtures for use with the modified D695 and ISO 2850 test standard, produced by Wyoming Test Fixtures [76]*

Current end-loading test methods are not appropriate for use with 3D composites. The test areas prescribed are small and since the size of a unit cell can vary dramatically depending on the chosen format design, it is not possible to encompass a representative area using this test method.

ASTM D3410 – Compressive Properties of Polymer Matrix Composite Materials with Unsupported Gauge Section by Shear Loading

ASTM D3410 focusses on the characterisation of compression properties via shear-loading [79], which is applied via wedge grips using a fixture such as that shown in Figure 22. The two halves of the fixture are loaded between compression platens, imparting a shear load through the clamped sections of the specimen, which results in a compressive load across the gauge-section. The standard uses straight-sided specimens with or without end tabs and with a short unsupported gauge-section. The choice of specimen dimensions is flexible as long as several key requirements are fulfilled. The first requirement is based on the use of an unsupported gauge-length and the importance of avoiding Euler buckling. This can be achieved by reducing the gauge-length relative to the thickness and can be calculated using equation (5), which is based on a linear elastic material response and pinned-end conditions. It is suggested that back-to-back strain gauges are used to monitor for buckling. Secondly, the gauge-length should be long enough to allow the successful introduction of a uniform compressive load into the gauge area. Lastly, there must be enough material contained within the width and thickness of the specimen to be representative of the bulk material. While specimen dimensions can be chosen, the standard does provide recommendations for specimen width, minimum thickness and gauge-length based on estimated compression strength and stiffness values. Recommended gauge-length and width dimensions tend to range between 10 and 25 mm, with the greater of the two suggested as the width for composite lay-ups such as multidirectional and woven fabrics.

$$h \geq \frac{l_g}{0.9069\sqrt{\left(1-\frac{1.2F^{cu}}{G_{xz}}\right)\left(\frac{E^c}{F^{cu}}\right)}} \quad (5)$$

E^c = longitudinal modulus
F^{cu} = ultimate compressive stress
G_{xz} = through-thickness shear modulus
h = specimen thickness
l_g = length of gauge-section

Failure in compression can occur via different mechanisms depending on factors such as material type and lay-up/material architecture. Generally, most compressive failure mechanisms are acceptable so long as they occur within the gauge-section; the exception is Euler buckling. Whilst it can be difficult to observe visually during and/or after the test it can be detected easily using back-to-back strain gauges. Failures that occur within the clamped regions, including end-crushing, are not acceptable. Figure 23 details acceptable and unacceptable failure modes as defined in ASTM D3410.

The flexibility of ASTM D3410 with regards to specimen geometry provides suitability for use with 3D FRP composites that may require large gauge areas to accommodate a representative number of unit cells. In addition, ASTM D3410 recommends that at least one unit cell across the

gauge-length is covered by a strain gauge for materials such as woven composites, unlike standards such as ISO 14126 that allows gauge elements no longer than 3 mm to be used.

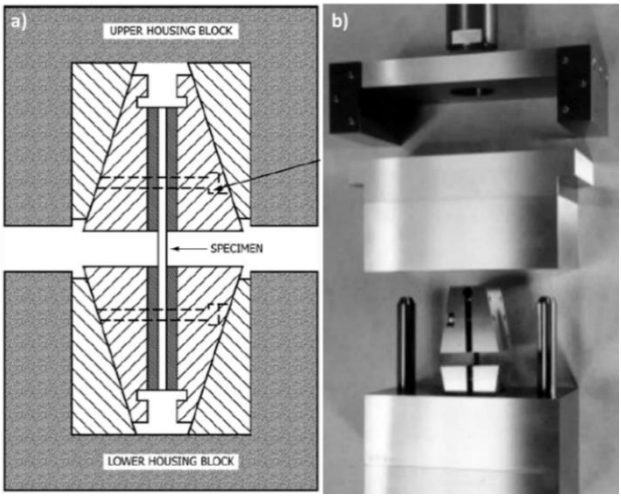

Figure 22. *ASTM D3410 shear-loading compression test fixture; a) illustration from the test standard [79]; b) image of fixture supplied by Wyoming Test Fixtures [76]*

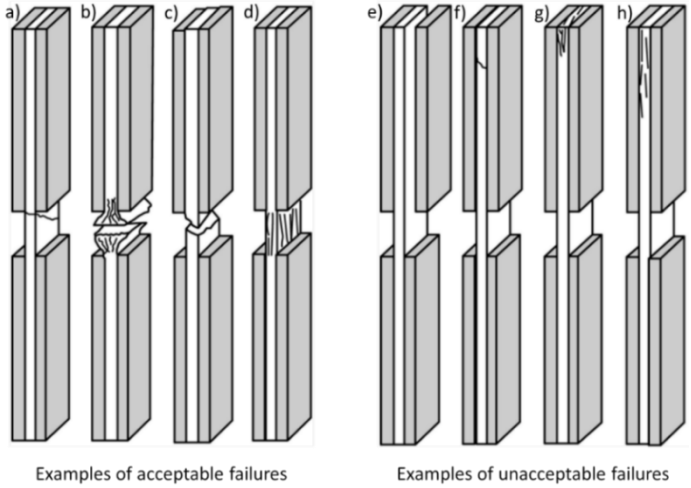

Figure 23. *Examples of acceptable and unacceptable compressive failure modes [79, 80]. Acceptable failures (all within gauge-section): a) transverse shear; b) brooming; c) through-thickness shear; d) splitting. Unacceptable failures (all in the clamped sections): e) debonding of tabs; f) through-thickness shear; g) end-crushing; h) delamination.*

ASTM D6641 – Compressive Properties of Polymer Matrix Composite Materials Using a Combined Loading Compression (CLC) Test Fixture

ASTM D6641 can be used for determining compressive properties via a combination of shear- and end-loading [80]. Specimens are clamped via bolts between two serrated grip faces with the ends of the specimen flush with the test fixture. The fixture (Figure 24) is made up of four steel blocks clamped together in pairs. Alignment rods connect the top and bottom halves of the fixture through bearings that serve to reduce frictional contact during loading. Load is applied through both the ends of the specimen and the test fixture, with the latter transferring load to the gauge-section of the specimen via shear through the clamped portions of the specimen. Through the combination of loading modes, load is introduced into the test specimen more smoothly, providing greater uniformity of test results with reduced scatter [81]. Adjustment of the clamping forces can be used to control the ratio of end- to shear-loading. In practice, the shear-loading contribution should be enough to reduce the potential for end-loading to cause crushing of the specimen ends. The use of serrated or roughened grip faces means that the clamping forces, and thus the shear loading contribution, can be reasonably small.

ASTM D6641 uses straight-sided rectangular test specimens with an unsupported gauge-length. End tabs are not necessary but are suggested for highly orthotropic materials e.g. 0° unidirectional. As for the modified D695 / ISO 2850 methods, the use of end tabs further reduces the potential for end-crushing by transferring some of the end-load into the tabs. Typical specimen dimensions are 140 mm long, 13 mm wide and with a gauge-length of 13 mm. The use of other dimensions is permitted, with a standard fixture capable of clamping specimens up to 30 mm wide. According to Donald Adams of Wyoming Test Fixtures [81], successful loading of 125 mm wide specimens has been achieved which illustrates the flexibility of the standard for testing large coupon sizes. Unlike shear-loading fixtures, the combined loading fixture allows any thickness of material to be used. However, for a chosen thickness the unsupported gauge-length must be sufficiently small to avoid Euler buckling. Additionally, measurement of strain and detection of bending/buckling is suggested via the use of back-to-back strain gauges. As such, consideration of the gauge-length versus grid size of the strain gauges used must be made. Acceptable and unacceptable failures are also outlined in ASTM D6641 using the same convention as shown for ASTM D3410.

For 3D composites, where the size of a representative volume of material may vary considerably between different formats, ASTM D6641 is very appealing due to both the flexibility of specimen dimensions and test fixture scaling.

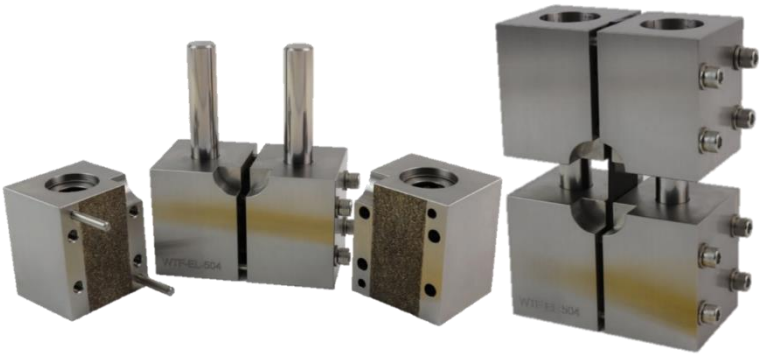

Figure 24. *Combined loading compression test fixture produced by Wyoming Test Fixtures [76]*

ASTM D8066 – Unnotched Compressive Testing of Polymer Matrix Composite Laminates

ASTM D8066 [82] is an unnotched compression test standard for polymer composites that is supplementary to the open-hole compression (OHC) test standard ASTM D6484 [83], discussed later. Compressive load is introduced via shear-loading using hydraulic wedge action grips and the support fixture as per ASTM D6484 for open-hole compression. This fixture acts as a lateral support for specimens restricting out-of-plane deformation though the support does not contact the central gauge-section of the specimen. An image of the support fixture is provided in Figure 25a, and is designed to be gripped between hydraulic grips (Figure 25b). ASTM D6484 allows either shear-loading or end-loading of the support fixture but ASTM 8066 only allows shear-loading to reduce the potential for end brooming/crushing failures that are more likely to occur in unnotched specimens. Care should be taken when testing using the support fixture as the lateral pressure applied to the specimen by the support fixture can influence the test results.

Unlike other compression test standards, ASTM D8066 uses long and wide specimens, of the order of 300 mm and 36 mm, respectively. The test standard is designed to be used with multidirectional composite materials and is especially suitable for formats of material with large unit cells such as woven fabrics. However, the specimen thickness is limited to 3-5 mm. Measurement of strain is permitted in three ways, either using back-to-back strain gauges, edge mounted extensometers, or a suitable non-contact strain measurement technique. Failure is only considered valid if it occurs within the 100 mm long gauge-section. Like other compression standards, end-crushing and Euler buckling are unacceptable failures, as is failure outside the gauge-section.

BS EN ISO 14126:1999 – Fibre-reinforced plastic composites – Determination of compressive properties in the in-plane direction

ISO 14126 [84] is flexible with choice of test method allowing either shear-, end- or combined loading to be used. Each of these loading methods are based on established tests suggested within existing ASTM and industrial test standards, with the idea of rationalising and harmonising them into one standard. As such, ISO 14126 allows any test fixture to be used so long as it fulfils the requirements for the chosen load introduction method. This test standard is similar to other test methods in that straight-sided specimens with or without end tabs are used. However, most of the flexibility in specimen dimensions is in the choice of thickness, and only really for end/combined loading methods. The choice of total length, widths, and gauge-lengths is restricted to those recommended with no allowance for alternatives to be used.

Summary of compressive test standards

The following table provides a summary of the advantages and disadvantages of the compression standards reviewed. Only those using end-loading tend to be unsuitable for testing 3D composites mostly due to limitations on the test specimens allowed and observable gauge area. In contrast, test standards using shear- and/or combined loading methods are generally more flexible with specimen dimensions, making them more likely to be suitable for the testing of 3D composites.

Test Method	Advantages	Disadvantages
ASTM D695	• Various specimen geometries • Used for a variety of unreinforced and reinforced plastic materials	• Limited material modulus ≤ 41.37 GPa • Limited specimen widths – 12.7 mm • Dog-bone specimens for materials thinner than 3.2 mm • Not suitable for materials with large unit cell areas such as 3D composites
Modified ASTM D695 (EN 2850)	• Uses straight-side specimens • Fixture provides better specimen alignment between platens	• Thin specimens (order of 2 mm) • Separate test specimens for strength and modulus measurements • Not formally standardised but included in EN 2850 • EN 2850 only for UD CFRP • Not suitable for materials with large unit cell areas such as 3D composites
ASTM D3410	• Straight-sided specimens with flexible dimensions • Potentially suitable for testing 3D composites	• Requires reverse wedge grip fixture • Specimen thickness limited by the test fixture

ASTM D6641	• Straight-sided specimens with flexible dimensions • Smoother load transition into specimen due to combined end- and shear- loading • Scalable test fixture • Potentially suitable for testing 3D composites	• Requires special test fixture
ASTM D8066	• Straight-sided specimens • Non-contact strain measurement techniques allowed • Suitable for multidirectional and woven composite formats with large unit cell areas, i.e. 3D composites	• Long test specimens requiring greater amounts of material than other test standard specimens • Lateral supports required to avoid Euler buckling • Limited to specimen width of 36 mm and thickness of 3-5 mm
ISO 14126	• Straight-sided specimens • Allows user to choose method of load introduction • Flexibility in the choice of test fixture • Potentially suitable for testing 3D composites	• Relatively limited test specimen dimensions

Open-hole (notched) compression (OHC)

For open-hole compression testing there are fewer international test standards available. As such, those that have been developed tend to cater to multiple methods of compressive load introduction, as indicated within the table below.

Test standard	End-loading	Shear-loading	Combined loading
ASTM D6484	✓	✓	×
BS-ISO 12817	✓	✓	×

The following section provides a brief overview of the open-hole compression test standards.

ASTM D6484 – Open-Hole Compressive Strength of Polymer Matrix Composite Laminates

ASTM D6484 can be used to determine the open-hole compressive strength of composite materials [83]. The standard details two methods for compressive load transfer into the test specimen, i.e. shear- and end-loading. Shear-loading uses hydraulic wedge action grips (Figure 25b), as described for ASTM D8066, whereas end-loading places the test fixture between loading

platens (Figure 25c), applying the compressive load through the ends of the specimens. ASTM D6484 requires the use of a long test specimen, nominally 300 mm, with the test fixture acting as an anti-buckling guide. Specimen dimensions are restricted i.e. 36 mm wide, 6 mm diameter holes, and thickness in the range of 3-5 mm. However, these dimensions can be altered if the effect of width-to-hole diameter ratio is to be investigated. All the failure modes typically observed during compression are acceptable failures for open-hole specimens, as long as they occur through and around the region of the notch. Failures outside of the notch area are unacceptable.

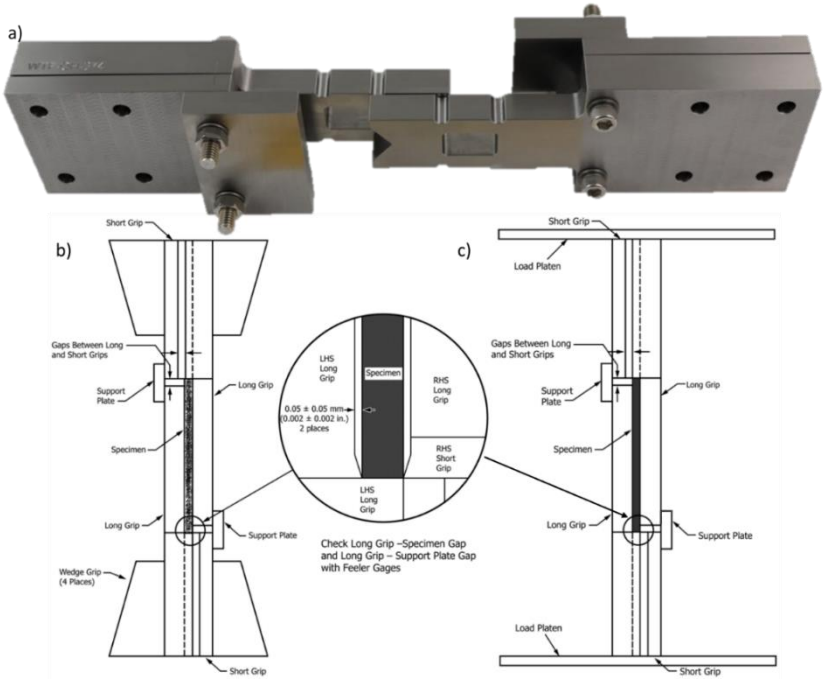

Figure 25. *a) Example of an ASTM D6484 test fixture produced by Wyoming Test Fixtures [76]; b) Test fixture clamped between grips for shear-loading and c) Test fixture loaded between compression platens for end-loading [83]*

BS ISO 12817:2013 – Fibre-reinforced plastic composites – Determination of open-hole compression strength

ISO 12817 can be used to determine the open-hole compressive strength of composite materials [85], providing the choice of three test methods:

1. Method 1: End-loaded with anti-buckling support fixture
2. Method 2: Shear- or combined-loading without anti-buckling support fixture
3. Method 3: The same as in ASTM D6484

Unlike ASTM D6484, methods 1 and 2 are conducted on short specimens, with lengths similar to those recommended in ISO 14126. The fixture for end-loading is shown in Figure 26 and has similarities with the fixtures used in the modified D695/ ISO 2850 compression test methods. However, this fixture is both taller and wider than those fixtures in order to accommodate the open-hole test specimens. For shear-loading, no test fixture is required as the specimens can be directly gripped using hydraulic grips, though the standard does also suggest the use of a combined loading fixture as shown in Annex C of ISO 14126.

For all the test methods included, the specimen width and hole diameter are the same, i.e. 36 mm wide with a 6 mm diameter hole located centrally along the length and width. The main differences between specimen dimensions are total length and thickness of material. End-loading specimens are suggested to have a length of 118 mm and a thickness of 2.5 mm, whereas shear-loaded specimens are 125 mm long with a minimum thickness of 4 mm. While the length of the specimens is restrictive, there is flexibility with regards to the thickness of specimens that can be used. In addition, the standard indicates that alternative width and hole diameters can be used so long as the width-to-hole diameter ratio remains equal to 6.

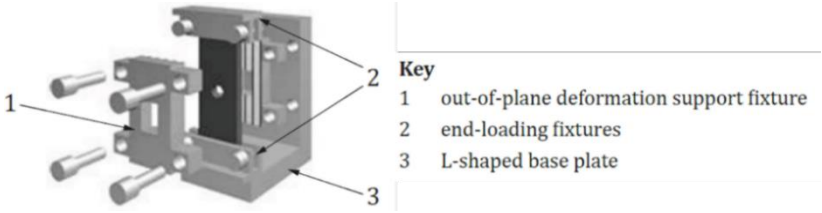

Figure 26. *End-loading test fixture recommended in ISO 12817 [85]*

Summary of open-hole compression test standards

The table below provides a summary of the advantages and disadvantages of both open-hole compression test standards. Both test standards should be applicable for 3D composites since the standard test specimen dimensions are sufficiently large.

Test Method	Advantages	Disadvantages
ASTM D6484	• Choice of end- or shear-loading • (Optional) Strain measurements using extensometers	• Long test specimens requiring greater amounts of material than other test standard specimens • Lateral supports required to avoid Euler buckling • Limited specimen dimensions • Restricted to specimens with a width-to-hole diameter ratio of 6
ISO 12817	• Choice of end- or shear-loading • (Additional) Allows testing using ASTM D6484 methods and specimens • Shear-loading – no fixture required – hydraulic grips used	• Lateral supports required for end-loading and ASTM D6484 specimens • Limited specimen dimensions depending on method chosen • Restricted to specimens with a width-to-hole diameter ratio of 6

Compressive testing of 3D composites in the literature

A number of studies have been undertaken to examine the performance of, and damage mechanisms in, 3D woven materials under compressive loading [43, 60, 86, 87]. 3D woven architectures tested include various forms of orthogonal, angle-interlock, and layer-to-layer weaves, with the most common failure modes observed being fibre tow debonding, micro-buckling and kink band formation. Examples of these damage modes, observed in a CFRP layer-to-layer material, are shown in Figure 27. Each of these damage mechanisms develop due to geometric flaws within the fabric such as fibre misalignment of the in-plane load bearing tows. The degree of fibre misalignment in load bearing tows is influenced by the z-binder weaving pattern and consolidation forces during composite manufacture. Sections of load bearing tows with the greatest misalignment tend to be located near the material surface around z-binder cross-over points, as shown schematically in Figure 28a. Fibre misalignment promotes localised axial shear stresses that can lead to fibre tow debonding, reducing constraining forces that inhibit buckling [86]. In turn, fibres become free to rotate, typically in an out-of-plane direction, forming kink bands. It has been suggested that the suppression of delamination and Euler buckling caused by z-binders tends to promote kink bands as a dominant failure mode [87]. Figure 28b shows a schematic of kink bands in a warp tow near the specimen surface, indicating the influence of buckling suppression caused by the z-binder.

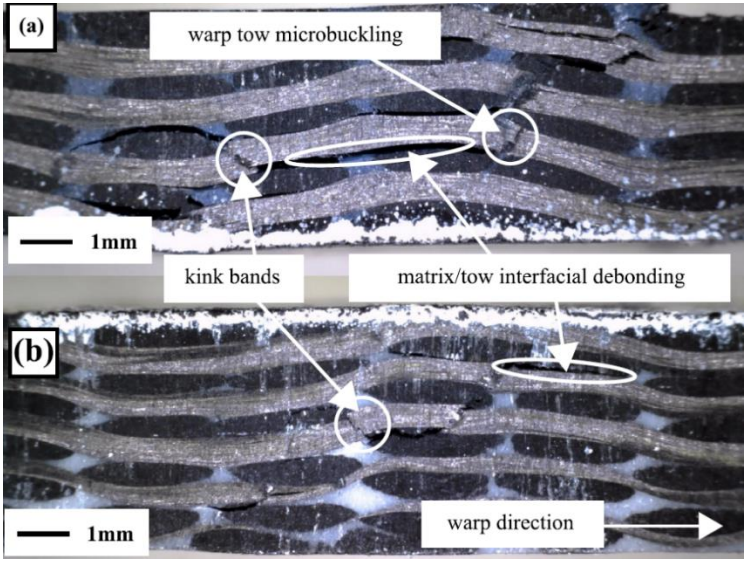

Figure 27. *Compressive damage observed in the warp-direction in a CFRP layer-to-layer material [60]*

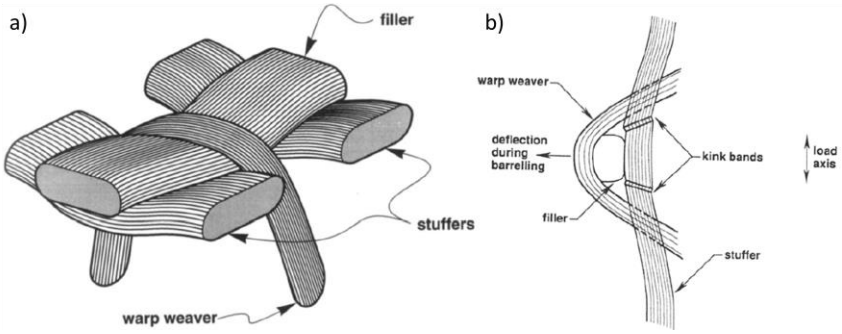

Figure 28. *a) Influence of z-binders on the misalignment of tows near the specimen surface [65]; b) kink banding in warp tows [86]. Note: stuffers and warp weavers are referred to as warp tows and z-binders, respectively in the text.*

The effect of adjusting weaving parameters on the mechanical performance of 3D woven composites has also been examined by Dahale et al. [44]. Here, a glass fibre/epoxy layer-to-layer 3D woven material had the pick density, i.e. the number of weft tows/unit length, adjusted from 4 picks/cm to 14 picks/cm; the number of ends/cm, i.e. warp tows, was kept the same. For the highest pick density, a more compact fabric was produced, which reduced the overall crimp within the fabric structure and increased the constraint on fibre tow movement. In turn, there

was a significant improvement in the weft-direction strength and strain-to-failure when pick density was increased. It was also observed that the dominant failure mechanism changed from interlaminar or brooming failure to the higher energy mechanism of micro-buckling. The improvement in strength was attributed to the increase in weft-direction fibre volume fraction and change of failure mode. A less significant improvement in strength and strain-to-failure was observed for the warp-direction, with any improvements thought to be due to higher geometric regularity of the material. Cox et al. [65] saw a similar improvement in the strength of 3D woven composites by increasing the compaction pressure during consolidation. Higher compaction pressure resulted in an increased compressive strength of 2-3 times that of the lower compaction pressure. This was suggested to be related to an increase in the fibre volume fraction. However, increasing the compaction pressure led to large geometric distortions, most notably in the weft tows and z-binders. As a result, the strain-to-failure of the higher compaction pressure specimens was substantially lower than the lower compaction specimens. Failure in both variations of material was due to the development of kink bands initiated by delaminations.

The choice of test method varies from study to study, with some using end-loading of the form described in ASTM D695 [5, 43, 44], some using shear-loading [13, 65, 86, 87], and others using combined-loading from ASTM D6641 [60]. As for 2D composite materials, there does not appear to be a clear consensus for the loading of 3D composites in compression. The choice of loading mode needs to be made considering the flexibility for using larger test coupons depending on the size of the unit cell.

Compression and open-hole compression testing

Test methods

Compression

From the overviews of each standard provided it is clear that shear- or combined loading methods are better suited to testing 3D composites. As such, compression testing reported in this Guide was conducted according to Method 2 (combined loading) of ISO 14126. The decision to test using only ISO 14126 was based on its flexibility to choose both the method of load introduction and the test fixture.

Specimen geometry

In Method 2 of ISO 14126, there are two different test specimens available: Type B1 and Type B2. Type B1 specimens have a width and gauge-length of 10 mm and can be used for material with a thickness of 2-10 mm, whereas for Type B2 specimens it is 25 mm and is suitable for use with material with a thickness greater than or equal to 4 mm. Type B2 specimens are recommended for multidirectional and woven materials. From consideration of the unit cell

dimensions of the two materials evaluated in this Guide (see Chapter 1), the Type B1 specimen was selected for the GFRE ORT material and the Type B2 specimen for the CFRE LTL material. For the GFRE ORT material, the Type B1 specimen dimensions only just encompass a unit cell along both the width and gauge-length, whereas for the CFRE LTL material the Type B2 specimen width of 25 mm covers more than one unit cell. To ascertain the importance of encompassing sufficient numbers of unit cells, non-standard dimension specimens were also tested as shown in Table 7. All test specimens covered at least one unit cell across both the width and the gauge-length.

***Table 7**. Average dimensions of GFRE ORT and CFRE LTL compression test specimens*

Distance between grips (mm)	Loading direction	Length (mm)	Width (mm)	Thickness (mm)
GFRE ORT				
10	Warp	110.03 ± 0.01	9.97 ± 0.01	3.30 ± 0.02
	Weft	109.99 ± 0.01	10.00 ± 0.03	3.07 ± 0.01
	Warp	110.02 ± 0.02	24.96 ± 0.00	3.39 ± 0.05
	Weft	109.98 ± 0.00	24.88 ± 0.03	3.07 ± 0.01
	Warp	109.30 ± 0.00	35.89 ± 0.04	3.08 ± 0.06
	Weft	110.00 ± 0.01	35.93 ± 0.04	3.08 ± 0.03
20	Warp	119.83 ± 0.02	25.00 ± 0.05	3.13 ± 0.02
	Weft	119.84 ± 0.02	25.01 ± 0.06	3.13 ± 0.03
	Warp	119.87 ± 0.05	35.97 ± 0.03	3.15 ± 0.03
	Weft	119.88 ± 0.03	35.96 ± 0.04	3.12 ± 0.03
CFRE LTL				
25	Warp	125.01 ± 0.01	25.02 ± 0.02	5.01 ± 0.02
	Weft	125.00 ± 0.02	25.01 ± 0.02	5.08 ± 0.02
	Warp	124.99 ± 0.02	35.95 ± 0.05	5.01 ± 0.01
	Weft	125.01 ± 0.01	35.99 ± 0.01	5.10 ± 0.03

Specimen preparation

Compression testing is sensitive to rough and uneven surfaces as these can produce nonuniform loading of the specimen that could promote bending and/or ultimately lead to premature failure. To minimise the potential for these unacceptable failures and achieve repeatable results, it is important to ensure that test coupons are prepared appropriately. Initial preparation is similar to that for tensile specimens, i.e. specimens are machined in plaques and use 2 mm thick GFRP end tabs with a ±45° fibre orientation (Figure 29). A recommended end tab material and adhesive is Tufnol® 10G/40 and 3M™ Scotch-Weld™ Structural Paste Adhesive EC-9323-2 B/A, respectively.

Note 1: Machine specimens and end tabs larger than the required specimen dimensions as these will be reduced to size during a grinding stage.

Note 2: Using spacers during the attachment of end tabs ensures that the unsupported gauge-length is as required on both sides of the test specimen.

For uniform loading, each of the faces that contact the test fixture need to be sufficiently flat and parallel to each other. Tolerances of the order of 0.02 mm are stipulated in each test standard and are achievable through machining processes such as grinding.

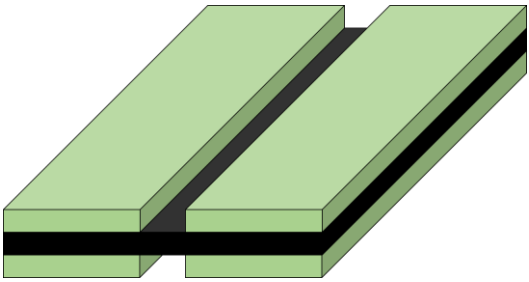

Figure 29. *Tabbed and ground panel from which individual specimens can be machined*

Test setup

For the compression testing discussed in this Guide, specimens were tested using a four-pillar combined loading fixture as shown in Figure 30. Minimisation of bending-buckling of specimens can be achieved through good alignment of the test fixture and specimens relative to the test frame. Interchangeable support blocks are used to ensure specimen alignment and prior to testing these are aligned using a ground steel bar. The support blocks available contain recesses that can accommodate 10, 25 and 36 mm wide specimens. Flat or serrated metal inserts are used to clamp specimens in place and are tightened via a pair of bolts in each block. For this test

fixture it is recommended that a torque of 5 and 10 Nm is applied to the inner and outer bolts, respectively.

Note 3: Ensure that the specimen ends are fully seated and in contact with the base of each recess within the support blocks before testing. This can be achieved by loosely clamping the specimen in place and lowering the crosshead until a small load (100-200 N) is registered by the load cell. When fully seated, reduce the load to 10-30 N and tighten the inner and outer bolts. Tighten the bolts incrementally following an inside-out pattern until the recommended torque levels are reached.

Tests were conducted on an Instron 1197 test frame with a 500 kN load cell, at a rate of 1 mm/min until failure.

Figure 30: *Four-pillar die set combined loading compression test fixture*

Strain measurement

ISO 14126 states that the measurement of strain should be conducted using strain gauges or suitable extensometers and shall be measured on both surfaces of the specimen. To reduce the potential for buckling during loading, the gauge-length of specimens are kept short. Small gauge sections restrict the measurement of strain to the use of strain gauges, especially when using shear-loading and some end-loading fixtures where space for an extensometer is often inadequate. For many coarse 2D and 3D fabrics, the use of small gauge sections will result in measurement of localised strain responses rather than global strain. For 3D composites this is due to the size of the unit cell and the influence of components within it, i.e. z-binders,

warp/weft tows, and resin-rich regions, on the local strains. Whilst not prescribed by any compression test standard, non-contact optical strain measurement techniques such as DIC are more suitable for testing these materials. DIC can provide full-field strain mapping across the entire gauge-length and width of a test specimen and can be post-processed numerous times. This makes it ideal for determining the appropriate size of gauge area across which strain can be measured and from which compressive modulus, Poisson's ratio and strain-to-failure can be determined.

For the compressive tests undertaken, strain was measured using back-to-back stereo DIC, i.e. a pair of cameras on each side of the test specimen. Four 5Mpx resolution LaVision cameras, each with a 50 mm fixed focal length lens, were used. A black speckle pattern on a white mat background was sprayed onto each sample to aid correlation. Image capture and processing was performed using the LaVision software DaVis 8.4 utilising a subset size of 31 and step size of 8.

Note 4: For information on DIC good practice, such as recommended speckle pattern sizes, refer to the International Digital Image Correlation Society (iDICs) Good Practice Guide [73].

To assess the influence of averaging strain over different areas on the calculation of compressive modulus, strain measurements were made using virtual strain gauges of varying sizes. As per ISO 14126, the compressive modulus was measured from the stress-strain response between 0.05% and 0.25% strain using equations (6) and (7).

The degree of bending can be calculated using equation (8) where the suffixes $1a$ and $1b$ indicate longitudinal strains on opposing faces of the specimen. ISO 14126 requires that bending be less than 10% strain for a test to be considered valid.

$$\sigma_c = \frac{F}{bh} \quad (6)$$

$$E_c = \frac{\sigma_{2c} - \sigma_{1c}}{\varepsilon_2 - \varepsilon_1};\ \sigma_{1c}@\varepsilon_1 = 0.05\%\ and\ \sigma_{2c}@\varepsilon_2 = 0.25\% \quad (7)$$

$$\left|\frac{\varepsilon_{1b} - \varepsilon_{1a}}{\varepsilon_{1b} + \varepsilon_{1a}}\right| \leq 0.1 \quad (8)$$

Open-hole compression (OHC)

OHC tests were conducted in accordance with ISO 12817. Method 2 allows the use of a combined-loading test fixture such as that used for plain compression testing (Figure 30). However, Method 2 only allows the use of materials with a minimum thickness of 4 mm. The thickness of the CFRE LTL material fits within the prescribed thickness requirements of ISO 12817 but, at 3 mm, the GFRE ORT does not. Method 1 (supported end-loading) allows specimens with

a thickness of 2.5 mm and a slightly reduced length compared to Method 2; these specimen dimensions were chosen for the GFRE ORT material, though its thickness remained at 3 mm. Since Method 2 tests with an unsupported gauge area, reducing the gauge-length to accommodate a lower material thickness will reduce the potential for buckling.

The standard recommends 36 mm wide specimens with a 6 mm diameter open-hole, though other dimensions can be used so long as a width-to-hole ratio of 6 is maintained. As such, tests were also carried out with a width of 24 mm and a hole diameter of 4 mm to assess the dimensional variability of measured open-hole compressive strength. The average dimensions of the OHC specimens tested are detailed in Table 8.

***Table 8**. Dimensions of GFRE ORT and CFRE LTL open-hole compression test specimens*

Distance between grips (mm)	Loading direction	Length (mm)	Width (mm)	Thickness (mm)	Hole (mm)
GFRE ORT					
18	**Warp**	118	24.24 ± 0.02	3.10 ± 0.03	4.00
	Weft	118	24.22 ± 0.04	3.03 ± 0.04	4.00
	Warp	118	35.93 ± 0.02	3.07 ± 0.03	6.00
	Weft	118	35.93 ± 0.02	3.07 ± 0.06	6.00
CFRE LTL					
25	**Warp**	125	24.03 ± 0.02	5.04 ± 0.01	4.00
	Weft	125	24.01 ± 0.07	5.05 ± 0.05	4.00
	Warp	125	35.99 ± 0.03	5.04 ± 0.03	6.00
	Weft	125	36.00 ± 0.01	5.12 ± 0.02	6.00

Specimen preparation

The preparation of OHC test specimens is similar to the preparation of OHT specimens; the specimens do not require end tabs. In addition, as for plain compression specimens, the ends of the OHC specimens should be flat and parallel to ensure uniform loading; this can be achieved by grinding. For hole drilling it is recommended that a sickle-shaped carbide drill bit is used to minimise damage at the periphery of the hole.

Test Setup

OHC testing was undertaken using the same test machine, fixture, and loading rate as used for plain compression. No strain measurements were performed. Open-hole compressive stress/strength was calculated using equation (6).

Results and analysis

Plain compression (ISO 14126)

Elastic property measurement

For many composite formats, strain is not uniform across its surface during loading but varies in accordance with the material structure. For the determination of properties such as the elastic modulus or Poisson's ratio, measurement of the global strain is required. The following example is provided to better understand the influence of the material structure on the strain induced during loading.

Example: Influence of gauge area on the measurement of strain

DIC can be used to visualise the strain distribution across a material surface as shown in Figure 31. Here, a GFRE ORT warp-direction specimen has been loaded to approximately 250 MPa in compression. A clear pattern of strain can be observed that corresponds well with features of the material structure; a schematic representative of this specimen has been provided for reference.

Compressive strain range	**Feature**
0.25≤ ε ≤0.75% (Dark blue)	Z-binder crowns, i.e. regions where the z-binder crosses over the surface weft tows
0.75≤ ε ≤1.25% (Light blue)	Weft tows
1.25≤ ε ≤1.75% (Green)	Resin-rich regions at the surface of the material
2.25≤ ε ≤2.75% (Red)	Resin-rich regions located where the z-binder traverses through-the-thickness of the material

Note 5: Warp tow strains are not visible in these strain distributions as they are located below the material surface and are obscured by the weft tows.

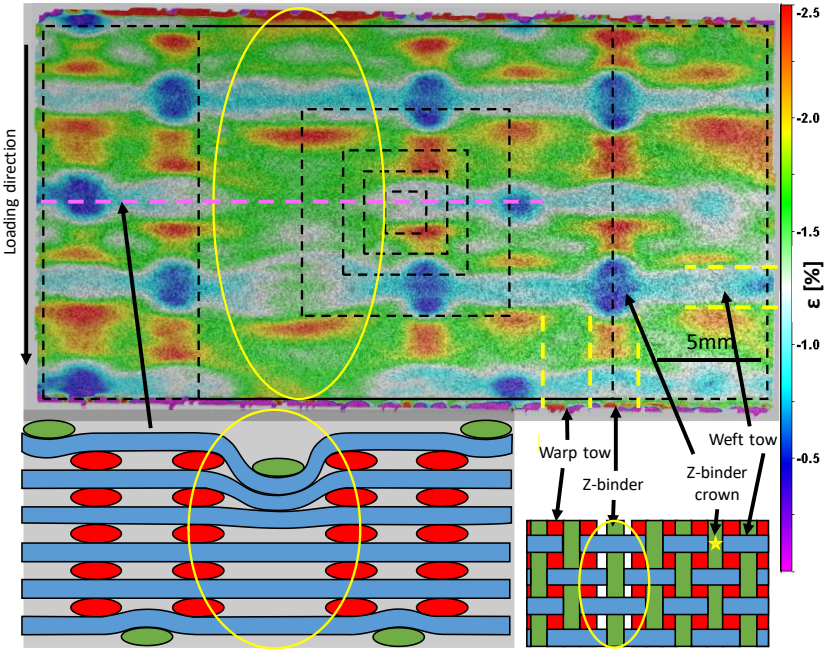

Figure 31. *DIC captured strain map for a GFRE ORT warp-direction loaded specimen alongside a side- and plan-view schematic of the material structure. Hatched squares relate to virtual strain gauges used for strain and modulus measurements shown in Figure 32.*

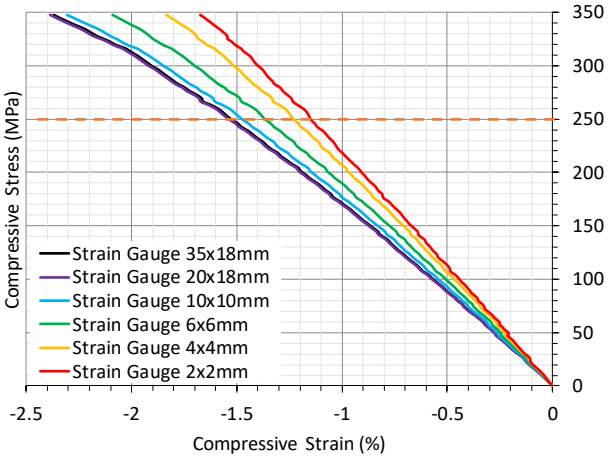

Gauge [mm]	E [GPa]
2x2	22.40
4x4	19.94
6x6	18.28
10x10	17.75
20x18	17.61
35x18	17.64

Figure 32. *Effects of strain gauge size on the measurement of average strain and compressive modulus for a GFRE ORT warp-direction loaded specimen – measurements taken from DIC image shown in Figure 31.*

By looking at the full-field strain distribution, it is possible to not only observe features of the material but also structural irregularities. For instance, from the strain distribution highlighted by the yellow ellipse in Figure 31 it appears as though a section of the material structure is missing. A plan view schematic representative of this test specimens shows that this is due to an irregularity in the spacing between one of the z-binders and the neighbouring warp tows. This has the consequence of causing longer sections of weft tows to span the gap between warp tows, which are subsequently pulled centrally by the z-binder in a similar manner to that shown in the cross-sectional schematic of Figure 31. At these depths, these components provide little influence on the distribution of strains along the surface and therefore are not registered on the strain map. Instead, strain in the resin that occupies this region is observed.

It is important to recognise that the measurement of bulk strain for materials with a strain distribution such as the one shown in Figure 31 can vary depending on where and over what area the measurements are taken. This has been demonstrated in the compressive stress-strain responses for varying sizes of virtual strain gauge shown in Figure 32; the corresponding gauge areas have been drawn over the full-field strain distribution for reference (Figure 31). By virtue of the area each gauge covers, differences in the average strain response are observed, most notably for gauges less than 10 mm x 10 mm. The strain responses converge as the gauge sizes increase thereby representing a more global strain distribution. Consequently, the relationship between average strain and gauge area has an effect on the determination of the compressive modulus, values of which are also included in Figure 32. When evaluated on multiple specimens, not only does the average modulus measurement converge with increasing gauge area, but there is also a reduction in the scatter between measurements as shown in Table 9. Given that the unit cell size of this material is ~8 mm x ~10 mm, this suggests that the use of at least one unit cell within the gauge area for average strain measurement should be sufficient. However, larger gauge areas will capture a more representative global strain response, especially if periodic defects are present in the material structure.

Recommendation 1: The minimum area required for measuring a strain response representative of the bulk material should be equivalent to at least the area of one unit cell. Ideally, the measurement area should cover as many unit cells as practical.

Table 9: *Effect of strain gauge size on the measurement of compressive modulus when averaged across multiple specimens – example here is from GFRE ORT warp-direction loaded specimens. Results presented in the form of mean +/- std. dev. (CoV).*

Specimen gauge area	Test direction	Virtual strain gauge area	Compressive modulus
		mm x mm	GPa
36 mm wide, 20 mm long gauge-section	Warp	2x2	19.6 ± 1.8 (9.0%)
		4x4	19.5 ± 0.8 (3.9%)
		6x6	18.9 ± 0.3 (1.8%)
		10x10	18.5 ± 0.5 (2.6%)
		20x18	18.4 ± 0.5 (2.5%)
		35x18	18.3 ± 0.5 (2.6%)

GFRE ORT property measurement

For the GFRE ORT material, testing was conducted using several different specimen dimensions, whereby both the width and the gauge-length were increased compared to the standard test dimensions (Table 7). The virtual strain gauge area was chosen to be as large as possible with regards to the specimen dimensions; virtual strain gauge areas used for each specimen size are shown in Table 10. Whilst one unit cell area is sufficient for the measurement of bulk strain, the use of larger gauge areas ensures greater accuracy. In addition, given the flexibility of DIC to measure across areas of the user's choice, it is recommended to use virtual gauge areas of a similar size to specimen gauge area.

Recommendation 2: If DIC is used for strain measurement, take average strain measurements across the entire unsupported gauge area to obtain a good representation of global strain response. Due to short gauge-lengths of compressions specimens, the entire gauge area should easily fit within the field-of-view of the DIC cameras used.

Table 10. *Sizes of virtual strain gauge used in the measurement of average compressive strains for each test specimen type*

Specimen gauge area	Virtual strain gauge area
GFRE ORT material	
10 mm x 10 mm	9 mm x 9 mm
25 mm x 10 mm	24 mm x 9 mm
36 mm x 10 mm	35 mm x 9 mm
25 mm x 20 mm	24 mm x 18 mm
36 mm x 20 mm	35 mm x 18 mm
CFRE LTL material	
25 mm x 25 mm	24 mm x 24 mm
36 mm x 25 mm	35 mm x 24 mm

Figure 33a shows a comparison of the compressive moduli measured for each specimen size plotted against the specimen width. For the GFRE ORT material, increasing both the width and gauge length produces negligible change in the compressive modulus and maintains a low scatter, similar to that observed for tension testing. This indicates that the ISO 14126 type B1 test specimen dimensions are sufficient for determining the compressive modulus of this material. However, it must also be recognised that strain was measured across the entire specimen gauge area, which is not possible using strain gauges or extensometers.

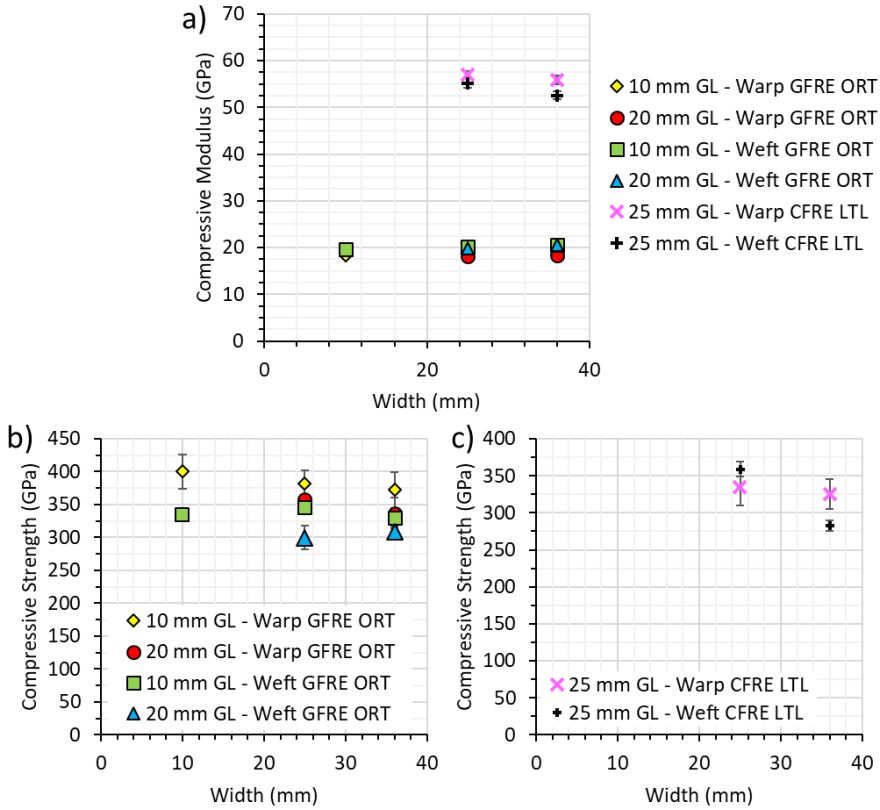

Figure 33: *Comparison of compressive modulus and strength measurements for both the GFRE ORT and CFRE LTL materials with different specimen widths and gauge lengths*

Compressive strengths for both loading directions of the GFRE ORT material are shown in Figure 33b plotted against the specimen width. There are two key observations that can initially be made with regards to the compressive strength: (1) the warp-direction decreases with increasing specimen width, while the weft-direction remains reasonably consistent; and (2) increasing the gauge-length produces a knockdown in strength regardless of loading direction related to the increased likelihood of buckling.

The decrease in strength for the warp-direction is related to the increased potential for defects such as the irregularity shown in the example above (Figure 31). Strain map and specimen observations show that irregularities in spacing are not uncommon in the warp-direction compression specimens. This can have the effect of reducing the number of load bearing tows

present across the width. It is worth noting that without the irregular tow spacing (from the example), all specimens tested here contain an equal number of warp tows and z-binders.

Unlike the tow spacing defects observed between warp tows and z-binders, spacing between weft tows is more regular across all test specimens. As such, increasing the width of the specimen does not appear to noticeably influence the results. The spacing defect observed in warp-direction specimens would only promote premature failure by increasing the misalignment of all weft tows in the out-of-plane direction – see the schematic illustration in Figure 31.

Table 11. *Maximum gauge-lengths for compression test specimens according to the Euler buckling criteria (equation (5)) provided in ISO 14126. E_c is the compressive modulus, σ_c is the compression strength, G_{13} is an assumed through-thickness shear modulus, h is the specimen thickness, and L is the gauge-length*

	GFRE ORT		**CFRE LTL**	
	h (mm)			
	3		5	
G_{13} (GPa)	**E_c (GPa)**			
4	18	20	55	57

	Warp	**Weft**	**Warp**	**Weft**
σ_c	**L (mm)**			
300	20.1	21.2	58.6	59.6
350	18.5	19.5	53.8	54.7
400	17.1	18.0	49.9	50.8

It can also be seen from Figure 33 that increasing the gauge-length produces a drop in the measured compressive strength regardless of loading direction or specimen width. Equation (5) can be used to determine the gauge-length at which buckling is suspected to occur during compressive loading. From Table 11 a 20 mm gauge-length is very close to the buckling limit for a range of compressive strength values. This suggests that these test specimens may fail by buckling. While this did not occur in all instances, some specimens showed a buckling-type loading profile from comparison of back-to-back strain measurements, i.e. difference in strain readings greater than 10%.

From the GFRE ORT material measurements, the standard 10 mm long gauge-length (as prescribed by ISO 14126) appears sufficient for the determination of compressive properties. For this material the standard Type B1 gauge-length represents approximately one unit cell in either material direction. Ensuring at least a unit cell is present within the gauge-length is recommended for a minimum representation of the bulk material performance. However, this does need to be balanced against the buckling limit. It is suggested that the gauge-length should be as short as possible to avoid buckling whilst still containing at least one unit cell length.

Measurements also indicate that the adjustment of the width of the test specimen above that of the standard Type B1 only affect the measurement of the compressive strength. Again, like the gauge-length, the standard width dimension is also representative of approximately one unit cell length of either loading direction of the GFRE ORT material. The effect of irregular tow spacing on warp-direction loading, as opposed to that of the regularity of the weft-direction, suggest that the width of the test specimen should be chosen based on structural uniformity across the material depending on the direction of loading. Observation of structural uniformity prior to testing may be achieved visually or by the use of a variety of non-destructive inspection (NDI) techniques.

CFRE LTL property measurement

Unlike the GFRE ORT material, only the width of CFRE LTL compression test specimens was varied while the gauge-length was kept constant. The decision to use the ISO 14126 Type B2 specimen was based on the minimum thickness allowable and the ability to contain more than one weft-direction unit cell; the warp- and weft-direction unit cell lengths are ~10 and 17 mm, respectively. Since DIC was used for the measurement of strain, the same approach with regards to virtual strain gauge size was used as described above for the GFRE ORT material. The virtual strain gauge sizes used can be seen in Table 10 and examples of the strain distributions across the surface of two specimens can be seen in Figure 34. Locations of z-binder crowns at the surface have been highlighted in the strain distribution and compared to surface images of the material. Other features on the surface of the specimen are harder to determine in the strain distribution. Resin-rich regions are more limited in the LTL format, especially between weft tows, due to the use of multiple z-binders through-the-thickness. To some extent this blurs the ability to clearly outline the structure of the material. However, the repeating features seen can still be used to determine the smallest area that could be used for strain measurements used in the calculation of the compressive modulus.

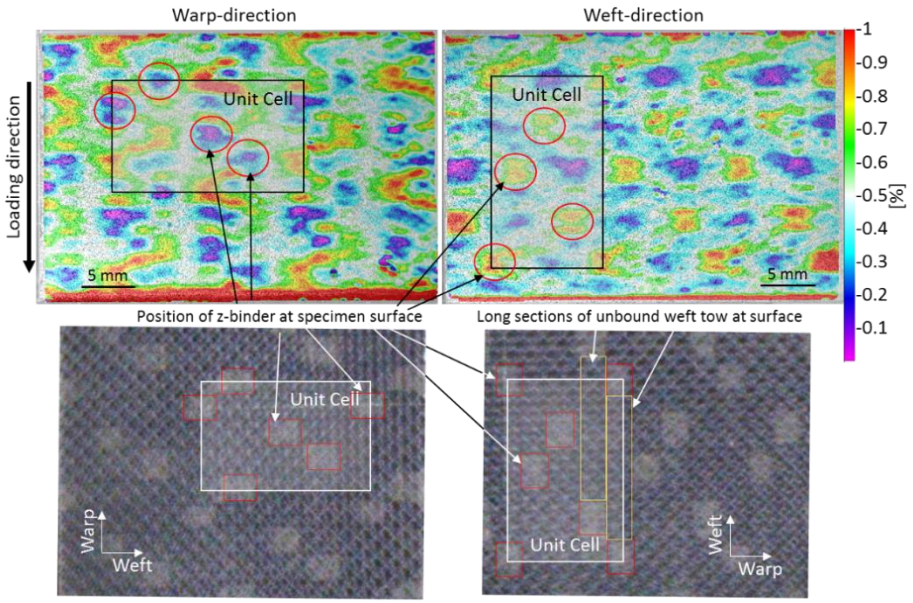

Figure 34: *Observed locations of z-binders in a DIC strain map of CFRE LTL specimens loaded in compression compared against images of the material surface. The DIC and surface images are not from the same specimens but are simply for z-binder location comparison. Note: the scale bar is only for the DIC images.*

The compressive moduli for both loading directions are detailed in Figure 33a. In both cases the compressive modulus decreases with increasing specimen width, though it is much more noticeable for the weft-direction. The compressive modulus is influenced by misalignment of in-plane fibres orientated along the loading direction. Whilst it is impossible to remove all fibre misalignment in a composite structure, the z-binders create misalignment in sections of weft tow, whilst less constraint is placed on the warp tows. Under initial loading, the misalignment of in-plane fibres provides a more immediate influence on the overall stiffness of the material. By increasing the width there is a greater chance for tows with greater misalignment to be present across the gauge area.

Figure 33c shows the compressive strength for both loading directions of the CFRE LTL material plotted against the specimen width. For the warp-direction, increasing the width produces a negligible change in the compressive strength. Since this LTL material has a tightly packed and uniform structure, and the warp tows are well constrained by the weft tows, this is not unexpected. In contrast, there is a considerable decrease in the compressive strength of the weft-direction. The interlacing pattern of the z-binders in this structure is such that long lengths of weft tow at the surface of the material remain unbound; an example of this has been

highlighted in the image of the material surface shown in Figure 34. Under compression, these free lengths of weft tow are susceptible to buckling. This susceptibility is increased further by the curvature present in all weft tows as a result of the interlacing of the z-binders, which creates misalignment from the intended in-plane loading direction. Increasing the width, increases the number of weft tows present and therefore increases the potential for failure at lower loads.

The standard Type B2 test specimen gauge-length dimensions are likely satisfactory for the testing of this type of material. As shown in Table 11, the gauge-length is well within scope to avoid buckling, and this was also confirmed in all strain responses captured. In the case of this material, just as for the GFRE ORT material, increasing the width appears to be a better test for determination of material strength so long as the gauge-length contains at least one unit cell and is below that determined by the buckling criteria.

Recommendation 3: To ensure the compressive strength and modulus is representative of the bulk material, the unsupported gauge area of a 3D composite compression test specimen should ideally contain at least one unit cell length across its length and width. However, this must be balanced against the estimated gauge-length to avoid Euler buckling.

Compressive failure modes

Acceptable failure modes according to ISO 14126 include in-plane shear, through-thickness shear, splitting, delamination and a complex mode that is a combination of these modes. Unacceptable failure modes generally occur outside of the gauge area between the end tabs, often towards the ends of the specimen. All specimens tested produced failure modes that would be considered acceptable. Figure 35 shows the side profile failure for warp- and weft-direction specimens of both the GFRE ORT and CFRE LTL material. While not explicitly shown here, a number of these specimens had a mixed mode type of failure, such that the damage observed along either side profile was different. This may occur as a result of the positioning of different parts of the structure relative to the edge of the specimen. Additionally, it is noted that none of the specimens tested separated into two pieces but remained together as a result of the z-binders.

Damage modes common to each material are as follows:

- GFRE ORT material — Mostly through-thickness shear and fibre fracture. Instances of splitting and delamination observed, but damage growth was limited due to the through-thickness reinforcement,

- CFRE LTL material — Through-thickness shear, delamination buckling, splitting and fibre fracture were all common damage mechanisms. The area of failure tended to be large and extended across much of the gauge-length. The z-binder pattern of this material is less restrictive to out-of-plane movement and more readily allows the development of delamination growth.

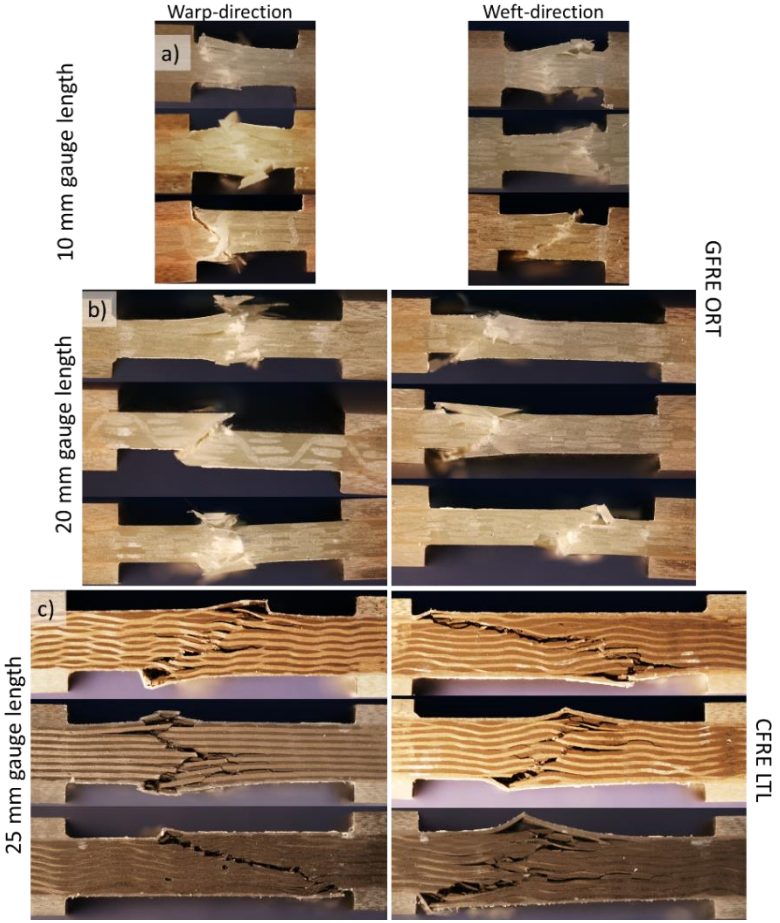

Figure 35: *Various damage modes observed along the edge of test specimens post-failure for both loading directions Note: Images shown here are single sides taken from a variety of test specimens: a) GFRE ORT specimens – 10 mm long gauge-length; b) GFRE ORT specimens – 20 mm long gauge-length; c) CFRE LTL specimens – 25 mm long gauge-length*

Open-hole compression (OHC)

Table 12 shows the OHC strengths for both materials tested in the warp- and weft-directions. The values are plotted as a proportion of the unnotched compressive strength in Figure 36. Both materials, regardless of loading direction, showed a 25-30% drop in strength with a 4 mm hole in a 24 mm wide specimen. Increasing the width and hole diameter leads to a further reduction of the strength by 10-15% for both materials and loading directions, except for the GFRE ORT weft direction.

For the GFRE ORT material, the loss of strength in the warp-direction increases with increasing width and hole diameter, whilst for the weft-direction it remains similar regardless of the hole diameter/specimen width. Both trends are similar to those observed for the unnotched compressive strength measurements. For the GFRE ORT weft-direction measurements, the relatively consistent notched strength suggests that each hole size removes similar proportions of load bearing material. Since the orthogonal woven z-binder restricts out-of-plane movement and leaves only short sections of weft tow exposed at the surface, the size of the hole may not overly influence failure above a general knockdown due to the removal of load bearing tows. Conversely, the drop in OHC strength with increase in width and hole diameter for the GFRE ORT warp-direction measurements is quite considerable. In addition, the scatter in the measurements is large, indicating that measurements are dependent on the position of the hole relative to the material structure (Figure 18). This is to be expected when both the coarseness of the material format and the irregular spacing between warp tows and z-binders are considered.

Table 12. *Comparison of the average open-hole compressive strengths for both loading directions of the GFRE ORT and CFRE LTL materials, tested with different widths and hole diameters. Results presented here as mean +/- std. dev.*

Test Direction	Open-hole compressive strength, MPa	
	24 mm wide – Ø4 mm	36 mm wide – Ø6 mm
GFRE ORT		
Warp	270 ± 20	229 ± 20
Weft	248 ± 14	233 ± 8
CFRE LTL		
Warp	226 ± 9	208 ± 15
Weft	244 ± 8	210 ± 12

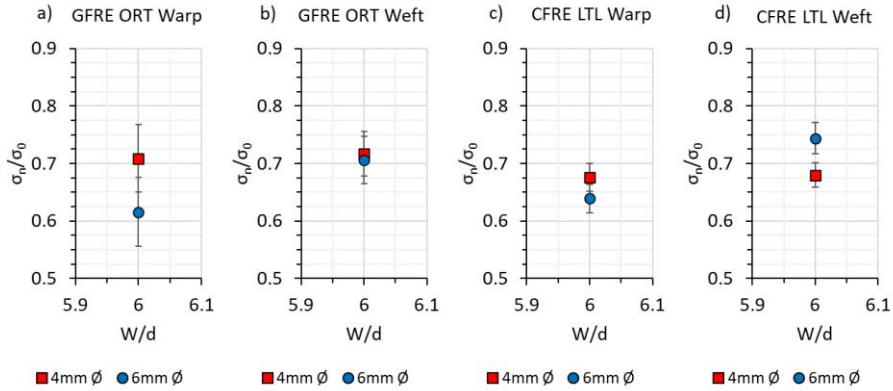

Figure 36. *Effective knockdown in compressive strength produced by open-holes shown as a ratio of the measured open-hole (notched) strengths to the unnotched compressive strength plotted against the ratio of specimen width-to-hole diameter for both the GFRE ORT and CFRE LTL warp- and weft-direction*

The OHC strength values of the CFRE LTL material decrease by a greater percentage for the warp-direction than for the weft-direction. Due to there being z-binders between each warp tow column, there are proportionally less warp tows across the width of a test specimen when compared to the number of weft tows. As such, removing the load carrying ability of one or two warp tows has a much larger influence on the OHC strength. The knockdown in strength of the CFRE LTL weft-direction is similar to the weft-direction knockdown of the GFRE ORT material. However, in this case there is a greater reduction in strength when increasing the width and hole size, likely related to longer sections of exposed weft tow at the surface. Here, the stress concentration around the hole will induce buckling failure in cut weft tows.

As for OHT testing, OHC testing produces a varied loading response, with the results influenced by the size and position of the hole relative to the material structure. It is likely that not all 3D composite materials will show the same degree of notch sensitivity. To fully evaluate the notch sensitivity of a material it is suggested that testing is not conducted only using the standard test dimensions. Maintaining a width-to-hole diameter ratio of 6 is useful for initial testing of a materials performance but can be varied should further analysis be required.

In addition, while the scatter for most of the tests conducted here is low, this could be coincidental with respect to the position of the drilled hole. This would therefore produce an unrealistic representation of the material performance. In conditions where holes are to be machined into composite components, it is unlikely that they will be repeatedly placed in the same position relative to the material structure each time. As such, for understanding the material performance relative to hole size and position, it is recommended that more than five

tests should be conducted. Potentially, a Weibull statistical distribution would be required to capture the influence of hole position on material performance.

Recommendation 4: For 3D composite materials, conduct OHC testing using multiple test specimen dimensions, maintaining a width-to-hole diameter ratio of 6, to determine the degree of notch sensitivity of the material structure. Optional further testing can be undertaken with other width-to-hole diameter ratios.

Recommendation 5: Depending on the size of the hole and the coarseness of the material structure, increasing the number of test specimens beyond the minimum of five suggested by the test standard is recommended.

Conclusions and recommendations

Compression testing presented in this Chapter has been conducted in accordance with ISO 14126. Both materials were tested using standard and non-standard dimensions in order to assess the influence on property measurements, especially with regards to bulk material representation. From the work reported, a number of observations and recommendations can be made, including:

- Strain measurement: For materials with a coarse structure or large unit cell area, small strain gauges only produce a local, rather than global, measure of the strain during loading. This is most evident by the scatter between multiple test specimens but can also be observed when looking at full-field strain images. Increasing the strain gauge area allows a better representation of the bulk material to be measured. Beyond the size of a unit cell, minimal changes to the strains measured are observed indicating that this should be the minimum area used for strain measurement of materials with these characteristics.

  Recommendation: The measurement of strain should be taken across an area of at least a unit cell, though the larger the area the better the representation of the bulk material.

  The use of non-contact measurement techniques such as DIC is a valuable tool for determining the coverage required when measuring strain.

- Specimen gauge area dimensions:

  For representation of the bulk material the gauge-length should contain at least one unit cell length. However, this does need to be balanced against the buckling limit imposed by the Euler buckling criteria.

  Similarly, the specimen width should contain at least one unit cell length, though it is also worth considering the uniformity of the material when selecting a width as this will also influence measurements.

  Recommendation: The unsupported gauge area of a test specimen should contain one unit cell length across its length and width.

OHC testing was conducted in accordance with ISO 12817 using standard and non-standard dimensions maintaining a width-to-hole diameter ratio of 6. The OHC strengths of the materials presented here show strong notch sensitivity with there being a clear dependence of measured strength on the position and size of the hole relative to the material structure.

Recommendation: Vary the dimensions of the test specimen, maintaining a width-to-hole diameter ratio of 6. Two to three variations of specimen dimensions will provide an indication of material performance relative to hole size.

Additional recommendation: Depending on the coarseness of the material structure, increase the number of tests undertaken. This will produce a better representation of the material performance due to an increase in the random distribution of a hole relative to the material structure. It may be necessary to produce a Weibull statistical distribution to characterise the material sufficiently.

Chapter 4

Flexure

- Standard test methods for determining flexural properties
- Flexural testing of 3D composites in the literature
- Flexural testing
- Conclusions and recommendations

Introduction

Flexural loading occurs in many structural applications of composite components and as such is a common test method used to evaluate performance. Typically, flexural characterisation is performed for material screening and/or quality control purposes. It is a very simple test to perform, but unlike many other composite test methods, the strength and stiffness measurements made here are not basic material properties. Instead, the stress state and failure modes are complex and contain a combination of tensile, compressive and shear elements. During loading, the surface nearest the loading point/s is loaded in compression, whilst the outer surface is in tension. The maximum bending stresses occur along the outer surfaces and failure is usually determined by which stress state has the lower strength. It is noted that shear is independent of specimen length, while bending moments are proportional. Therefore, it is common to reduce the shear proportion during flexural loading by using long support spans relative to the material thickness for failure to occur via tension or compression.

Standard test methods for determining flexural properties

Flexural testing of FRP composite materials is typically conducted in three- or four-point bending. ISO 14125 [88] and ASTM D7264 [89] cover both three- and four-point bending methods, whereas ASTM D790 [90] and ASTM D6272 [91] detail three- and four-point methods, respectively. The choice of test method is made such that deformation due to shear is minimised and interlaminar shear failure is avoided. For three-point bending (3PB), load is applied via a central loading point and reacted by two support points, which results in both maximum bending and shear stresses at the loading position. In contrast, load is applied at two points along the specimen's length for four-point bending (4PB), creating a constant maximum bending stress between these points and no shear stress. Considering the stress states present, 4PB appears to be the more desirable choice of test method for composite materials due to the reduced shear between the loading points. For flexural testing, acceptable failure is via tensile or compressive surface failure without interlaminar shear failure or crushing under loading or support points.

Both ASTM D790 and D6272 recommend test specimen dimensions for reinforced and unreinforced plastic material formats, whereas ASTM D7264 focusses only on fibre-reinforced polymer composites. In all ASTM flexural test standards, regardless of loading method, a support span length-to-specimen thickness ratio of 16:1 is suggested for fibre-reinforced composites, so long as the ratio of the in-plane tensile strength to out-of-plane shear strength is approximately 8:1. However, if the ratio of tensile strength to shear strength is much larger than 8:1, the support span length should be increased in order to minimise the influence of shear on the

flexural loading; here, ratios of 32:1, 40:1, and 60:1 are recommended as necessary. It is worth noting that the test spans suggested in the ASTM standards can be used for any fibre-reinforced composite.

Note 1: With regards to 4PB, the distance between loading points is generally equal to either $\frac{1}{3}L$ or $\frac{1}{2}L$, where L is equal to the support span length, as shown in Figure 37. ASTM D6272 allows either of these setups to be used, while ISO 14125 and ASTM D7264 only allows $\frac{1}{3}L$ and $\frac{1}{2}L$, respectively. The main difference between these two setups is the force required to achieve the same bending moments. A $\frac{1}{3}L$ setup requires one quarter less load to achieve the same bending moment as a setup using $\frac{1}{2}L$.

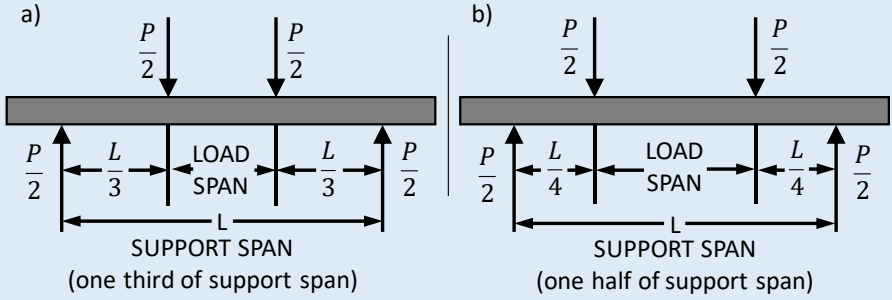

Figure 37. *Two different loading setups for four-point bending (4PB)*

ISO 14125 focusses on fibre-reinforced composites but provides dimension recommendations based on the format of the reinforcement material. Examples of material formats covered by ISO 14125 include, but are not limited to, discontinuous fibre-reinforced thermoplastics, composite mats, unidirectional and multidirectional FRPs. By separating reinforcement formats into various classifications, ISO 14125 allows the user to more effectively select appropriate test dimensions. Unlike the ASTM test standards, support span length-to-specimen thickness ratios recommended in ISO 14125 differ slightly depending on whether 3PB or 4PB is being used. For 3PB the available ratios are 16:1, 20:1 and 40:1, while for 4PB the ratios increase to 16.5:1, 22.5:1, and 40.5:1 in order to accommodate the spacing between support and loading points as shown in Figure 37.

Flexural modulus measurements can be particularly influenced by the presence of shear during loading. ASTM test standards suggest using a support span length-to-specimen thickness ratio of 60:1 to ensure the influence of shear is minimised. However, it is unlikely that flexural strength measurements can be achieved using a 60:1 span length-to-thickness ratio due to test fixture limitations. As such, measurement of flexural modulus and strength may need to be

conducted separately. In contrast, ISO 14125 does not make this same suggestion, opting to use singular test specimens for all measurements.

While support span ratios are chosen to reduce the influence of shear on flexural properties, the equations used for the determination of these properties also influence the derived property values. Equations for flexural strength are based on beam theory of homogeneous materials and in their simplest form are only valid for materials displaying Hookean-type behaviour. Since composite materials are heterogeneous, and many are designed to be highly orthotropic, the maximum stresses may not occur along the outer surface as assumed by the beam theory equations. As such, these equations only provide an apparent strength that is dependent on the ply-stacking sequence. The maximum stress at failure can be determined using laminate beam theory. In addition, if large bending deflections occur during loading, large end forces at the support points can develop that will influence the bending moments. Additional terms to the beam equations can be applied in order to correct for the larger bending deflection influences. In all flexural test standards, deflections greater than 10% of the support span length are considered large and should be corrected for. To minimise bending deflections, ASTM test standards suggest tests should be terminated when an upper limit of 5% flexural strain is reached.

The table below is a summary of the key features of each of the flexural test standards.

Test Method	Key features
ASTM D790	• Used for three-point bending (3PB) • For unreinforced and reinforced plastic materials • Standard support span ratio of 16:1 – increase to minimise influence of shear • Long specimens (support span 60:1) for modulus measurements • Maximum fibre strain allowed is 5%
ASTM D6272	• Used for four-point bending (4PB) • For unreinforced and reinforced plastic materials • Standard support span ratio of 16:1 – increase to minimise influence of shear • Long specimens (support span 60:1) for modulus measurements • Load span = ⅓ and ½ support spans • Maximum fibre strain allowed is 5%
ASTM D7264	• Used for both 3PB and 4PB • For fibre-reinforced polymer composites only

	• 3PB and 4PB dimensions are the same – standard support span16:1– increase to minimise influence of shear • Long specimens (support span 60:1) for modulus measurements • [4PB] Load span = ½ support span
BS EN ISO 14125	• Used for both 3PB and 4PB • For fibre-reinforced polymer composites • Suggests dimensions depending on material format • 3PB and 4PB dimensions differ slightly • Same specimens used for modulus and strength measurements • [4PB] Load span = ⅓ support span

Flexural testing of 3D composites in the literature

Flexural testing of 3D composites is limited within the literature [43, 65, 92, 93, 94, 95, 96, 97], with available studies focusing more on understanding the failure mechanisms during loading than measurement of the flexural properties. Common failure mechanisms found in 3D composites include transverse matrix cracking and fibre fracture, kink bands, and delamination damage. The presence of delamination damage indicates that interlaminar shear stresses are present during loading. Being common to many studies, delamination growth appears to be an unavoidable failure mechanism for these types of materials. However, the extent of delamination growth appears to be a function of both the physical size of the z-binders, their path through the preform, and their position relative to other z-binders [43]. Each of these factors can determine how much energy is absorbed during loading, which in turn will slow, or even halt, delamination growth.

Of the flexural test standards available, ASTM D790 tends to be the most widely used, with test spans varying between studies. Zhang et al [96] chose to use test spans lower than the minimum required 16:1, citing the lack of material availability and thickness of materials tested as a reason. However, it was acknowledged that comparisons between each material would not be possible but could be used to provide some understanding of loading configurations on the materials under investigation.

Despite 4PB appearing to be the more desirable method due to the elimination of shear forces between the loading points, 3PB seems to be the most common method of testing 3D composites in the literature [43, 65, 92, 93, 94, 95, 96, 97]. As such, the development of interlaminar shear failures, i.e. debonding and delamination, is not unexpected. Cox et al [65] initially tested 3D woven composite specimens using both 3PB and 4PB but found consistent evidence of interlaminar shear failure in both loading cases. Since 4PB did not appear to limit the development of shear failures as beam theory would suggest, further testing was conducted

using 3PB only. No other studies appear to provide any explanation for using 3PB over 4PB. However, the ease of performing 3PB over 4PB, and potential difficulties in avoiding shear failures, may be contributing factors.

Flexural testing

Test methods

Flexural testing reported in this Guide was conducted following the 4PB procedure outlined in ISO 14125 [88]. Four-point bending was chosen to eliminate shear failure between the loading rollers and provide pure bending. Here, the choice to use ISO 14125 was made based on its material classification system (described below) which is aimed at helping the user determine suitable specimen dimensions and test spans depending on the material format. Table 13 shows the specimen dimensions of all the flexural tests conducted.

Test specimen dimensions

ISO 14125 provides recommended specimen dimensions for four different material classes, with materials being classified via consideration of the composite structure and ratio of longitudinal flexural stiffness to through-thickness shear stiffness (E_{f1}/G_{13}). The descriptors for each class indicate that 3D woven composites would likely be considered either a class III or class IV material. The distinction made between each of these classes is based on ranges of E_{f1}/G_{13} values. Class III covers a small range of E_{f1}/G_{13} values and is suggested for use with glass-fibre composites, while class IV covers higher E_{f1}/G_{13} values with a larger range, than class III, typically chosen for carbon-fibre composites. Since G_{13} was not known for either of the 3D woven composites presented in this Guide, and glass-fibre and carbon-fibre materials are both being tested, initial testing was conducted using the classes recommended for each material type. ISO 14125 offers some flexibility with regards to specimen dimensions by providing width- and span-to-thickness ratios that can be used for material formats that do not comply with the preferred specimen recommendations.

From the results that will be discussed later, it was thought that testing specimens with span lengths between class III and class IV may result in more valid failures. Both standard and non-standard test dimensions were used on the GFRE ORT material as it was much easier to see the various damage mechanisms that developed during loading. Table 14 shows the test setup dimensions based on the different classes used, where the nominal thickness, h, of the GFRE ORT and CFRE LTL materials were 3 and 5 mm, respectively.

Table 13. *Sample dimensions for the GFRE ORT and CFRE LTL woven materials*

Material	Direction	Width, b	Thickness, h
		mm	mm
GFRE ORT	Warp	15.02 ± 0.08	3.00 ± 0.04
	Weft	15.4 ± 0.07	3.02 ± 0.04
CFRE LTL	Warp	15.04 ± 0.02	5.02 ± 0.01
	Weft	15.06 ± 0.05	5.09 ± 0.02

Table 14. *Test setup dimensions and test speeds used for the flexural testing of the GFRE ORT and CFRE LTL weaves based on material class.*

Material Class as per ISO 14125	Direction	Length, l		Outer span, L		Inner span, L'	Test speed
		$[l/h]$	mm	$[L/h]$	mm	mm	mm/min
GFRE ORT							
Class IV	Warp	50	150	40.5	121.5	40.5	10
	Weft						
Class III.75	Weft	45	135	36	108	36	8
Class III.5	Warp	40	120	31.5	94.5	31.5	6
	Weft						
Class III.25	Warp	35	105	27	81	27	5
Class III	Warp	30	90	22.5	67.5	22.5	2
	Weft						
CFRE LTL							
Class IV	Warp	50	250	40.5	206	68.7	18
	Weft						

Note 2: Non-standard test span lengths have been given a material class designation based on their length relative to those of material class III and IV, e.g. a test span length halfway between class III and class IV is named class III.5.

Specimen preparation

The preparation of flexural specimens is very simple compared to many other testing methods, such as tension and compression, as there is no requirement for specialist geometries or application of tabs. Flexural specimens can be machined directly from panels following the chosen orientation; here, the use of a diamond saw is recommended.

Test setup

Flexural testing should be undertaken using a suitable testing fixture, such as the one shown in Figure 38. This fixture is freely adjustable, such that the distance between, and diameter of, both support and loading points can be altered as required. ISO 14125 recommends that the distance between each support and loading point is equal to a 1/3 of the length of the support span. The length of the support span (outer span) and loading span (inner span) used for each material class is shown in Table 14.

Note 3: Both the support and loading points should be symmetric about the centreline of the test frame. This can be achieved by first setting the distance between the loading points, which is fixed directly into the load cell, and then setting the position of each support point from the nearest corresponding loading point. It is assumed here that the load cell is aligned centrally within the test frame. It is recommended that the position of each loading and support point is done using slip gauges to ensure the correct spans are obtained.

According to ISO 14125 the diameter of each support and loading point depends on the thickness of the material being tested; 4 mm diameter for thicknesses less than and equal to 3 mm, and 10 mm for thicknesses greater than 3 mm. For testing reported in this Guide, support and loading points of diameter 4 mm and 10 mm were used for the GFRE ORT and CFRE LTL, respectively.

Note 4: The size of the support and loading points may influence flexural measurements but the recommend dimensions in both ASTM and ISO test standards are usually reasonable for most materials tested. However, it should be recognised that if the support and loading points are too small, localised stress concentration failures may be induced. In this situation, increasing the size of the support and loading points is recommended.

The test fixture was mounted on an Instron 4507 test frame with a 20 kN load cell. As per ISO 14125, the test speed should be varied according to the outer span length using equation (9) below; the test speeds used in this Guide are shown in Table 14. In addition, deflection of the bottom, or tensile, face of the test specimen should be measured with a suitable device such as a Linear Variable Differential Transformer (LVDT). The LVDT used here had a total travel of 25 mm. Flexural stress and strain can be calculated using equations (10) and (12), or equations (11) and (13) if the measured deflections are greater than 10% of the support span length. Here, F is the load, L the outer span, b and h are the specimen width and thickness, and s is the flexural displacement of the bottom face. Flexural modulus should be calculated with equation (14) between 0.05 and 0.25% strain using flexural deflections determined by rearranging equation (12) or (13).

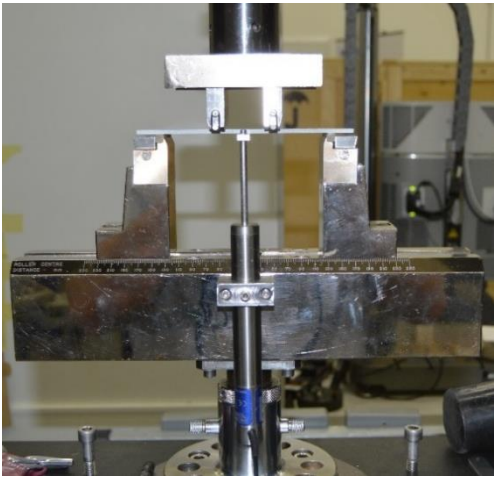

Figure 38. *Image of the four-point bend test setup used.*

$$V = \frac{\varepsilon' L^2}{4.7h} \quad (9)$$

$$\sigma_f = \frac{FL}{bh^2} \quad (10)$$

$$\sigma_f = \frac{FL}{bh^2}\left\{1 + 8.78\left(\frac{s}{L}\right)^2 - 7.04\left(\frac{sh}{L^2}\right)\right\} \quad (11)$$

$$\varepsilon = \frac{4.7sh}{L^2} \quad (12)$$

$$\varepsilon = \frac{h}{L}\left\{4.70\frac{s}{L} - 14.39\left(\frac{s}{L}\right)^3 + 27.70\left(\frac{s}{L}\right)^5\right\} \quad (13)$$

ε' = strain rate of 0.01 (i.e. 1%/min)
F = Load
σ_f = Flexural stress
E_f = Flexural modulus of elasticity
L = span
h = specimen thickness
b = specimen width
s = beam mid-point deflection

$$E_f = \frac{0.21L^3}{bh^3}\left(\frac{\Delta F}{\Delta s}\right) \quad (14)$$

Results and analysis

Flexural loading observations for the GFRE ORT material

For the GFRE ORT material, testing was conducted using a variety of test span dimensions, starting with an outer span ratio of 22.5:1 (class III) and then followed by 40.5:1 (class IV). For both loading directions, class III specimens exhibited damage by tensile and interlaminar shear failure mechanisms, which is an unacceptable failure mode and therefore this type of specimen is not suitable for use with this material. In contrast, the class IV specimens produced solely tensile failures with slight debonding of the z-binder but due to very large deflections all tests were stopped before a failure load was reached. These deflections came close to the travel limit of the LVDT. While the reduction in shear failure is positive, the inability to fail at a reasonable deflection also means the dimensions of class IV are not acceptable for use with this material. Images of failed specimens for each class are shown in Figure 39, with various damage mechanisms highlighted. The large degree of bending observed for class IV specimens is shown in Figure 40.

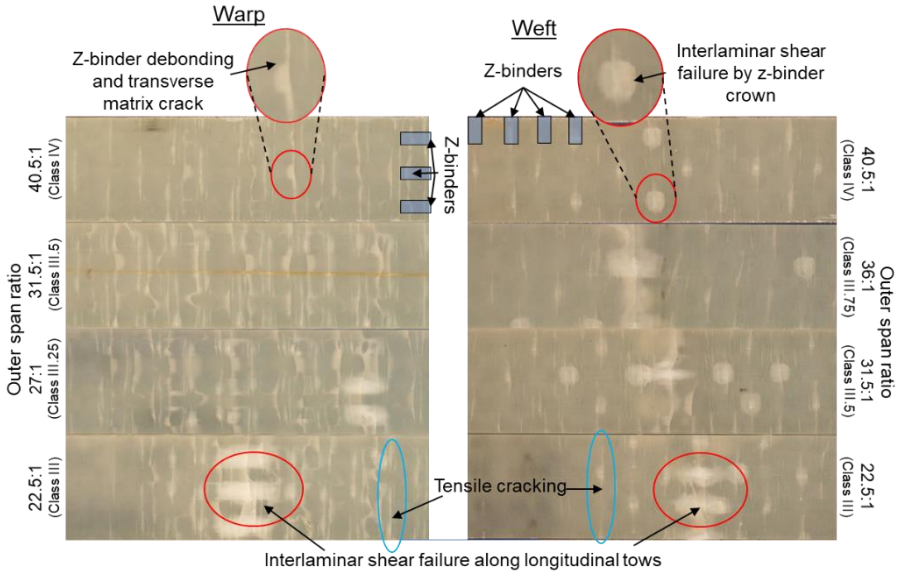

Figure 39. *Bottom (tensile) face damage of the GFRE ORT specimens under four-point bending*

It is clear that the standard dimensions recommended within ISO 14125 are not suitable for use with the GFRE ORT material. Further refinement of the testing spans was attempted and provided the following observations:

- Class III.5: Tensile cracking and small amounts of z-binder debonding were observed for both loading directions but warp-direction testing had similar levels of bending deflections to class IV specimens, with tests terminated before failure, and weft-direction testing showed the development of interlaminar shear failures.
- Class III.75: (Weft only) Peak load is reached but in addition to tensile failures, interlaminar shear failures are also observed.
- Class III.25: (Warp only) Same as for class III.75

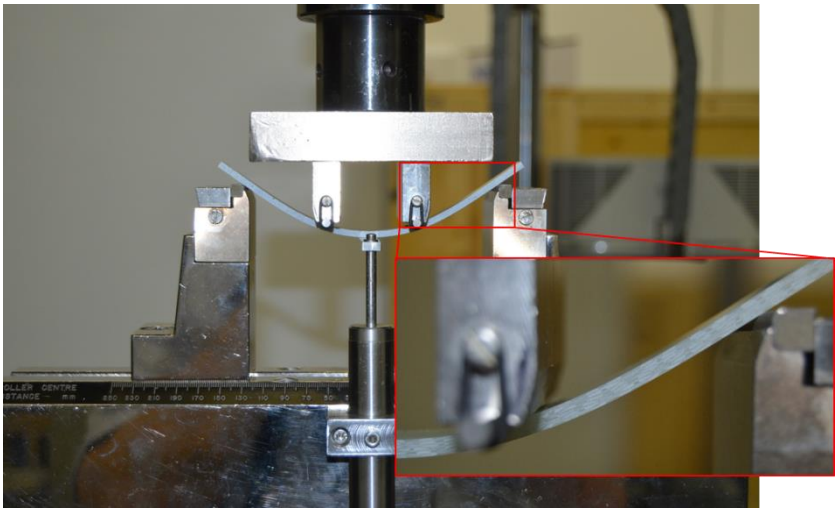

Figure 40. *Example of large bending deflections observed in a class IV GFRE ORT test specimen.*

Evidence of compressive failure was also observed in weft-direction specimens as shown in Figure 41. Here, the compressive failure appears to be in the form of surface tow buckling around the centre of the loading span. Due to the presence of the z-binders, the development of this mechanism is restricted to a small area.

For the GFRE ORT material, the tensile and compressive strengths of the weft-direction specimens are similar, whereas the compressive strength of the warp-direction is higher than the tensile strength, see Figure 16 and Figure 33. As such, it would be expected that warp-

direction specimens should fail in tension, whilst the weft-direction should fail under either tension or compression. This coincides well with the damage mechanisms observed to develop in this material for the individual loading directions.

For the GFRE ORT material it appears that even with the use of non-standard test spans, it is difficult to achieve successful flexural failure whereby the specimen reaches a peak load without excessive bending deflections or the development of interlaminar shear damage. While not performed here, further investigation would be required to determine an acceptable loading span. It can be noted that in all cases tested for this material, the level of bending deflection was large enough, i.e. greater than 10% of the support span length, to require the use of the large deflection correction equation shown above as equations (11)and (13).

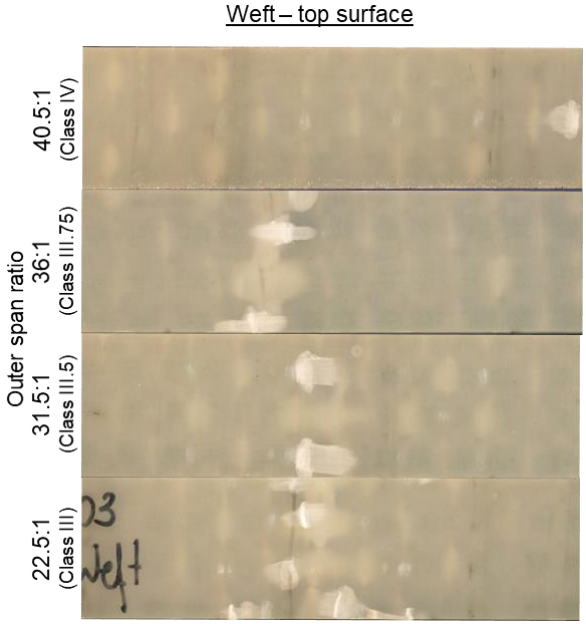

Figure 41. *Compressive damage observed along the top surface of GFRE ORT weft-direction loaded specimens during four-point bending*

Flexural loading observations for the CFRE LTL material

For the CFRE LTL material, testing was only conducted using specimens with outer test spans of 40.5 (class IV). It was not possible to observe the development of damage during loading for the carbon-fibre composite due to its opacity. As a result, observations of damage were made using optical microscopy. The micrographs in Figure 42 and Figure 43 were taken post-peak load from

CFRE LTL specimens loaded in flexure along the warp- and weft-directions. All damage mechanisms observed were common for both loading directions and, while some tensile damage can be observed, failure appears to be predominately compressive. Since the compressive strength of the CFRE LTL material is much lower than the tensile strength, failure in this way was expected. Evidence of compressive failure can be seen by the development of kink bands on all tows present along the longitudinal axis of test specimens. Kink bands develop in regions of compressive stress as a result of the degree of fibre tow waviness and sensitivity of the matrix to shear loading. Given the natural waviness of the z-binders, due to their interlacing pattern around multiple layers of weft tows, the development of kink band damage is not unexpected. For warp and weft tows, the observed fibre tow waviness occurs via a combination of the weaving design and consolidation during laminate manufacture, which ultimately enables kinking to develop during loading.

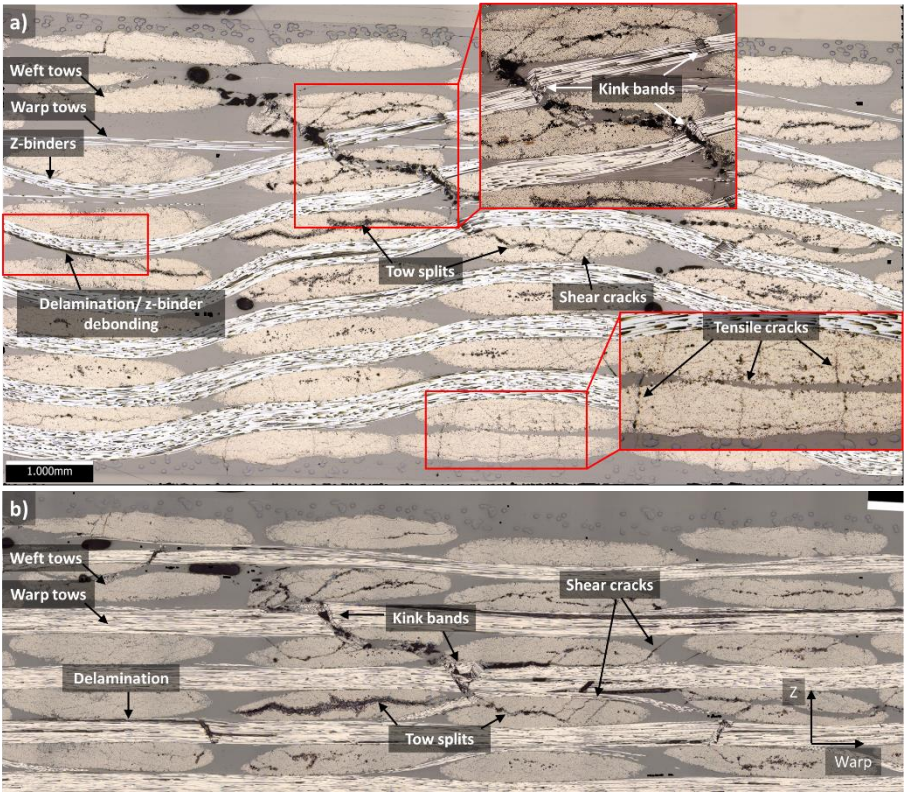

Figure 42. *Cross-sectional damage in a CFRE LTL loaded in four-point bending along the warp-direction: a) cross-section through z-binder plane; b) cross-section through warp tows*

While compressive failures appear dominant, it can be seen in Figure 42 and Figure 43 that delamination damage has also developed along the compressive half of the test specimen. The development of delamination damage indicates the presence of shear during flexural loading despite beam theory suggesting its removal when testing with four-point bending. As for the GFRE ORT specimens, increasing the span lengths should further increase the bending moment and reduce the potential for shear failures. However, despite not exceeding 10% of the support span length, the bending deflections for each loading direction were still large; for the warp- and weft-directions, bending deflections reached approximately 80% and 60% of the 25 mm travel limit of the LVDT, respectively. Due to the inherent waviness in the material structure, especially in the z-binders, it may not be possible to eliminate the development of interlaminar shear stresses and achieve successful flexural failure. Whilst longer support spans and the ability to measure much greater deflections enable acceptable flexural failure, the maximum flexural capability of the test fixture must also be considered.

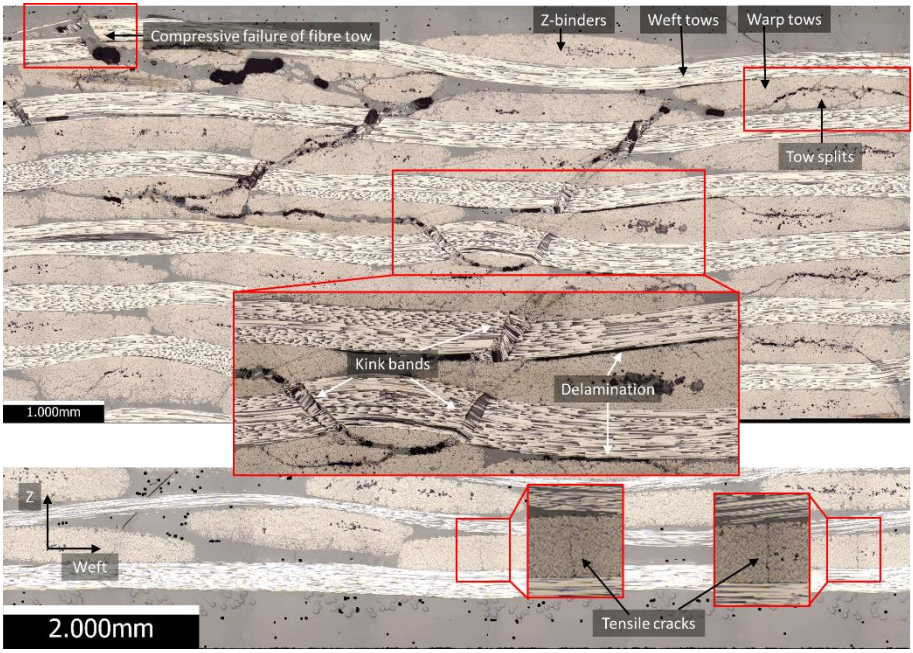

Figure 43. *Cross-sectional damage developed in a CFRE LTL loaded in four-point bending along the weft-direction*

Recommendation 1: When testing 3D composites, use support span ratios greater than 30:1 as an initial starting point for the minimisation of shear during loading. However, it must be recognised that the influence of shear during loading is highly dependent on both the 3D composite format being tested and its loading direction.

[***Additional***] Test spans greater than 40:1 generally produce bending that can exceed the limits of flexural test fixtures and should be avoided unless used solely for flexural modulus measurements.

Flexural performance of the GFRE ORT and CFRE LTL materials

Figure 44a is a plot of flexural modulus against outer (support) span length for both the GFRE ORT and CFRE LTL materials. Here, the weft-direction is stiffer for both materials. This is due to there being weft tows located near to the surface of the material, as well as there being an extra tow layer available to carry load. Despite some scatter, the flexural modulus remains relatively consistent regardless of the test spans for each loading direction. However, long test spans are recommended in order to reduce shear influence on the measured values.

Note 4: Flexural modulus is influenced by the material structure/layup and shear present during loading, and as such cannot directly be compared with the tensile, or compressive, modulus.

Flexural strength as a function of the outer span length is shown in Figure 44b. Although some consistency is observed for the various test directions, these cannot be treated as correct measurements of the flexural strength for each material. For the CFRE LTL materials, as well as most of the GFRE ORT (as outlined in previous sections), this is due to the presence of shear influencing the loading. Additionally, for the GFRE ORT material, the class IV specimens for both test directions, and the class III.5 specimen for the warp-direction, were stopped due to large bending deflections nearing the travel limit of the LVDT.

Note 5: From beam theory it is known that under flexural loading stresses are greatest along each surface and decrease linearly toward the neutral axis. Stresses are compressive along the topside and tensile along the underside.

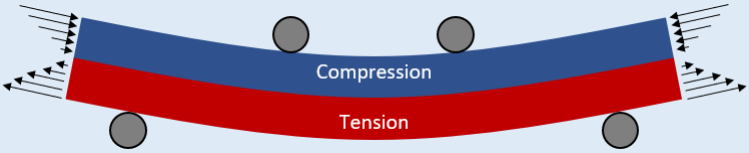

Flexural failure occurs when one of the stress states reaches the respective strength of the material, i.e. tensile or compressive. However, it is not uncommon for the measured flexural strengths to be higher than either of these strengths. Unlike tension or compression testing, the volume of material under each stress state is much smaller during flexural loading, and therefore the potential for defects is reduced. As such, the measured flexural strengths cannot be compared directly with, or considered representative of, the material's tensile or compressive strengths.

Recommendation 2: Avoiding shear failure during flexural testing may not be entirely possible in many 3D composite materials. As such, it is recommended that an acceptable level of shear failure is agreed prior to testing (see conclusions and recommendations). Since the qualitative comparison of specimens is important, the development of small amounts of shear failure can enable easier and faster testing.

It is difficult to recommend sufficient test spans that would enable successful measurement of the flexural strength as this is influenced not only by material structure, but also by test direction. Generally, a shorter test span would be required for warp-direction specimens, when compared to the weft-direction, since these produce greater bending deflections to peak loads. For large bending deflections, consideration of the deflection measurement device, i.e. LVDT, and the capability of the test fixture must be taken into account.

Recommendation 3: In attempting to minimise the influence of shear when making flexural strength measurements, it may be difficult to avoid large bending deflections. In these instances, it may be worth choosing a suitable strain limit at which to stop the test such as the 5% flexural strain limit used in ASTM D790 and D6272. It should be recognised that these cannot be representative of the flexural strength but can be used for qualitative comparison of different materials.

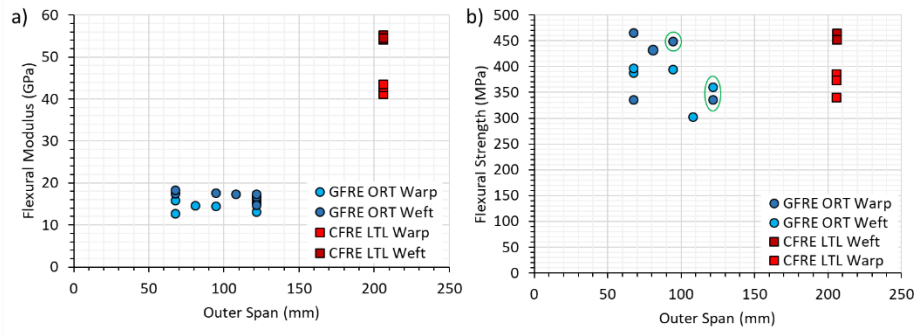

Figure 44. *Flexural modulus (a) and strength (b) for GFRE ORT and CFRE LTL materials against outer span length. Circled in green are tests stopped due to deflections reaching the travel limit of the LVDT.*

Conclusions and recommendations

Flexural testing of 3D composites was conducted in accordance with the four-point bend method in ISO 14125. As per the test standard, it is unacceptable for interlaminar failures to occur during loading as it indicates the presence of shear stresses. The development of interlaminar failures are not uncommon in 3D composites and have been observed in several studies. These studies showed that delamination growth tended to be restricted by the presence of a through-thickness reinforcement, with the lengths depending on the pattern and path of the z-binder. Interlaminar shear failures were observed for both materials used in this work but as per the observations from the literature, the extent was restricted to small regions.

Using dimensions based on recommended material class as per ISO 14125, the following observations were made:

- GFRE ORT: Class III (support span ratio of 22.5:1) dimensions develop interlaminar shear failures alongside tensile failures for both loading directions

  Class IV (support span ratio of 40.5:1) dimensions only develop tensile failures but show very large bending deflections.

- CFRE LTL: Class IV dimensions develop interlaminar shear failures alongside tensile and compressive failures. Compressive failure is the dominant mechanism.

Using the GFRE ORT material test span lengths varying between class III and IV indicate a fine balance is required between eliminating shear and limiting the bending deflections. While not investigated in this study, the same applies to the CFRE LTL since deflections were quite large

relative to the travel of the LVDT used and yet shear failures still developed within these specimens.

While it is difficult to suggest a suitable test span for acceptable determination of the flexural strength for these materials, some recommendations can be made:

- Choose a test span that minimises shear contribution and ensure deflection can be measured fully – a support span ratio greater than 30:1 but less than 40:1 should be considered for 3D composites to minimise the influence of shear and avoid excessive bending. A long travel LVDT or another suitable device should be used. This option also requires consideration of test fixture capabilities, i.e. how much can a specimen be flexed before reaching the fixture's limit.
- Determine an acceptable level of interlaminar shear failure (the smaller the better) that can occur before a peak load is reached during testing. While shear is ideally removed from these specimens, the qualitative comparison between specimens is important and small amounts of shear may not be easily avoidable. Allowing a small proportion of shear failure to develop may enable easier and faster testing.
- [***Optional***] Select a suitable strain limit to stop the test at if large bending deflections occur – this can be very much dependent on the material being tested but stopping the test at 5% flexural strain, as suggested within ASTM D790 and D6272, seems reasonable.

Chapter 5

Shear

- Standard test methods for determining shear properties
- Shear testing of 3D composites in the literature
- Shear testing
- Conclusions and recommendations

Introduction

In many composite materials, the resistance to shear loading tends to be relatively low when compared to tension and compression, especially along matrix dominated planes. Improvement of the shear performance can be achieved somewhat through the arrangement and orientation of fibre layers within the composite laminate. A weak shear performance can potentially lead to premature failures if not effectively taken into consideration during the design stage of a component. It is therefore essential shear properties are measured correctly to enable successful design of composite components.

Pure shear loading of composite materials is difficult to achieve. Ideally, an effective test method would produce a uniform shear stress state within the gauge section of a test specimen. However, in practice it is difficult to achieve a uniform shear stress state without inducing tensile or compressive stress components that ultimately influence the loading. Due to the difficulties in producing acceptable shear loading conditions, much effort has been put into the development of suitable methods that minimise the contribution of other stress states compared to shear state required.

As for tension and compression, both in-plane and out-of-plane shear properties of composite materials need to be characterised. This can be difficult to achieve using a single test method. Numerous test methods have been developed and standardised, with some considered more successful than others. Compared to the number of standardised test methods for the determination of tensile and compressive properties, there are a much greater number available for measuring shear properties. In the following section, several of the standards available will be discussed.

Standard test methods for determining shear properties

±45° tension

One of the simplest methods for determining the in-plane shear response of composite materials is to apply a uniaxial tensile load to a specimen with fibres orientated at ±45° to the loading direction. During loading, the off-axis fibres reorientate towards the loading direction, thus producing a shearing response. This is a relatively easy test method to perform and specimens can be produced using the same techniques used to make typical tension specimens. There are currently two standards that prescribe ±45° tension methods for in-plane shear property determination; these are ISO 14129 and ASTM D3518 [98, 99].

While a shear stress/ shear strain response is produced using this test method, it should be noted that the specimen is never placed in a state of pure in-plane shear. Each fibre layer is

subjected to a biaxial stress state in the form of in-plane normal stresses. The effects of in-plane normal stresses are minimised through the presence of neighbouring fibre layers acting as a form of ply constraint. However, surface layers are only constrained on one side and therefore undergo a mixed mode failure rather than a pure shear one.

The initial shear response can be used for the measurement of in-plane shear modulus [53] but care must to be taken when interpreting shear strength and strain results. The measurement of shear strength at failure is believed to be an underestimate of the true shear strength.

Note 1: It is possible for fibre scissoring to occur which, if excessive, can violate the assumption of testing a ±45° layup. As a result, both ASTM D3518 and ISO 14128 recommend that testing is terminated once 5% shear strain is reached, regardless of whether the load continues to increase or not.

When performing shear strain and modulus measurements on a ±45° tension specimen, material inhomogeneity on a local scale needs to be considered carefully. Some composites, such as those constructed using layers of textile preforms can produce variations in strain across their surface. It is important to ensure that measurements of strain are taken across a large enough region to be representative of the bulk material strain when under load. If strain gauges are used, they must cover enough material to be considered representative, and be able to measure up to sufficiently high strains. In contrast, extensometers can easily cover a representative region, but need to be removed prior to failure over concern of damage to the device. Alternatively, the use of non-contact optical measurement tools, such as video gauges or DIC, are an option as they are capable of measuring over large areas across the entirety of a test.

V-notch test methods

There are currently two standards that use test specimens containing V-notches: ASTM D5379 – V-notch beam (Iosipescu shear) [100] and ASTM D7078 – V-notch rail shear [101]. Both methods use flat rectangular test pieces with a pair of opposing V-notches located centrally along the specimen length, but the specimen size and application of load differ. Examples of specimen size and shape, along with test fixtures can be seen in Figure 45. In both cases, shear loading is produced using asymmetric four-point bending. V-notch testing is often the preferred shear testing method, as it is capable of measuring both in-plane and interlaminar shear properties.

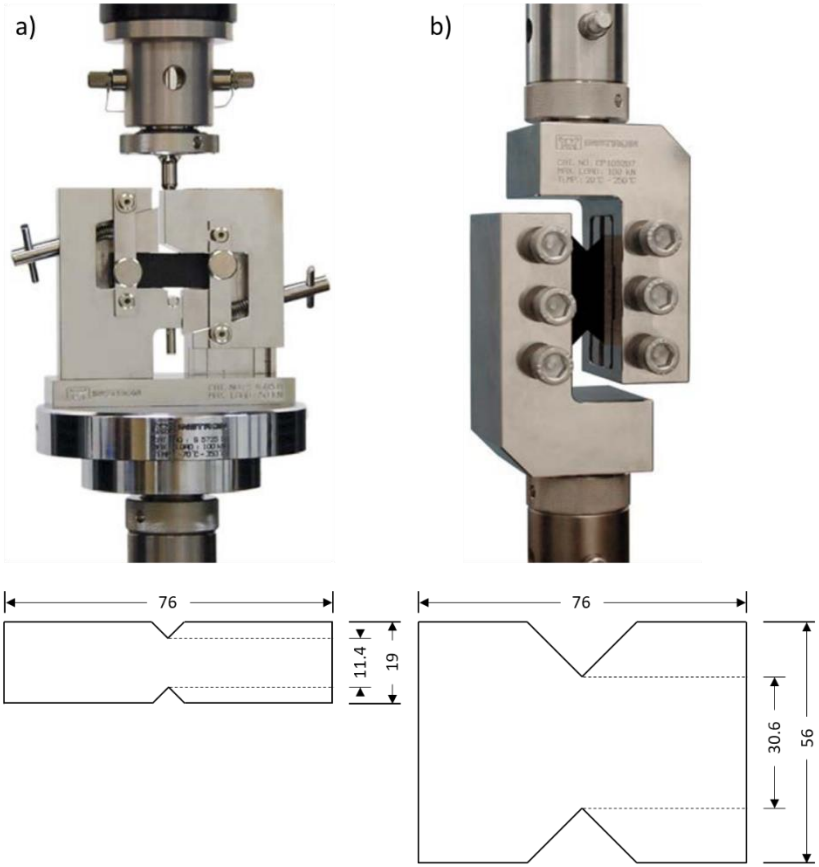

Figure 45. *V-notch shear test method rigs and general specimen dimensions; a) V-notch beam method (Iosipescu shear) ASTM D5379; b) V-notched rail shear ASTM D7078; All dimensions in mm. Images taken from Instron® [102].*

Note 2: Shear loading of an unnotched rectangular test specimen produces a parabolic shear stress distribution across its width, with zero shear at the edge and a maximum at its midplane Figure 46. The addition of notches removes regions of low shear stress, leaving a central section with a relatively uniform state of shear stress.

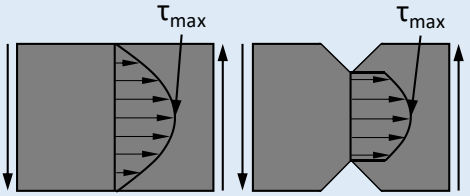

Figure 46. *Shear stress state across unnotched and notched coupons*

Note 3: In asymmetric four-point bending, there is a constant shear force and cancellation of the bending moments at mid-length of the test specimen Figure 47, enabling pure shear to be produced at this location.

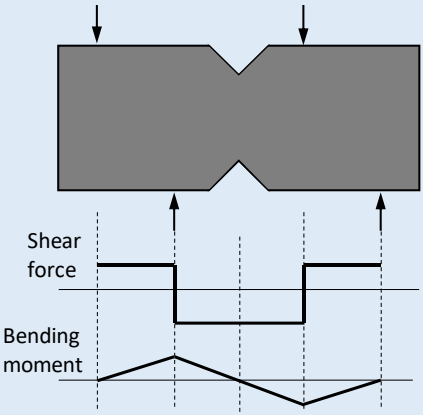

Figure 47. *Shear force and bending moments in asymmetric four-point bending*

For both test methods, shear strain is measured using two biaxial strain gauges, one on each face orientated at ±45° to the loading direction. As the region of uniform shear stress is relatively small in these test specimens, the size of the strain gauges is also kept small, with a gauge-length of 1-2 mm recommended. However, ASTM D5379 does also suggest using special shear strain gauges that can sit vertically between the notches in order to cover a larger area of material. Gauges on both surfaces allow for the measurement of specimen twist, which should remain low at less than 3%. Twist in the specimen can influence both shear strength and modulus

measurements, and therefore care must be taken to ensure that both specimen manufacture and test setup is adequate to reduce and/or eliminate twist from loading.

Note 4: Measurement of the elastic modulus assumes a uniform shear stress between the notches. However, the degree of uniformity varies with both the material orthotropy and the loading direction tested. Adjusting the notch dimensions, i.e. angle, depth, and tip radius, can potentially improve the shear stress uniformity between the notches. Unfortunately, there are no agreed recommendations for notch dimensions based on material orthotropy. As such, ASTM 5379 and D7078 each provide only a single specimen geometry.

ASTM D5379 – Shear Properties of Composite Materials by the V-Notched Beam Method

ASTM D5379 [100] is a V-notch beam (sometimes referred to as Iosipescu) test method that loads the specimen along its top and bottom edges in asymmetric flexure. It was the first of the V-notch test methods to be developed and standardised and is a preferred method for measurement of shear property design data. Although it is versatile in its ability to test all material orientations, the test method does have drawbacks:

- Edge crushing: Due to the application of load through the specimen edges, some materials may be susceptible to edge crushing. This is especially true for thin specimens, typically with a thickness of less than 3 mm, and it is recommended in these cases that end tabs be bonded onto the test specimens. This increases the area under contact with load and reduces the potential for edge crushing. Bonding of end tabs can also be used to minimise twisting during loading.
- Material homogeneity: One of the assumptions made by this test method is that the materials being tested are relatively homogeneous with respect to the size of the test section. This means that the specimen geometry may not be applicable for use with materials containing coarse features, such as some textile composites with large unit cell areas.
- Thickness requirements: While this test method is capable of measuring properties in all six shear planes, most of these can only be done on thick materials due to geometric requirements of specimens. For many composite materials this limits the shear properties that can be measured.

ASTM D7078 – Shear Properties of Composite Materials by the V-Notched Rail Shear Method

The V-notch rail shear method, ASTM D7078 [101], improves upon the V-notch beam test through more efficient loading and the inclusion of a much larger area of uniform shear stress between the notches. Specimens are clamped between grip faces allowing more efficient face loading of the specimen. In turn this allows wider specimens to be tested whilst maintaining the same length as the V-notch beam test specimens. For V-notch beam test specimens a similar increase in specimen width would require a proportional increase in length in order to minimise edge crushing effects. The distance between notches in V-notch rail shear specimens is almost three times that of the V-notch beam test specimen, enabling testing of relatively coarse composite formats (i.e. textile composites) containing reasonably large unit cell sizes. In addition, the increased efficiency of loading in V-notch rail shear test fixture allows for a greater loading capability than the V-notch beam test fixture. This is especially useful when testing multidirectional composites such as those containing ±45° plies [103, 104]. The load limit of this test method is often governed by slippage of the test specimen in the grips, and therefore it is suggested that the test specimens must be kept relatively thin in order to avoid this.

Short beam shear (SBS)

A common method for measuring the interlaminar shear strength of composite materials is by short beam testing. There are two main standards which cover this procedure, ISO 14130 [105] and ASTM D2344 [106]. Both test methods use three-point bending (3PB) of short composite coupons to produce failure in shear. The magnitude of the bending stresses is a linear function of the support span length, while shear stresses are independent. Therefore, both standards limit the specimen dimensions in order to maintain a shear failure and reduce the effects of bending stresses.

Under 3PB, there is no region of pure shear during the loading of SBS test specimen. Test specimen failure can occur via a variety of different modes, each of which are dependent on, but not limited to, factors such as the type of composite material, laminate layup and material thickness. As such, this method produces a measure of the “apparent” interlaminar shear strength (ILSS) and testing is often used for quality assurance (QA) purposes, rather than the generation of design data.

BS ISO 19927 – Fibre-reinforced plastic composites – Determination of interlaminar strength and modulus by double beam shear test

ISO 19927 [107] is a relatively new test standard aimed at improving the measurement of interlaminar shear properties. The test method, known as double beam shear (DBS), uses three support and two loading points. It is an alternative to SBS, using five-point bending to produce interlaminar shear stresses along the midplane of a test specimen. Like SBS, DBS uses short test

coupons. As indicated by the free body diagrams in Figure 48, the test arrangement produces regions of pure ILS, and no bending stresses. According to Zhou et al. [108] and the interlaboratory test data provided in the test standard, ILSS values measured using this method are 20-30% higher than those obtained using SBS. Failures are only considered valid if interlaminar failure occurs on or near the midplane.

In addition to the measurement of ILSS, this test method can also be used to the measure interlaminar shear modulus. This is achieved by using a suitable displacement transducer such as an LVDT. Due to both the size of the test specimen and the region of high ILSS being small, the transducer used must also be small and accurately positioned.

Testing is limited to composites with a symmetric and balanced layup, chosen to avoid bending/twisting or bending/extension coupling deformations. The method is suitable for either glass-fibre or carbon-fibre thermosetting composites with either a UD or $[0/90]_{ns}$ layup. It is possible to use other layups, matrices or fibres but trials must be undertaken to ensure that an acceptable failure mode occurs.

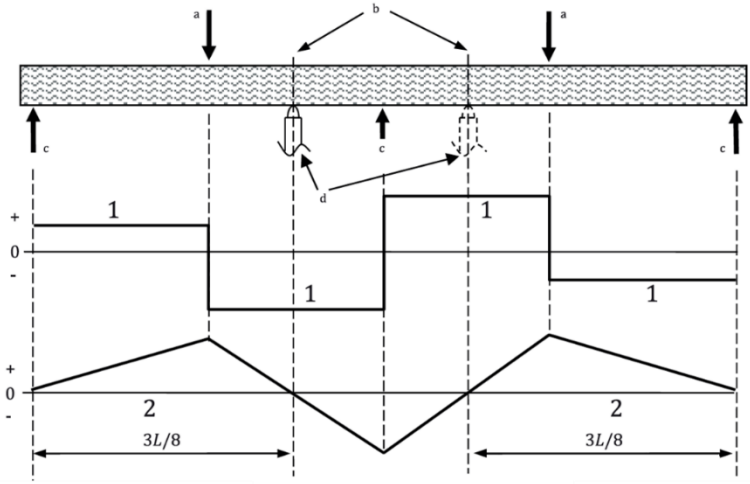

Key

1	ILS stress
2	bending stress
a	Load.
b	Sections of pure shear.
c	Support.
d	Displacement measurement points.

Figure 48. *Loading conditions of the double beam shear test with shear stress and bending moment free body diagrams.*

ASTM D3846 – Standard Test Method for In-Plane Shear Strength of Reinforced Plastics (Double notch shear)

ILSS can also be measured via the double notch shear method detailed in ASTM D3846 [109]. In this method, a notch is machined across the width of each surface of a test coupon. The notches are set a distance apart and cut through half of the specimen thickness. The specimen is end-loaded in compression and a shear plane is induced along the specimen mid-thickness between the notches. The method requires the use of a lateral specimen support to avoid buckling.

A fundamental problem with the double notch shear test method is the development of significant stress concentrations at the roots of the notches, which can lead to premature failure of the test specimen [110]. It is suggested that reducing the spacing between notches to less than or equal to the thickness of the specimen will result in an apparent interlaminar shear strength measurement closer to the actual interlaminar shear strength of the material.

Two NPL reports [111, 112], one of which includes a round-robin interlaboratory study, have found that the notch depth can influence the measured shear strength. It has been observed that higher strength values are produced if the notch depth is less than half of the specimen thickness, due to the increased cross-sectional area of the fracture path. Conversely, notch depths greater than half of the specimen thickness produce low strength values, with bending and peeling type failures occurring. Schematics of typical failure modes observed depending on notch depth can be seen in Figure 49. Notch depths under or over cut by less than ± 0.1 mm produce minimal differences in measurements. As such, accurate notch depth machining is critical to producing consistent ILSS measurements.

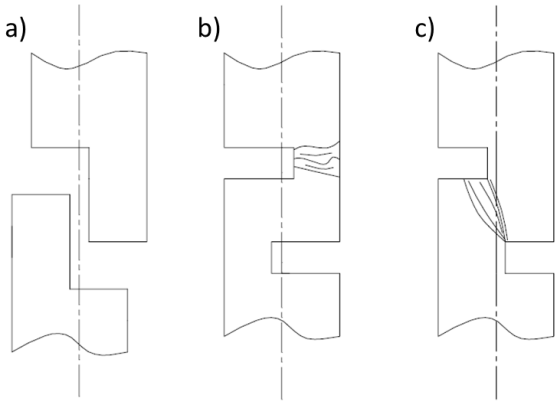

Figure 49. *Typical double notch shear failure modes; a) acceptable failure; b) and c) unacceptable failure [112]*

BS EN ISO 15310:2005 – Reinforced plastics – Determination of the in-plane shear modulus by the plate twist method

ISO 15310 [113] is a method that is limited to measuring the in-plane shear modulus of FRP composites using plate specimens. Specimens are supported on one diagonal and loaded on the other, as shown in Figure 50. The test fixture is essentially two crossbeams with adjustable support/loading points placed perpendicular to each other. Loading in this manner induces a near pure shear stress state across the material. To minimise the influence of through-thickness shear, plate dimensions are typically quite large at 150 mm x 150 mm with thicknesses of 2 mm or 4 mm depending on the format of the reinforcement. This test is suitable for most FRP composite materials, though it is preferred if the material is approximately homogeneous in the through-thickness direction.

To measure the in-plane shear modulus, specimens are loaded to a maximum displacement equal to half of the specimen thickness. Specimens loaded in this way tend to remain elastic and can then be sectioned for testing in other modes. All displacement measurements are taken directly from the crosshead.

Figure 50. *Plate twist fixture*

Summary of shear test standards

The table below provides a brief overview of the key feature of each test standard reviewed.

Test Method	Key features
ASTM D3518 and BS EN ISO 14129 (±45° tension)	• Tensile test similar to ASTM D3039 and ISO 527 where fibres are orientated ±45° to the loading direction • Only measures in-plane shear strength and modulus
ASTM D5379 (V-notch beam)	• Test coupon – Two opposing V-notches – fixed dimensions • Asymmetric four-point bend (4PB) • End-loaded – requires special test fixture • Used to measure shear strength and modulus in all six shear planes
ASTM D7078 (V-notch rail shear)	• Test coupon – two opposing V-notches – fixed dimensions (~3x wider than V-notch beam specimens) • Shear-loaded – requires special test fixture • Used to measure shear strength and modulus in all six shear planes • Designed for testing coarse composite formats (i.e. textile)
ASTM D2344 and BS EN ISO 14130 (Short beam shear)	• Small test specimens – dimensions based off material thickness – not the same in both methods • Three-point bending (3PB) • Apparent interlaminar shear strength only
BS ISO 19927 (Double beam shear)	• Small test specimens – dimensions based off material thickness • Five-point bending (5PB) • Measures interlaminar shear strength and modulus
ASTM D3846 (Double notch shear)	• Two notches machined to mid-thickness a set distance apart on either side of specimen • End-loaded in compression – lateral supports required • Interlaminar shear strength only
BS EN ISO 15310 (Plate twist)	• Square plate geometry – reasonably restrictive dimensions • Test specimens supported • Only measures in-plane shear modulus

Shear testing of 3D composites in the literature

Although there are several standards available for measuring shear properties, a survey of the literature shows that there is a lack of test methods that may applicable for determining the shear properties of 3D composites [114]. As stated in previous sections, due to the complex architecture of 3D composites and often large unit cell sizes, it is important to understand whether the properties measured are representative of the bulk material, rather than a local response [115].

Studies [115, 116] have been undertaken to compare the suitability of different shear test methods for determining a "true" in-plane shear modulus of 3D composites. Weissenbach et al. [115] compared the influence of unit cell size on modulus measurements made using the plate twist, V-notch beam, and 10° off-axis tension test methods. Of these, plate twist produced the most consistent values of in-plane shear modulus, with the V-notch beam performing the worst. This difference is due to both the test specimen size and the way in which strain is measured. The use of small strain gauges on V-notch beam specimens produce local rather than global measures of strain in materials with large unit cells. In contrast, the plate twist method uses much larger specimens, using the plate displacement rather than strain gauges in the measurement of the in-plane shear modulus. As such, measurements of the in-plane shear modulus are more representative of the bulk material. Buchanan et al. [116] observed very similar trends when comparing the plate twist method to the V-notch beam method. In this study, comparison was also made with V-notch rail shear, observing that measurements of the in-plane shear modulus were similar to those produced using plate twist. V-notch rail specimens have a gauge area almost three times that of the V-notch beam specimens and were designed for use with multidirectional and coarse composite formats. Both studies suggest that plate twist and V-notch rail are suitable for the determination of in-plane shear modulus of composites with large unit cell areas. However, the plate twist method is only suitable for measuring the in-plane shear modulus and therefore either the V-notch beam or V-notch rail methods must be used for the measurement of the shear strength.

In a study by Quin et al [114] for a 3D orthogonal woven composite loaded in shear by the V-notch beam method, the measurement of shear strain was shown to be sensitive to both the size of the strain gauges and their position relative to various features within the material unit cell, see Figure 51. The variation in strain across the material structure can be observed using DIC as shown in Figure 52. Here, distinct high and low regions of strain are representative of features withing the material structure. As such, the position of these features relative to the notches will increase the scatter in measurements of shear strain.

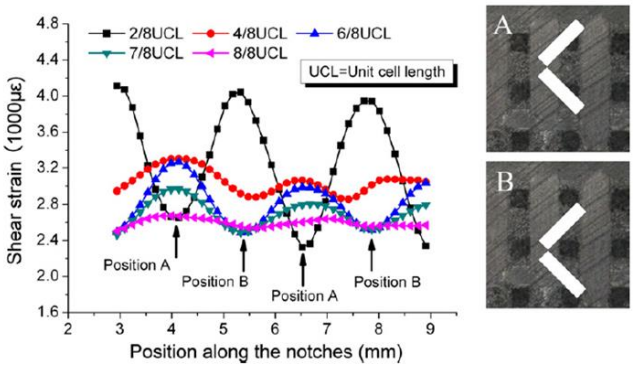

Figure 51. *V-notch beam test undertaken on a 3D orthogonal woven composite; effect of position and gauge size on the measurement of shear strain using virtual strain gauge rosettes [114]*

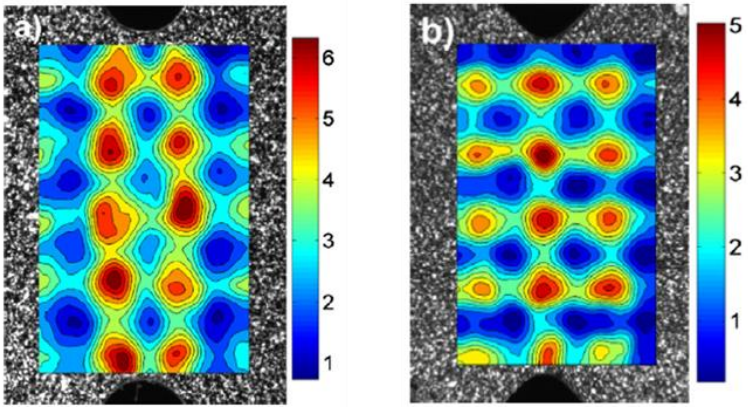

Figure 52. *Full-field strain maps of a 3D orthogonal woven composite loaded in shear using the V-notch beam test method: a) low strains between notches; b) high strains between notches; [114]*

Shear testing

Test methods

In this Guide several test standards are assessed for their applicability in the determination of shear properties of 3D composites. These include:

- ± 45° Tension (ISO 14129)
- V-notch beam (ASTM D5379)
- V-notch rail shear (ASTM D7078)

- Short beam shear (ISO 14130 and ASTM D2344)
- Plate Twist (ISO 15310)

±45° tension

For conducting ±45° tension testing, there is very little difference between ASTM D3518 [98] and ISO 14129 [99]. As such, the ±45° tension testing reported in this Guide is undertaken using ISO 14129 to measure in-plane shear properties.

Specimen preparation

Standard specimen dimensions for length, width and gauge-length are 250, 25, and 150 mm, respectively. To accommodate a larger number of unit cells within the test specimen width, 35 mm wide specimens were prepared alongside the standard 25 mm wide specimens. Average specimen dimensions for each material are shown below in Table 15. For both materials and specimen widths, five specimens were tested.

Table 15. *Average dimensions of ±45° tension test specimens. Measurements provided as mean ± std. dev.*

Test direction	Length (mm)	Width (mm)	Thickness (mm)	Distance between grips (mm)
GFRE ORT				
±45°	250	25.07 ± 0.02	3.19 ± 0.22	150
		35.04 ± 0.02	3.21 ± 0.04	
CFRE LTL				
±45°	250	25.07 ± 0.02	5.04 ± 0.03	150
		35.04 ± 0.01	5.13 ± 0.03	

Test specimens were prepared using the same techniques as reported for tensile testing. Specimens were cut from a panel using a diamond saw ensuring that the fibres were orientated ±45° to the loading direction. It is recommended that GFRP end tabs with a ±45° fibre orientation are used to provide a compliant gripping surface so as not to damage the test specimen and cause premature failure in or near to the gripped regions. A recommended end tab material and adhesive is 2 mm thick Tufnol® 10G/40 and 3M™ Scotch-Weld™ Structural Paste Adhesive EC-9323-2 B/A, respectively.

Test setup

Testing was conducted on an Instron 4507 test frame with a 200 kN load cell at a crosshead speed of 2 mm/ min. Mechanical wedge action grips were used to load the specimen in tension until either the load dropped, or the test was manually stopped. It is recommended that the mechanical grips are aligned in the test frame using a ground flat steel bar. It is also important to ensure that the test specimens are centrally aligned within the grips. Depending on the size of the grip faces used, this may require spacers to be placed between the grip housing and the test specimen.

ISO 14129 recommends that extensometers and/or strain gauges are used to measure strain during loading. However, for the work reported in this Guide, DIC was used. This was chosen as it allows full-field strains to be evaluated, as well as the influence of gauge area on the measurement of shear strain and shear modulus. Here, two stereo pairs of 3D DIC cameras were used, i.e. two cameras per specimen surface. 3D DIC allows out-of-plane measurements to be made and is generally preferred if setup is possible (see Note 10 in this chapter).

Calculations

The equation for shear stress/strength is provided below in equation (15) where τ_{12} is the shear stress, F is the load, and A is the cross-sectional area of the specimen. Equation (16) is used to calculate the shear strain, γ_{12}, through the summation of strains measured longitudinally (ε_x) and transverse (ε_y) to the loading direction. Shear modulus, G_{12}, is calculated using equation (17) via linear regression over the shear strain range 0.1-0.5% as recommended in the test standard. The shear modulus reported in this work is the average of the moduli measurements calculated from both sides of the specimen.

$$\tau_{12} = \frac{F}{2A} \quad (15) \qquad \gamma_{12} = \varepsilon_x - \varepsilon_y \quad (16) \qquad G_{12} = \frac{\tau_{12}}{\gamma_{12}} \quad (17)$$

V-notch beam test (ASTM D5379)

The V-notch beam test, also known as the Iosipescu test, was conducted according to ASTM D5379 [100] using rectangular specimens with V-notches located centrally along the length, as shown in Figure 53a. Despite the method being able to measure material properties in all six shear planes, the thickness of the materials presented in this Guide restricted the measurements to only the 1-2 and 2-1 shear planes, where 1 and 2 represents the warp- and weft-directions, respectively. Average test specimen dimensions for each material and test direction are shown in Table 16. Five specimens per material per direction were tested.

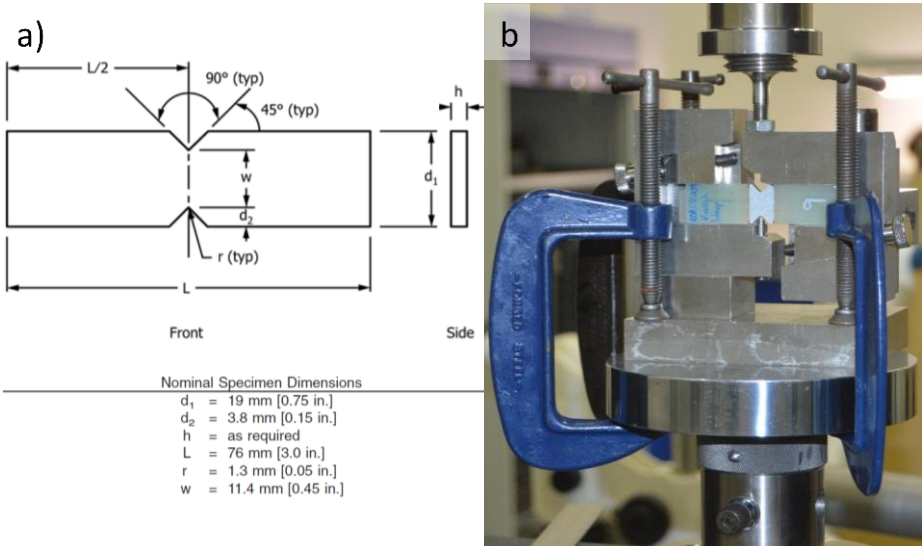

Figure 53. *a) Typical dimensions of a V-notch beam test specimen; b) V-notch beam test fixture with specimen*

Table 16. *Average V-notch beam test specimen dimensions. Measurements provided as mean ± std. dev.*

Test direction	Length (mm)	Width (mm)	Thickness (mm)	Notch-to-notch distance (mm)
GFRE ORT				
Warp (1-2)	76.03 ± 0.02	19.00 ± 0.03	3.11 ± 0.05	11.43 ± 0.03
Weft (2-1)	76.04 ± 0.01	19.01 ± 0.02	3.13 ± 0.03	11.40 ± 0.02
CFRE LTL				
Warp (1-2)	76.01 ± 0.02	19.03 ± 0.03	5.10 ± 0.02	11.42 ± 0.03
Weft (2-1)	76.03 ± 0.03	19.04 ± 0.04	5.01 ± 0.01	11.39 ± 0.04

Test specimen preparation

Due to the edge loading used in this test method, non-uniform loading can induce specimen twisting, which in turn can influence the measurement of the shear strength and modulus. This can be minimised through the correct preparation of test specimens. ASTM 5379 provides tight

parallel and perpendicular edge tolerances in order to make sure that reliable and repeatable measurements can be obtained.

Specimens tested in this Guide were all cut to the required size as rectangular blanks using an automated diamond saw. The V-notches were then machined using a special V-shaped grinding tool on a surface grinding machine.

Note 6: If the tolerances in the test standard cannot be achieved using the chosen cutting method, it is recommended that the edges are machined using a surface grinder or similar machine capable of achieving the tolerances necessary. It may be necessary for specimens to be initially cut oversize and then ground

Note 7: If edge crushing occurs during loading, end tabs can be used to increase the size of the loading edge and minimise the potential for this failure.

If end tabs are used, it is recommended that GFRP with a [0/90]ns fibre orientation (woven or unwoven) is used with a thickness of approximately 2 mm. It is suggested that preparation is done as a single piece such that rectangular blanks can be cut from the panel with end tabs attached. This should ensure that the edges remain flat and even. A spacer can be used during the attachment of end tabs to ensure that the area required for V-notches is not covered.

Test Setup

Testing was conducted on an Instron 4507 test frame with a 20 kN load cell at a crosshead displacement rate of 2 mm/min for all specimens.

A dedicated test fixture was used to grip the specimens and induce a shear stress state between the V-notches as shown in Figure 53b. The fixture is split into two parts:

- A base: Sits against a compression platen and holds one half of the test specimen,
- A loading arm: Attaches directly to the load cell via a clevis pin plate and holds the other half of the test specimen. The loading arm is connected to the base via an offset post.

Note 8: Good alignment of both parts of the test fixture is essential and must be set prior to testing. This can be done using either a test specimen or a special alignment specimen if one is available:

- Push the specimen flat against the back plate of both parts of the test fixture and gently clamp in place. This may require some adjustment of either part of the test fixture for the specimen to sit flat to the back plate.
- Clamp the base of the fixture to the bottom compression platen and tighten the nut connecting the loading arm to the load cell to avoid changes in alignment occurring during testing.

Specimens should be loaded into the test fixture ensuring that they are flat against the back plate. A central bar with a wedge-shaped end can be placed between the notches to align the specimen centrally within the fixture. To clamp the specimens in place, the thumb screws used to move the clamps only need to be finger tight.

Note 9: Incorrect loading of the specimen can occur as the clamps are tightened if the horizontal faces of the test fixture clamping region do not line up. Depending on the layup and format of the material being tested, this could induce premature damage to the test specimen. Therefore, it is useful to monitor the load applied to the specimen during clamping. Adjustment of the crosshead may be needed in order to maintain a low preload on the test specimen. A load less than 50 N is recommended.

Since there is only a narrow region of pure shear between the notches, it is typical to use short biaxial strain gauges on the order of 1-2 mm with an orientation of ±45° to the loading direction. Unfortunately, short gauges will only measure the local strain response of materials with large unit cell or coarse textile structures. Using DIC, virtual strain gauges of different sizes can be used to assess the representation of the shear strain between the notches.

For all V-notch testing conducted, strain was measured using 2D DIC. 5Mpx LaVision cameras, each with a 50 mm lens, were placed on either side of the test specimen as shown in Figure 54. A black speckle pattern on a white matt background was sprayed onto each sample to aid image correlation. The LaVision software DaVis 8.4 was used for both image acquisition and processing, with the latter using a subset and step size of 31 and 8, respectively. Shear strain was measured using virtual strain gauges orientated at ±45° to the loading direction and shear gauges orientated parallel to the loading direction. The size of the gauges varied in order to assess the influence of gauge-length on the measurement of shear strain.

Note 10: 3D DIC can be used to monitor the out-of-plane displacement of specimens, which can include the degree of twisting during loading. While it is desirable to use 3D DIC on both sides of the test specimen, it is not essential for measuring bending. If not using strain gauges, bending can be measured using 2D DIC, with a camera facing each specimen surface analogous to using back-to-back strain gauges.

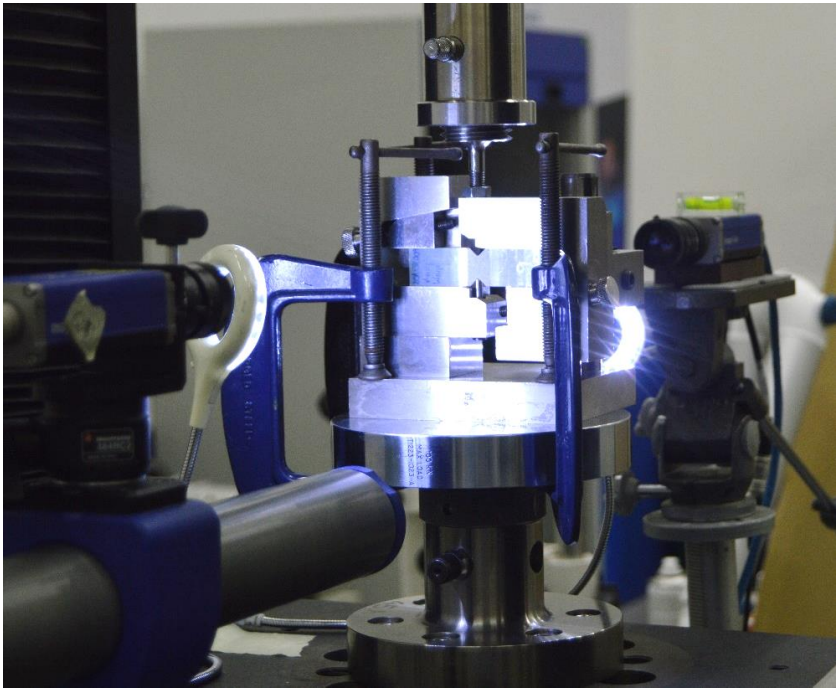

Figure 54. *V-notch beam test fixture setup with front and back 2D DIC*

Calculations

The equation for shear stress/strength is provided below in equation (18) where τ is the shear stress, F is the load, and A is the cross-sectional area between the notches. The shear strain, γ, can be calculated using equation (19) through the summation of strains measured longitudinally along each strain gauge that have been orientated at ±45° to the loading direction. Each strain component in equation (19) is the average of the same direction gauge on both faces of the specimen. Shear modulus, G_i, is calculated using equation (20) using linear regression over two different shear strain ranges, 0.15-0.55% and 0.25-0.65% as recommended by ASTM D5379. The reported shear modulus is the average of the shear moduli measured on each surface.

In addition to these measurements, it is important to monitor the percentage twist in the test specimen during loading. ASTM D5379 recommends that percentage twisting should not exceed 3%, with the test setup examined if twisting exceeds this value. Equation (21) uses the shear modulus of each surface to determine the percentage twisting, where the subscripts f and b denote the front and back surfaces, respectively. This equation can be reduced to only strain terms as shown in equation (22).

$$\tau = \frac{F}{A} \quad (18) \qquad \gamma = |\varepsilon_{+45}| + |\varepsilon_{-45}| \quad (19) \qquad G_i = \frac{\tau}{\gamma} \quad (20)$$

$$\left(\frac{G_f - G_b}{G_f + G_b}\right) \times 100 < 3\% \quad (21) \qquad \left(\frac{\gamma_b - \gamma_f}{\gamma_b + \gamma_f}\right) \times 100 < 3\% \quad (22)$$

V-notch rail shear (ASTM D7078)

V-notch rail shear testing was conducted in accordance with ASTM D7078 [101]. Like the V-notch beam test method, V-notch rail shear produces a narrow region of pure shear between the notches and is capable of measuring material properties in all six shear planes. In this Guide only the 1-2 and 2-1 shear planes were tested due to the thickness of the GFRE ORT and CFRE LTL materials.

Specimen preparation

The preparation of test specimens is conducted using the same techniques as described for the V-notch beam method. Nominal test specimen dimensions are shown in Figure 55. The average dimensions of the GFRE ORT and CFRE LTL test specimens are shown in Table 17. For each material and loading direction five specimens were tested.

Note 11: Although V-notch rail shear specimens are wider and have deeper notches than the V-notch beam specimens, the notch depth-to-width ratio is proportionally similar for both.

Note 12: Due to the use of face loading, the parallel and perpendicular edge tolerances of the V-notch rail shear specimens are larger than for the V-notch beam method.

Note 13: End tabs are not needed.

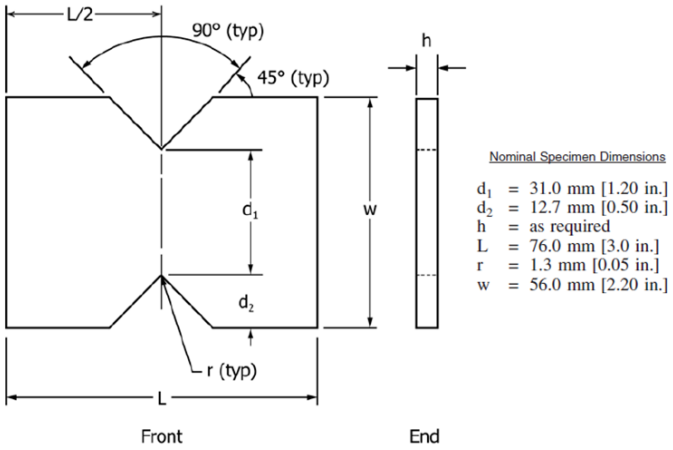

Figure 55. *Nominal dimensions of a V-notch rail shear test specimen*

Table 17. *Average V-notch rail shear specimen dimensions. Measurements provided as mean ± std. dev.*

Test direction	Length (mm)	Width (mm)	Thickness (mm)	Notch-to-notch distance (mm)
GFRE ORT				
Warp (1-2)	76.06 ± 0.04	56.02 ± 0.02	3.27 ± 0.11	30.63 ± 0.03
Weft (2-1)	76.04 ± 0.02	56.03 ± 0.02	3.10 ± 0.05	30.63 ± 0.03
CFRE LTL				
Warp (1-2)	76.07 ± 0.01	56.05 ± 0.02	5.09 ± 0.04	30.60 ± 0.03
Weft (2-1)	76.10 ± 0.02	56.06 ± 0.02	5.01 ± 0.02	30.63 ± 0.02

Test setup

Testing was conducted on an Instron 5969 test frame with a 50 kN load cell at a crosshead displacement rate of 2 mm/min.

The test fixture used is shown in Figure 56 and comprises of two halves that through the application of a tensile load, create shear stresses in the test specimen. Each half of the test fixture contains roughened grip faces that are used to secure the specimen in place during loading. The position of each grip face is adjusted using three bolts and should be set such that

the test specimen is aligned central within each half of the test fixture. Once set, only one set of grip faces needs to be tightened to secure the specimen or loosened for its removal. In addition, PTFE spacer blocks (Figure 56) are used to set the position of the specimen between the two halves of the test fixture,

Note 14: It is important to maintain good alignment between both halves of the test fixture to avoid twisting during loading. ASTM D7078 recommends that the degree of twisting should be less than 3%. Test fixtures usually have centre marks that can be used to aid setup and alignment of specimens.

Note 15: Due to the use of face loading, it is important to ensure that the specimen does not slip between grip faces during loading. The test standard suggests that each bolt should be tightened to a torque of 55 Nm to reduce the potential for specimen slippage. For materials tested in this Guide, a torque of 45 Nm was used and found to be adequate.

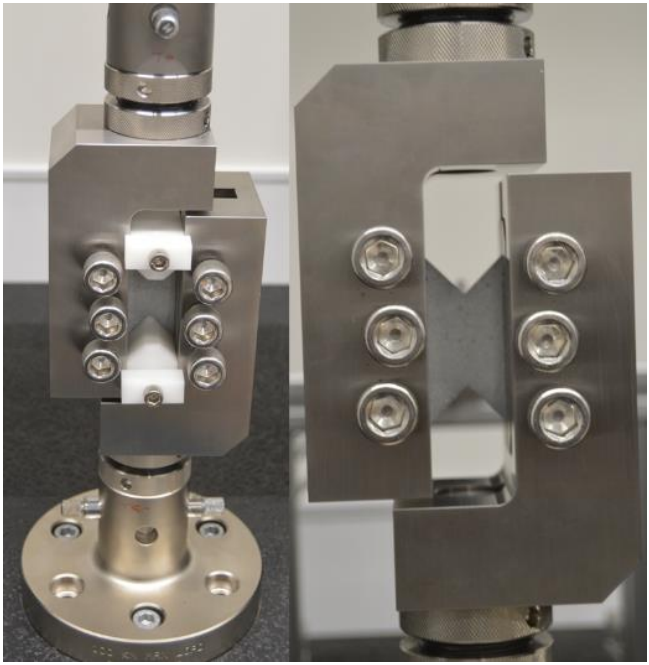

***Figure 56**. V-notch rail shear test fixture with PTFE spacer blocks (left) and setup for testing (right)*

The test specimen dimensions were prescribed to enable the testing of composites with large unit cell areas or coarse fabric formats. As such, strain was measured using DIC rather than strain

gauges to measure the full-field strain profiles and the influence of virtual strain gauge size on the measurement of shear strain. The DIC setup is the same as described for the V-notch beam test, and the general test setup with DIC is as shown in Figure 57.

Note 16: The V-notch rail shear test fixture provides a limited view of the test specimen during loading. As such, it is only possible to use 2D DIC on both surfaces. However, this is still adequate for measuring the percentage twist in a specimen.

Calculations

The calculations for the shear stress, strain and modulus use the same equations as for the V-notch beam method.

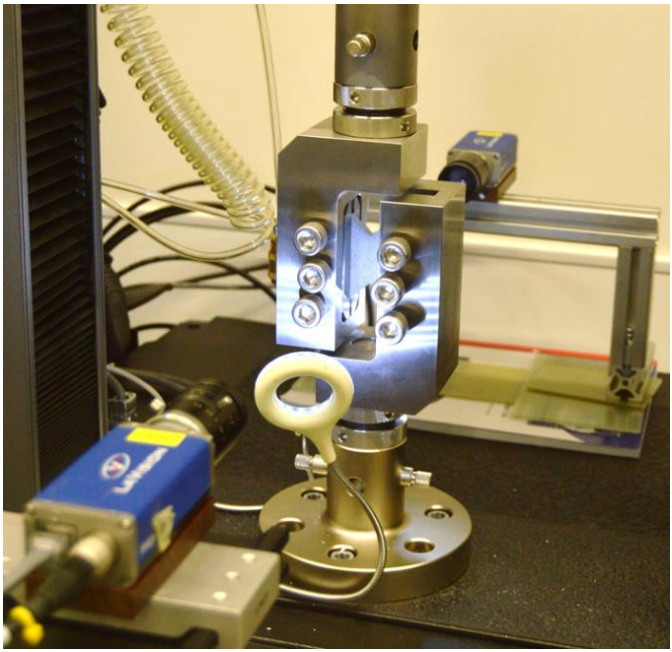

Figure 57. *V-notch rail shear test setup with DIC*

Short beam shear (ISO 14130 and ASTM D2344)

Test specimen dimensions

Short beam shear testing was conducted according to both ISO 14130 [105] and ASTM D2344 [106] as each standard provides slightly different allowances with regards to specimen

dimensions. Both standards provide recommended specimen dimensions, however since the 3D materials studied in this Guide have a thickness governed by the woven fabric thickness, these dimensions do not necessarily suit. Each standard does allow alternative specimens sizes to be used so long as they maintain specific length- and width-to-thickness ratios, as shown in Table 18. The dimensions of specimens were determined using the nominal panel thicknesses of 3 and 5 mm for the GFRE ORT and CFRE LTL materials, respectively. The average dimensions for the specimens tested are shown in Table 19. For both test standards, five specimens of each material and loading direction were tested.

Table 18. *Length-, width-, and span-to-thickness ratios recommended in ISO 14130 and ASTM D233*

Test standard	Length-to-thickness ratio	Width-to-thickness ratio	Span-to-thickness ratio
ISO 14130	10	5	5
ASTM D2344	6	2	4

Table 19. *Average SBS specimen dimensions and test spans. Measurements provided as mean ± std. dev.*

Test standard	Test Direction	Length (mm)	Width (mm)	Thickness (mm)	Span (mm)
GFRE ORT					
ISO 14130	**Warp**	29.98 ± 0.02	15.01 ± 0.03	3.22 ± 0.07	15.000
	Weft	30.01 ± 0.02	15.06 ± 0.05	3.14 ± 0.04	15.000
ASTM D2344	**Warp**	18.02 ± 0.02	6.07 ± 0.03	3.07 ± 0.02	12.000
	Weft	18.01 ± 0.04	6.02 ± 0.04	3.12 ± 0.02	12.000
CFRE LTL					
ISO 14130	**Warp**	50.01 ± 0.02	25.05 ± 0.01	5.05 ± 0.03	25.000
	Weft	50.00 ± 0.02	25.04 ± 0.01	5.03 ± 0.02	25.000
ASTM D2344	**Warp**	29.99 ± 0.04	10.00 ± 0.02	5.05 ± 0.01	20.000
	Weft	30.00 ± 0.03	9.99 ± 0.02	5.03 ± 0.01	20.000

Test Setup

Testing was conducted using an Instron 4507 test frame with a 20 kN load cell and a three-point bend fixture. The span-to-thickness ratios recommended in ISO 14130 and ASTM D2344 are shown in Table 18 and the corresponding span lengths used during testing are included in Table 19. The diameter of the support and loading points recommended by each test standard are shown in Table 20.

Table 20. *Support and loading point diameter for ISO 14130 and ASTM D2344*

Test standard	Support point diameter (mm)	Loading point diameter (mm)
ISO 14130	4	10
ASTM D2344	3	6

Shear stress calculation

The apparent interlaminar shear strength was calculated using equation (23), where τ_M is the interlaminar shear strength, F_M is the maximum load, and b and h represent the width and thickness of the specimen.

$$\tau_M = \frac{3}{4} \times \frac{F_M}{bh} \tag{23}$$

Plate Twist (ISO 15310)

Testing was conducted following the plate twist method test standard ISO 15310 [113]. This method is used to determine the in-plane shear modulus, G_{12} via the deflection of opposing corners of a plate test specimen.

Specimen preparation

ISO 15310 recommends test specimen dimensions 150 x 150 mm for materials with a thickness of 4 mm ± 0.5 mm. However, both the GFRE ORT and CFRE LTL do not fit that thickness criteria, having nominal thicknesses of 3 mm and 5 mm, respectively. Testing with non-standard dimensions is possible in ISO 15310, with the ratio of specimen width-to-thickness required to be greater than or equal to 35. Test specimens were cut to both standard and non-standard widths using a diamond saw. The average dimensions of the test specimens are given in Table 21.

Table 21. *Average plate twist test specimen dimensions. Measurements provided as mean ± std. dev.*

	Width, a_1 (mm)	**Width, a_2 (mm)**	**Thickness (mm)**
GFRE Ort	150.06 ± 0.04	150.01 ± 0.03	3.06 ± 0.08
	104. 99 ± 0.01	105.00 ± 0.01	2.98 ± 0.08
CFRE LTL	150.05 ± 0.05	150.07 ± 0.03	5.10 ± 0.07
	175.08 ± 0.06	175.10 ± 0.04	5.13 ± 0.03

Test setup

Testing was conducted on an Instron 5969 test frame with a 50 kN load cell at a rate 1 mm/min until a predefined displacement was reached. ISO 15310 recommends that the test specimens are only loaded to a displacement equal to half of the specimen thickness. Loading to this displacement ensures the specimen remains linear elastic.

The test fixture consists of two opposite facing flexural test fixtures oriented at 90° to each other as shown in Figure 58. The span length for the support and loading points are the same and equal to $0.95D$, where D is the diagonal distance between corners on the test specimens; D can be calculated using equation (24). Test specimens are loaded onto the test fixture such that opposite corners along the diagonal sit on the support and loading points. To ensure that the specimen sits centrally between the support and loading points, it is suggested that the location of these points is marked on the test specimen.

$$D = (a_1{}^2 + a_2{}^2)^{\frac{1}{2}} \tag{24}$$

Note 17: The support and loading points should be equidistant from the centre of the test frame. Here, it is assumed that both flexural test fixtures are centrally positioned in the test frame. Placing slip gauges between support, or loading, points and the side of the opposing flexural fixture, the distance between support/loading points can be set.

Note 18: The recommended support and loading points are cone shaped and therefore it is important to account for this when setting the support/loading span.

Figure 58. *Plate twist test setup*

Calculations

The in-plane shear modulus is determined using equation (25), where a_1 and a_2 are the specimen width and length, h is the specimen thickness, Δ is the slope of the load-displacement, and K is a geometric correction factor. The slope, Δ, of the load-displacement response is calculated between crosshead displacements equal to $0.1h$ and $0.3h$ using equation (26).

The geometric correction factor, K, is required due to the use of support and loading spans, s, equal to $0.95D$ and would not be needed if the support and loading points were positioned directly at the corners of the test specimen. However, span lengths slightly shorter than the diagonal length are preferred for ease of specimen placement. At $0.95D$, $K = 0.822$. Equation (27) can be used if any other span length is used, where s is the span length

$$G_{12} = \frac{3}{4}\frac{\Delta a_1 a_2 K}{1000h^3} \quad (25) \qquad \Delta = \frac{F_2 - F_1}{w_2 - w_1} \quad (26)$$

$$K = 0.822 \text{ @ } 0.95D \qquad K = 3s^2 - 2s - 2(1-s)^2 \ln(1-s) \quad (27)$$

Results and analysis

±45° tension

In contrast to other shear test methods such as the V-notch beam and V-notch rail shear methods, the entire gauge section of a ±45° tension test should be under shear loading. As such, average shear strain can be measured over much larger areas. The effect of strain gauge area on the measurement of shear strain was investigated using DIC. The smallest area used was 10 x 10 mm and the largest was 50 x 24 mm; all virtual strain gauge areas used can be seen in Table 22.

Table 22. *Comparison of shear modulus for the GFRE ORT and CFRE LTL materials tested via ±45° tension. The shear moduli were calculated using average strains obtained using different size virtual strain gauges. Measurements provided as the mean ± std. dev. (CoV) of five test specimens.*

Gauge Size (mm x mm) [Height x width]	**GFRE ORT**	**CFRE LTL**
	Shear Modulus, G_{12} (GPa)	
25 mm wide		
10 x 10	2.82 ± 0.16 (5.71%)	4.34 ± 0.17 (4.0%)
25 x 10	2.92 ± 0.08 (2.73%)	4.36 ± 0.14 (3.1%)
50 x 10	2.91 ± 0.05 (1.83%)	4.37 ± 0.13 (2.9%)
25 x 24	2.90 ± 0.05 (1.79%)	4.37 ± 0.15 (3.3%)
50 x 24	2.90 ± 0.05 (1.59%)	4.37 ± 0.13 (2.9%)
35 mm wide		
10 x 10	2.75 ± 0.19 (6.82%)	4.43 ± 0.15 (3.5%)
25 x 10	2.78 ± 0.07 (2.38%)	4.38 ± 0.15 (3.4%)
50 x 10	2.73± 0.03 (0.97%)	4.37 ± 0.08 (1.9%)
25 x 34	2.74 ± 0.05 (1.76%)	4.38 ± 0.10 (2.3%)
50 x 34	2.73 ± 0.03 (1.23%)	4.38 ± 0.07 (1.6%)

Using the average shear strain from each of the virtual strain gauges, the shear modulus, G_{12}, was calculated (Table 22). Here, the average shear modulus remains consistent for each material and specimen size, regardless of the size of the virtual strain gauge. Increasing the gauge area results in a reduction in the overall scatter for the modulus, though the scatter for both materials

is already relatively low for the smallest gauge area used. The small scatter produced by this method demonstrates the requirement for measuring shear strain over a larger area.

Recommendation 1: When using ±45° tension tests for determination of the in-plane shear modulus, ensure that the shear strain measurements are representative of the bulk material. For 3D composites, a coefficient of variation of less than or equal to 5% is acceptable and can be achieved by measuring strain across a minimum area 10 x 10 mm. The larger the area of measurement, the smaller the scatter and the better the representation of the bulk material.

Table 23 shows the shear strength for both materials measured at 5% shear strain. Two different specimen widths were used to investigate the influence on shear measurements. From Table 23 the shear strength measurements show low scatter, but do not remain consistent when increasing the specimen width.

Table 23. *Comparison of shear strengths measured for GFRE ORT and CFRE LTL loaded in ±45° tension, taken at 5% shear strain. Measurements provided as the mean ± std. dev. (CoV) of five test specimens.*

Material	Width (mm)	Shear strength, $\tau_{(12/21)}$ (MPa)
GFRE ORT	25	51.89 ± 0.87 (1.7%)
	35	46.35 ± 1.33 (2.9%)
CFRE LTL	25	54.77 ± 1.49 (2.7%)
	35	61.18 ± 1.00 (1.6%)

Failure was noticeably different for each of the materials. For the GFRE ORT material, the specimen failed by separating into two pieces, whereas the CFRE LTL material did not separate and instead continued to load, producing extreme scissoring of the in-plane fibres as can be seen in Figure 59. The distinct difference in failure modes is directly related to the through-thickness format of each material. For the GFRE ORT material, the z-binder is completely through-thickness and restricts much of the rotation of the fibres during loading. As such, there is a point where the z-binders fail and the material fractures (Figure 59). In contrast, the z-binders in the CFRE LTL material only cover two layers and leave sections of material less bound than in the GFRE ORT material. During loading, the tows can rotate with less constraint, while still being bound together overall.

Recommendation 2: Avoid using this test method for shear strength measurements, unless being used for qualitative analyses. Limit any measurements of shear strength to those representing a maximum of 5% shear strain but recognise that this is an arbitrary stopping point to minimise the influence of fibre scissoring on loading. For many 3D composite structures, large deformations will occur due to the through-thickness reinforcement restricting separation, making measurement of the true shear strength difficult.

Despite not producing pure shear during loading, measurements of the shear modulus are in line with measurements made using other test methods (as will be seen in the following sections) that have a purer shear stress state. In addition, the scatter remains very lower when measuring strain over a large gauge area. This suggests that this test method is adequate for determining a reasonable representation of the shear modulus. However, the differences seen for the shear strength, both when increasing the test specimen dimension and compared with other test methods, suggest ±45° tension is inappropriate for the determination of the shear strength.

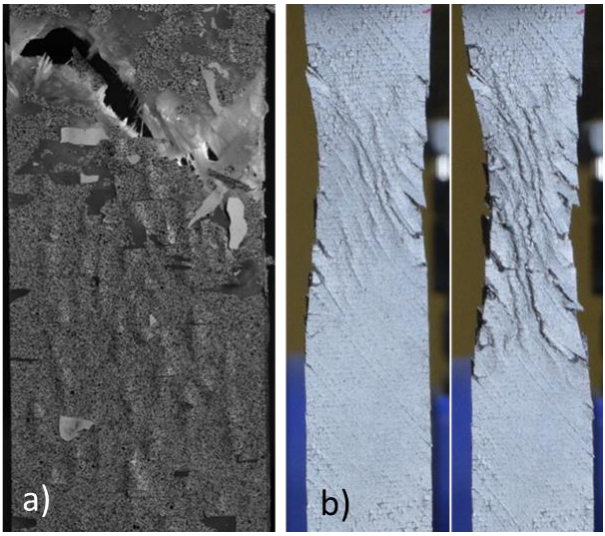

Figure 59. *Images of 3D woven specimens failed under ±45° tension testing; a) GFRE ORT, showing complete separation; b) CFRE LTL showing a large degree of fibre scissoring at failure*

V-notch beam test (ASTM D5379)

For both materials, average shear strain was measured using a 2x2 mm virtual strain gauge orientated at ±45° to the loading direction, and three virtual shear gauges of sizes 2x2 mm, 5x2

mm, and 10x2 mm orientated in line with the loading direction as indicated in Figure 60. The shear strain measurements were used to calculate the shear moduli for each loading direction and can be seen in Table 24. Here, increasing the coverage area reduces the overall scatter in the measurement of the shear modulus for both materials regardless of loading direction. The reduction in scatter with increasing gauge size suggests better representation of the bulk material under shear loading. For the CFRE LTL material, the scatter reduces to less than 4%, while for the GFRE ORT it remains reasonably large (~10%). The GFRE ORT material has a much coarser and more non-uniform fabric structure compared to the CFRE LTL; this is demonstrated in Figure 61 which shows examples of full-field strains that develop in the GFRE ORT and CFRE LTL for both loading directions.

For the best measurements of shear strain using this test method, it is recommended that gauges cover as much of the distance between notches as possible. As shown here, DIC provides an easy method adjusting the shear strain coverage area. However, if DIC is not available it is possible to buy shear strain gauges of varying lengths.

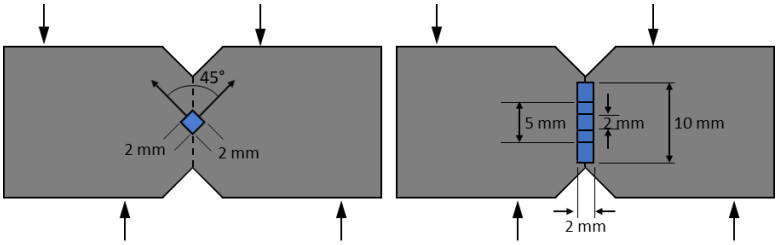

Figure 60. *Position and size of strain gauges used to measure average shear strain between the notches of a V-notch beam test specimen*

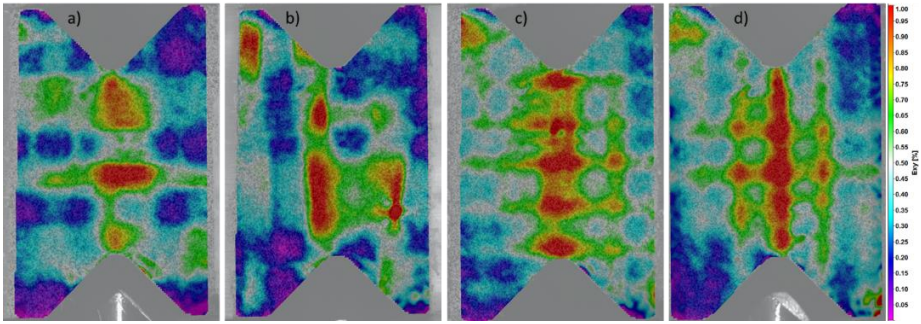

Figure 61. *Examples of full-field strain maps for V-notch beam specimens. a) GFRE ORT – weft-direction; b) GFRE ORT – warp-direction; c) CFRE LTL – weft-direction; d) CFRE LTL – warp-direction*

Table 24. *Shear modulus, $G_{(12/21)}$, measured using different size virtual strain gauges for the GFRE ORT and CFRE LTL materials tested using V-notch beam shear. Orientations, i.e. ±45° or 0°, indicate direction of the gauge relative to the loading direction. Measurements – mean ± std. dev. (CoV) of five test specimens*

Material	Loading direction	Gauge size (mm x mm)	Shear modulus, $G_{(12/21)}$ (GPa)
GFRE ORT	Warp (1-2)	2x2 (±45°)	2.88 ± 0.40 (14.0%)
		2x2 (0°)	2.72 ± 0.40 (14.8%)
		5x2 (0°)	2.84 ± 0.44 (15.7%)
		10x2 (0°)	2.91 ± 0.32 (10.8%)
	Weft (2-1)	2x2 (±45°)	3.16 ± 0.58 (18.4%)
		2x2 (0°)	3.19 ± 0.62 (19.5%)
		5x2 (0°)	3.11 ± 0.40 (12.8%)
		10x2 (0°)	3.00 ± 0.29 (9.7%)
CFRE LTL	Warp (1-2)	2x2 (±45°)	3.82 ± 0.26 (6.8%)
		2x2 (0°)	3.78 ± 0.27 (7.2%)
		5x2 (0°)	3.70 ± 0.13 (3.5%)
		10x2 (0°)	3.74 ± 0.14 (3.6%)
	Weft (2-1)	2x2 (±45°)	4.55 ± 0.34 (7.4%)
		2x2 (0°)	4.55 ± 0.41 (8.9%)
		5x2 (0°)	4.47 ± 0.12 (2.7%)
		10x2 (0°)	4.40 ± 0.11 (2.5%)

Table 25 shows the shear strength measured for both the GFRE ORT and CFRE LTL materials at 5% shear strain. ASTM D5379 recommends that shear strength is recorded at either peak load or the load at 5% shear strain, whichever is lower. For some toughened materials, where failure ultimately occurs via a mixed mode, the 5% shear strain condition is used to avoid reporting shear strength values which are not representative of the material. In the GFRE ORT and CFRE LTL materials used here, the z-binders enable continued loading well past 5% shear strain. The measurements of the shear strength at 5% shear strain have low scatter, indicating good repeatability and representation of the bulk using this test method.

In the GFRE ORT material, damage generally appears to initiate as an angled crack along one edge of a V-notch, which is considered unacceptable by ASTM D5379. This damage mechanism tends to develop prior to reaching 5% shear strain While acceptable damage in the form of angled cracking develops during continued loading, the formation of an angle crack invalidates the test with regards to strength measurements. Figure 62 highlights some of the damage that has developed in both materials once peak load is reached. Similarly, angled cracks along the edge of a V-notch develop in the CFRE LTL material, however this is not the initial damage that develops and forms well after reaching 5% shear strain. In this material, angled cracking develops between the notches for the weft direction and vertical cracking develops in the warp-direction, as shown in Figure 62. While the measurement of shear strength has very little scatter, the development of damage in these materials, especially the GFRE ORT material, suggests that this method may not be acceptable for measuring the shear strength for these materials.

Table 25. *Shear strength measured at 5% shear strain for both the GFRE ORT and CFRE LTL materials tested using the V-notch beam method. Measurements provided as mean ± std. dev. (CoV) of five test specimens*

Material	Loading direction	Shear strength, $\tau_{(12/21)}$ (MPa)
GFRE Ort	Warp (1-2)	61.31 ± 1.06 (1.7%)
	Weft (2-1)	59.64 ± 1.85 (3.1%)
CFRE LTL	Warp (1-2)	61.17 ± 0.58 (1.0%)
	Weft (2-1)	61.86 ± 1.26 (2.0%)

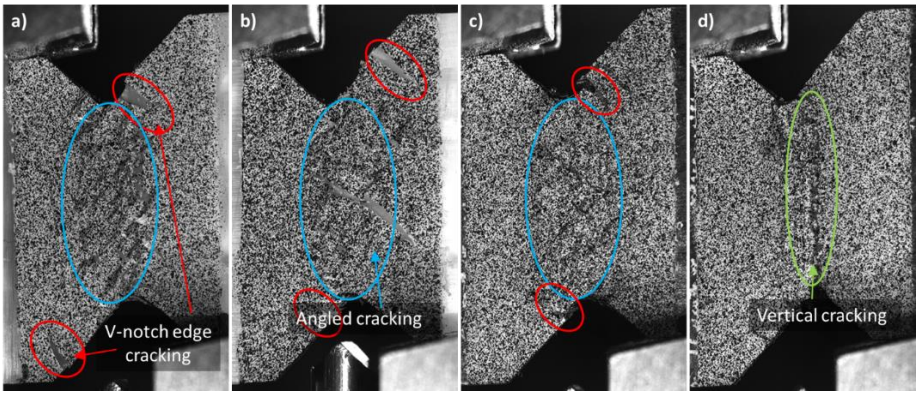

Figure 62. *V-notch beam test specimen damage near to peak load. a) GFRE ORT – weft-direction; b) GFRE ORT – warp-direction; c) CFRE LTL– weft-direction; d) CFRE LTL – warp-direction*

The shear properties shown here suggest that this method may be applicable for measuring shear modulus but not shear strength. For shear modulus the format and size of the unit cell will influence the degree of scatter but generally produce a reasonable representation of the shear modulus regardless of virtual gauge size. However, minimising the scatter is still recommended and therefore shear strain should be measured over as much of the distance between the notches as possible. Conversely, this method is not applicable for measuring shear strength despite the low scatter seen here. Unacceptable failure modes are generally found to develop prior to reaching 5% shear strain, invalidating the strength measurements.

Recommendation 3: When using V-notch test methods, take measurements of the shear strain over as much of the distance between the notches as possible to minimise the scatter as much as possible. Note, the region of pure shear across the notches is narrow. Measurements are best taken using DIC as the full-field measurements will help determine the best coverage for representation of the bulk material.

[Additional] Do not purposefully machine the V-notches at the same position within the structure of a material. This will artificially reduce the measurement scatter, at least with regards to shear strain, and therefore will not be a true representation of the bulk material.

V-notch rail shear (ASTM D7078)

Average shear strain was measured using a 2x2 mm virtual strain gauge orientated at ±45° to the loading direction, and five virtual shear gauges of sizes 2x2 mm, 5x2 mm, and 10x2 mm, 20x 2 mm and 30 x 2 mm, each orientated along the loading direction as indicated in Figure 63. Shear moduli were calculated for both materials and loading directions using the virtual strain gauge measurements and are shown in Table 26. In a study by Buchanan et al [116], it was shown that the V-notch rail shear specimens produced a much lower scatter in measurements than V-notch beam specimens for materials with large unit cell areas of 30 x 50 mm. For the work presented in this Guide, this has not been shown to be the case for these particular materials. The measurement of the shear modulus produced either similar or greater levels of scatter, especially noticeable for the GFRE ORT warp-direction. While the average shear modulus for each material and loading direction remains comparable between both test methods, the overall scatter does not decrease as expected. This suggests that for the GFRE ORT and CFRE LTL materials tested, the V-notch beam or V-notch rail shear are equally as effective at measuring the shear modulus. Examples of the full-field strain for both materials and loading directions can be seen in Figure 64. Despite the increased distance between the notches, the overall shear profile is similar when comparing Figure 61 for V-notch beam to Figure 64 for V-notch rail shear.

It is possible that the scatter could reduce if the width of strain gauges were increased. However, since the shear stress state between the notches is narrow, an increase in the width of a strain gauge may not be considered representative of the real shear deformation of the material.

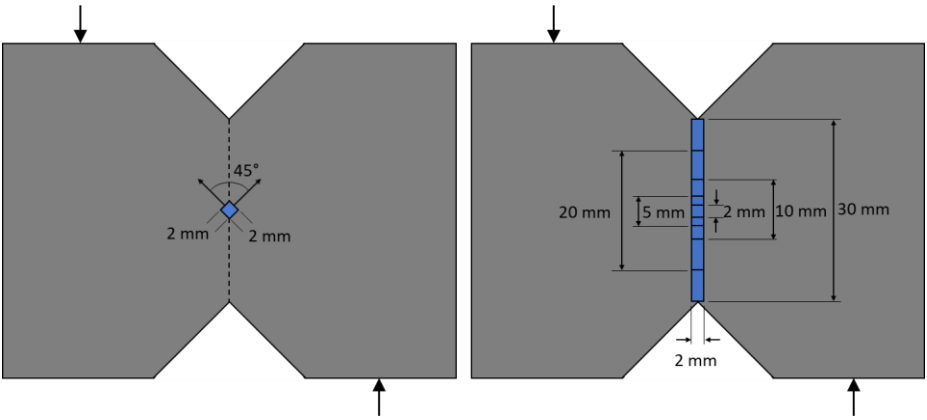

Figure 63. *Position and size of strain gauges used to measure average shear strain between the notches of a V-notch rail shear test specimen*

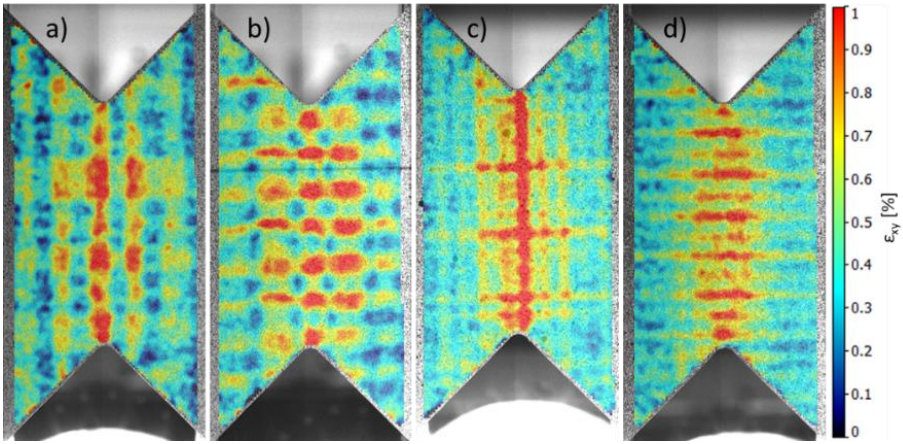

Figure 64. *Examples of full-field strain maps for V-notch rail shear specimens. a) GFRE ORT – warp-direction; b) GFRE ORT – weft-direction; c) CFRE LTL – weft-direction; d) CFRE LTL – warp-direction*

Table 26. *Shear modulus, $G_{(12/21)}$, measured using different size virtual strain gauges for the GFRE ORT and CFRE LTL materials tested using V-notch rail shear. Orientations, i.e. ±45° or 0°, indicate direction of the gauge relative to the loading direction. Measurements – mean ± std. dev. (CoV) of five test specimens*

Material	Loading direction	Gauge size (mm x mm)	Shear modulus, $G_{(12/21)}$ (GPa)
GFRE ORT	Warp (1-2)	2x2 (±45°)	2.92 ± 0.26 (8.7%)
		2x2 (0°)	2.98 ± 0.35 (11.8%)
		5x2 (0°)	3.08 ± 0.38 (12.3%)
		10x2 (0°)	3.07 ± 0.48 (15.6%)
		20x2 (0°)	3.02 ± 0.56 (18.5%)
		30x2 (0°)	2.86 ± 0.47 (16.3%)
	Weft (2-1)	2x2 (±45°)	3.08 ± 0.46 (14.9%)
		2x2 (0°)	3.05 ± 0.52 (16.9%)
		5x2 (0°)	3.24 ± 0.33 (10.2%)
		10x2 (0°)	3.25 ± 0.37 (11.4%)
		20x2 (0°)	3.19 ± 0.34 (10.8%)
		30x2 (0°)	3.02 ± 0.33 (10.9%)
CFRE LTL	Warp (1-2)	2x2 (±45°)	4.29 ± 0.24 (5.6%)
		2x2 (0°)	4.31 ± 0.25 (5.9%)
		5x2 (0°)	4.25 ± 0.27 (6.3%)
		10x2 (0°)	4.24 ± 0.26 (6.2%)
		20x2 (0°)	4.19 ± 0.24 (5.8%)
		30x2 (0°)	4.07 ± 0.22 (5.5%)
	Weft (2-1)	2x2 (±45°)	4.51 ± 0.28 (6.2%)
		2x2 (0°)	4.62 ± 0.25 (5.6%)
		5x2 (0°)	4.45 ± 0.14 (3.0%)
		10x2 (0°)	4.41 ± 0.16 (3.6%)
		20x2 (0°)	4.36 ± 0.18 (4.0%)
		30x2 (0°)	4.24 ± 0.15 (3.5%)

Table 27 shows the shear strength for both materials and loading directions measured at 5% shear strain. Loading using the V-notch rail shear method is very similar to the V-notch beam method, whereby loading continues well past 5% shear strain. Comparison between the

strengths for both test methods (Table 25andTable 27) show that the strength at 5% shear strain is the same. The main difference is the amount of scatter which, like the scatter for the shear modulus, tends to be similar or greater for the V-notch rail shear than the V-notch beam. Damage development is also comparable between both methods with the development of angled or vertical cracks in the gauge area between the notches. For the GFRE ORT material multiple angled cracks develop along the edge of the notches. In many cases this is the first apparent damage and initiates prior to reaching 5% shear strain. Angled cracks along the V-notches do not appear to develop in the CFRE LTL material, with damage restricted to around the gauge area between the notches.

Table 27. *Shear strength measured at 5% shear strain for both the GFRE ORT and CFRE LTL materials tested using the V-notch rail shear test method. Measurements – mean ± std. dev. (CoV) of five test specimens*

Material	Loading direction	Shear strength, $\tau_{(12/21)}$ (MPa)
GFRE Ort	Warp (1-2)	60.12 ± 3.15 (5.2%)
	Weft (2-1)	60.43 ± 4.6 (7.5%)
CFRE LTL	Warp (1-2)	59.56 ± 1.06 (1.8%)
	Weft (2-1)	59.18 ± 0.97 (1.6%)

The increased scatter seen for measurements made using the V-notch rail shear method is unexpected. Increasing the area across which measurements are made was expected to reduce the variability due to the increased representation of the bulk material. It is not clear why the scatter does not behave as expected but is likely related to the material structure. As shown by Qin et al. [114] (Figure 52), the position of the material structure relative to the V-notches will effect the measurement of the shear strain. It is possible that the structure of the material between the notches varies enough to produce scatter that cannot be minimised beyond a certain value when using this method due to the very narrow region of pure shear.

Recommendation 4: For V-notch testing, measurements of shear strength should be limited to those relating to 5% shear strain since 3D composites will continue to load well beyond this limit. However, caution should be taken as these values are not representative of the true shear strength. In addition, observe closely the damage development leading up to the 5% shear strain measurement to check for validity of the loading – angled cracking along the V-notches is not uncommon for these materials.

Short beam shear (ASTM D2344 and ISO 14130)

Table 28 shows a comparison of the average interlaminar shear strength (ILSS) measured for both the GFRE ORT and CFRE LTL materials when tested using the SBS methods of ASTM D2344 and ISO 14130. Differences in ILSS are to be expected when considering the relationship between the span length, shear stress and bending moments in flexural loading, but the difference in test spans used clearly produces minimal difference when testing at these specimen sizes. Additionally, the through-thickness reinforcement in these materials will influence the ILSS, by increasing the load required for interlaminar shear failure. However, the influence of through-thickness reinforcement on the ILSS of these materials is not easy to quantify.

Interestingly, ILSS measurements for the GFRE ORT material have a considerably larger scatter than for the CFRE LTL. For these materials, the size of the test specimens related to the size of their unit cells will provide some influence on the values measured. This is most noticeable for the GFRE ORT material, where the width of the ASTM test specimen does not even cover one unit cell. This suggests that loading of these test specimens does not produce a global measure of ILSS, thus increasing the measured scatter. For the CFRE LTL material, the superior regularity and uniformity of the material structure along with the larger test specimen dimensions enable a reduced measurement scatter.

Table 28. *Comparison of the ILSS for the GFRE ORT and CFRE LTL materials measured using the SBS test methods ASTM D2344 and ISO 14130. Measurements – mean ± std. dev. of five test specimens*

Test standard	Span (mm)	τ_{13} (MPa)	τ_{23} (MPa)
		Warp	Weft
GFRE ORT			
ISO 14130	15	41.28 ± 4.47 (10.8%)	46.30 ± 4.01 (8.6%)
ASTM D2344	12	50.04 ± 3.84 (7.7%)	47.89 ± 2.86 (6.0%)
CFRE LTL			
ISO 14130	25	36.54 ± 0.57 (1.6%)	37.57 ± 0.26 (0.7%)
ASTM D2344	20	38.81 ± 0.73 (1.9%)	39.14 ± 1.21 (3.1%)

For the measurement of ILSS, failure is only acceptable by interlaminar shear. Both tensile and compressive failures, with or without shear failure, are considered unacceptable. In the GFRE ORT material, regardless of the test specimen dimensions, failure always occurred via mixed mode tensile and shear, as indicated in Figure 65. Here, damage initiated as tensile cracking along the underside of the material prior to reaching peak load, with interlaminar shear failure

along warp/weft tow interfaces proceeding shortly after. The development of interlaminar shear failure appears to coincide with the locations of tensile cracks, suggesting these are acting to initiate shear failure in these materials. It is therefore unlikely that interlaminar shear failure could develop solely using this test method.

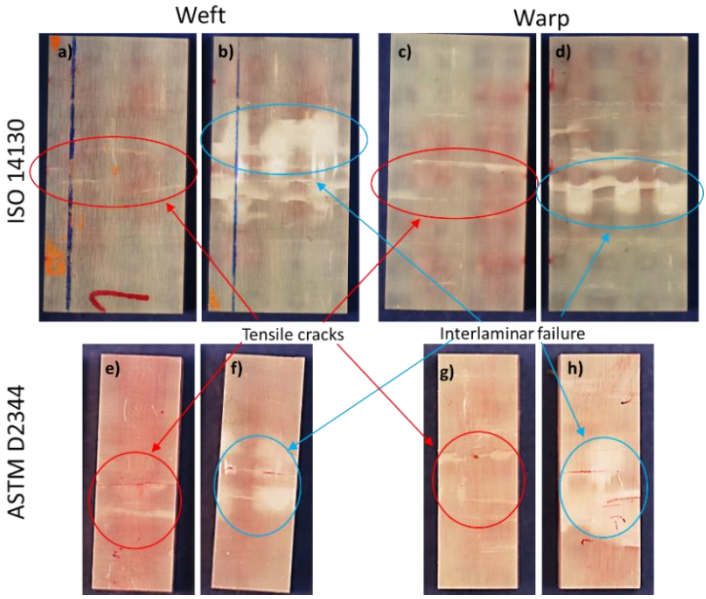

Figure 65. *Damage development in the GFRE ORT material during SBS loading. ISO 14130 – a) weft damage after first audible damage event; b) weft damage near peak load; c) warp damage after first audible damage event; d) warp damage near peak load. ASTM D2344 – e) weft damage after first audible damage event; f) weft damage near peak load; g) warp damage after first audible damage event; h) warp damage near peak load.*

For the CFRE LTL material, tensile failure was observed in all SBS test specimens regardless of dimensions used for testing, as indicated in Figure 66. Interlaminar shear failure is not as clear in the CFRE LTL material. From side profile micrographs (see Figure 67), the only shear damage observable appears to be shear splitting of transverse tows, with minimal interlaminar shear failure being observed. It is possible that some interlaminar shear failure has developed in this material, however it likely localised.

Recommendation 5: When testing 3D composites, avoid using any SBS test method for anything other than very simple qualitative analysis. The development of unacceptable failure modes is highly probable for 3D composite materials and therefore makes this test method unsuitable.

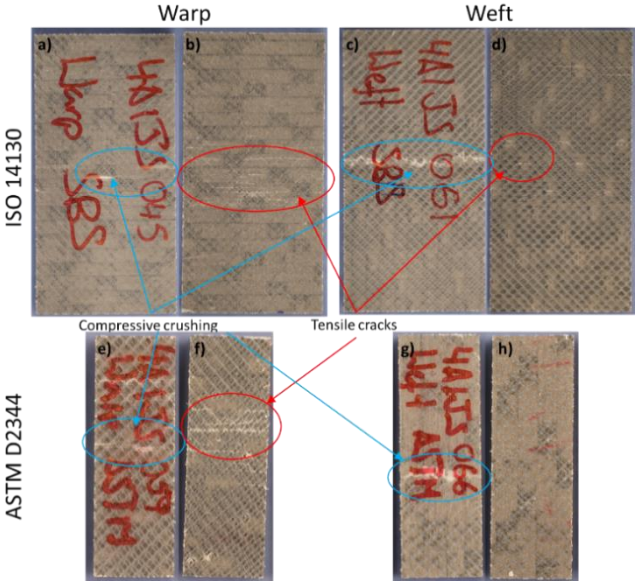

Figure 66*. Damage developed in the CFRE LTL woven material during SBS loading. ISO 14130 – a) warp damage top surface; b) warp damage bottom surface; c) weft damage top surface; d) weft damage bottom surface; ASTM D2344 – e) warp damage top surface; f) warp damage bottom surface; g) weft damage top surface; h) weft damage bottom surface;*

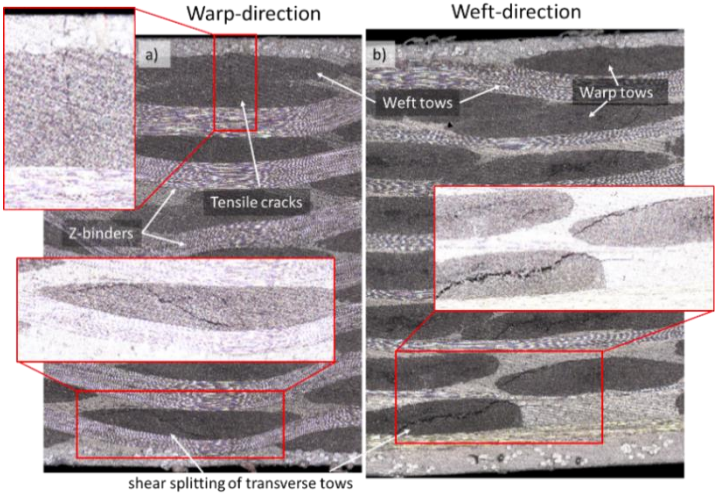

Figure 67. *Side profile micrograph showing damage in a CFRE LTL specimen loaded in SBS; a) warp-direction load; b) weft-direction loaded*

Plate Twist (ISO 15310)

Table 29 shows the in-plane shear modulus as measured using the plate twist method. For each material, two different size plates were tested to assess any influence on the measurement of shear modulus. It can be seen in Table 29 that for each material, the different plate sizes produce very similar modulus values and very low scatter. In fact, increasing the size of the plate does produce a slight reduction in the overall measured scatter. The similarities in measurements was expected as the size of the test specimens are very large, encompassing a large number of unit cells and therefore providing a strong representation of the bulk material. Compared to both V-notch beam, V-notch rail, and ±45° tension, the shear strain measured here is highly comparable. This indicates that not only is this method appropriate for the determination of the shear modulus, but that all three other methods can be used successfully.

Table 29. *In-plane shear modulus determined for both the GFRE ORT and CFRE LTL materials by plate twist. Measurements – mean ± std. dev. (CoV) of five test specimens*

Material	Plate dimensions (mm x mm)	Shear modulus, G_{12} (GPa)
GFRE Ort	105 x 105	3.07 ± 0.12 (3.9%)
	150 x 150	2.96 ± 0.10 (3.2%)
CFRE LTL	150 x 150	4.23 ± 0.15 (3.5%)
	175 x 175	4.22 ± 0.11 (2.7%)

Recommendation 6: If only shear modulus is required, plate twist is the simplest and most effective method to use. This method needs very little setup or specimen preparation and produces measurements comparable to other shear methods, with very little scatter. The only downside is the size of the specimens required is quite large.

Conclusions and recommendations

In this Chapter six test standards have been evaluated for their applicability in determining shear properties of 3D composites. Each standard uses a different method of introducing shear stresses into the material. Of these six test standards, four have been used for measuring in-plane shear properties and two have been used to measure interlaminar shear strength.

Measurements of the in-plane shear modulus were undertaken using the test methods ±45° tension (ISO 14129), V-notch beam (ASTM D5379), V-notch rail shear (ASTM D7078) and Plate Twist (ISO 15310). From these tests, the following general observations were made:

- All four test methods produced average shear modulus measurements of very similar values, but with varying degrees of repeatability,
- Repeatability of shear modulus measurements was best for the ±45° tension and plate twist methods for both materials,
- V-notch beam and V-notch rail shear produced very similar degrees of scatter between measurements, but this scatter was generally higher than for measurements made using both the ±45° tension and plate twist methods. Repeatability was better for the CFRE LTL regardless of loading direction which is more related to the uniformity of the material structure than the 3D woven fibre architecture.

Observations indicate that each of these methods appear suitable for determining the shear modulus of 3D composites. However, material uniformity and unit cell size should be considered when choosing which method to use. As such **it is recommended that the ±45° tension, V-notch beam, V-notch rail shear or plate twist test methods could be used to measure shear modulus depending on the user's preference**.

In-plane shear strength was measured using the ±45° tension (ISO 14129), V-notch beam (ASTM D5379), V-notch rail shear (ASTM D7078) test methods. For both materials, test specimens were loaded well beyond 5% shear strain due to the influence of the through-thickness reinforcement on loading. Since the 5% shear strain is an arbitrary test termination point, to minimise the influence of other loading modes on the measurement of the shear strength, the true shear strength cannot be obtained using any of these methods. In addition, despite good repeatability of shear strength at 5% shear strain for all three test methods, invalid failures, especially in the V-notch beam and V-notch rail shear test specimens, suggest that none of the tests are acceptable for measuring the shear strength. Therefore, **it is not recommended that the ±45° tension, V-notch beam, or V-notch rail shear test methods are used for measuring shear strength**. However, due to the good repeatability of measurements, these methods could be used for QA purposes. Further work is required to determine an acceptable method for measuring shear strength.

SBS test methods ASTM D2344 and ISO 14130 were used to assess the differences in material dimensions and test spans on the measurement of ILSS. Despite good repeatability of the ILSS values, both materials developed tensile cracking damage along the underside regardless of test method dimensions. This is considered an unacceptable failure mode and therefore not representative of ILSS. As such, **it is not recommended that either of the SBS test methods are used to measure ILSS**.

Chapter 6

Fracture Toughness

- Standard test methods for determining fracture toughness properties
- Fracture toughness testing of 3D composites in the literature
- Fracture toughness testing
- Conclusions and recommendations

Introduction

Traditional 2D composite materials are well known to have many desirable traits that can be utilised in component design, especially in the form of specific in-plane properties. However, the out-of-plane/ interlaminar properties are often much lower than the in-plane properties of these materials. Under loading conditions such as cyclic loading and impact, high interlaminar stresses can develop from material and/or structural discontinuities initiating delamination failure [117], which can induce failure. Examples of these discontinuities include, but are not limited to, a mismatch of properties between interfaces at free edges, out-of-plane bending, stress concentration at the tips of matrix cracks, ply-drops, and loading of bonded or bolted joints. The deformation of crack faces can be described using three fracture modes termed mode I, mode II and mode III. Mode I describes the parting of surfaces under tensile loads, while mode II and mode III occur through sliding shearing and tearing shearing motions, respectively [118]. It is generally observed that the development of various damage mechanisms, such as delamination, will occur as a combination of the three modes, though the proportion of each can vary greatly. Improving the interlaminar properties increases the resistance to fracture, or fracture toughness, which can ultimately improve the suitability of composite materials for use in various applications. Several suggestions for improving interlaminar properties have been suggested and studied, including toughened resins, interleafing, and through-thickness reinforcement [119]. In the present work, only studies related to through-thickness reinforcement will be discussed.

Standard test methods for determining fracture toughness

Although delamination initiation and propagation are typically a combination of modes I, II and III, it is common practice to characterise the fracture toughness of each mode individually and/or for mixed modes. Ideally, this is achieved using test methods designed to initiate and propagate a delamination via a single mode. In reality it is difficult to ensure pure loading in any of these modes. As such, it should be realised that measurements obtained during mode I, II, III or mixed mode loading are representative of an apparent fracture toughness rather than absolute.

Note 1: Fracture toughness is a measure of the energy loss required to increase the delamination front by a unit area of material. It is often discussed as the critical strain energy release rate, which is denoted with the symbol G_C and has the unit of Joules per square metre (J/m^2). Fracture toughness test standards determine the critical energy release rate required to initiate and propagate a delamination crack front.

There are currently several test standards available for determination of the fracture toughness of composite materials:

- Mode I ISO 15024 [120] and ASTM D5528 [121]
- Mode II ISO 15114 [122] and ASTM D7905 [123]
- Mixed mode I/II ASTM D6671 [124]

Note 2: There are currently no test standards for mode III.

Mode I

Mode I is often considered the easiest fracture toughness mode to characterise. The most common test method utilises a double cantilever beam (DCB) specimen to apply a tensile load to each surface at one end of the specimen that will initiate and propagate a delamination crack front. Here, a starter delamination is introduced along the mid-plane producing two beam arms that can be separated to enable delamination crack growth to occur as shown in Figure 68a. The starter delamination is produced by placing a thin (~13 µm) non-stick film at mid-thickness during laminate manufacture. The use of a thin film is to simulate the presence of a sharp crack and to limit changes in the material structure. Resin-rich regions can develop around thicker films that may produce unrepresentative initial fracture toughness values [53].

ISO 15124 and ASTM D5528 are very similar standards in that they both produce mode I loading using DCB specimens utilising the same dimensions, loading methods and data reduction techniques. Load can be introduced using either piano hinges or loading blocks like those shown in Figure 68b and c. Each of the data reduction techniques are energy based, such that the critical strain energy release rate for mode I loading, G_{IC}, is calculated. These are achieved either using beam theory or compliance calibration methods, the choice of which is made by the user. It should be realised that the data reduction techniques are based on linear elastic fracture mechanics and do not take into account fibre bridging, which can influence the measurement of fracture toughness.

Although many applications of composites require the use of multidirectional laminates, both test standards prescribe use with 0° unidirectional composite materials. ASTM D5528 infers that the method could be applied to other materials, lay-ups, and architectures; however, it should be realised that if crack branching occurs a pure mode I fracture may not be achieved. In addition, materials with high through-thickness strengths, such as many 3D composites, may fail in the loading arms rather than through the interlaminar mechanisms expected.

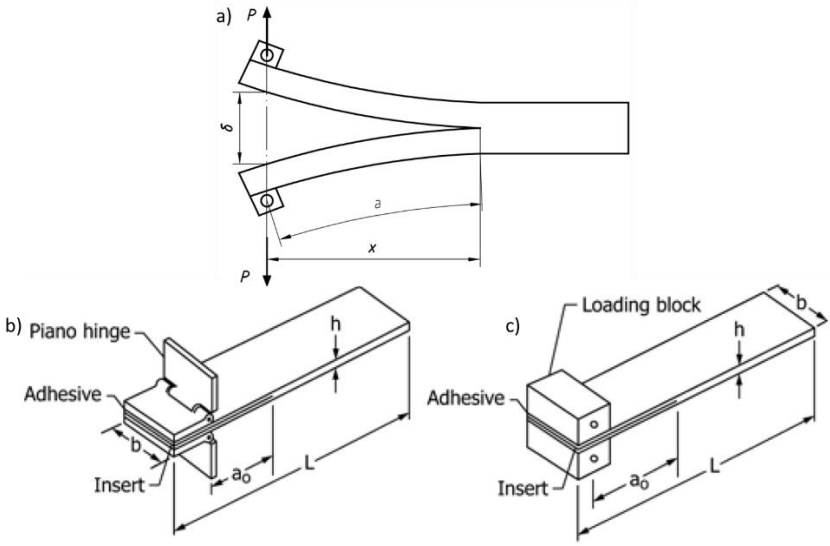

Figure 68. *Mode I DCB test specimens indicating a) the loading direction; and the different methods of loading allowed by both ISO 15024 and ASTM D5528, i.e. using b) piano hinges and c) loading blocks.*

Mode II

Mode II is a fracture mode that enables the propagation of a delamination crack front through shear sliding of two crack surfaces. Several mode II test methods have been proposed, including:

- End loaded split (ELS)
- End notched flexure (ENF)
- Stabilised end notched flexure (SENF)
- Four-point end notched flexure (4ENF)
- Centre notched flexure (CNF)

Of these methods only two have been standardised, ELS (ISO 15114) and ENF (ASTM D7905). Each of these methods produce mode II fracture via beam bending. As for mode I standards, both test methods are limited to use with unidirectional carbon and glass fibre-reinforced materials mostly due to limited experiences gained from interlaboratory comparison testing prior to standardisation. Use of these test standards for testing other fibres and lay-ups is not strictly prohibited, but care must be taken as mode II testing is sensitive to several factors such as the thickness of initial delamination, friction, geometric non-linearities and laminate stacking sequence [53].

Note 3: It should be recognised that measuring an accurate mode II crack length is difficult since there is no crack opening as per mode I. Magnification of the crack front region may reveal other forms of damage, making it harder to distinguish the location of the mode II crack front [126].

ISO 15114 – Fibre-reinforced plastic composites – Determination of the mode II fracture resistance for unidirectionally reinforced materials using the calibrated end-loaded split (C-ELS) test and an effect crack length approach

ISO 15114 is used to determine the mode II fracture toughness using the calibrated end-loaded split (C-ELS) test method. This test works on the principle of applying a cantilever point load to one end of a test specimen with an initial delamination crack located along its mid-plane (Figure 69a). Test specimens are produced using the same techniques as for mode I specimens, but only require one loading block to be bonded to specimens. Except for the specimen length, the recommended dimensions are also the same as for mode I test specimens. The length of the specimens must be such that one end can be sufficiently fixed (clamped) and adequate crack growth for analysis of the fracture toughness can be achieved. This test method produces stable crack growth so long as the ratio of the initial crack length, a, to distance from the load line to the clamp, L, is at least 0.55, i.e. $^{a}/_{L} \geq 0.55$ [53, 125].

As for mode I testing, the mode II fracture toughness, G_{IIC}, can be determined from measurement of the crack length using compliance or beam theory data reduction techniques. ISO 15114 also provides an option for calculating G_{IIC}without needing to visually measure the actual mode II crack length. This data reduction technique is known as the '*corrected beam theory using effective crack length (CBTE)*'. Here, an effective crack length is calculated using the measured compliance, flexural modulus and a clamp correction factor; the latter correcting for beam root deflections and rotations at both the crack tip and clamping point, as well as correcting for transverse shear effects in the composite arms. Both the flexural modulus and clamp correction factor are determined using an inverse ELS test that essentially 'calibrates' the clamping fixture and is achieved by applying a cantilever point load to the uncracked end of a mode II specimen prior to mode II loading [126].

ASTM D7905 – Determination of the Mode II Interlaminar Fracture Toughness of Unidirectional Fiber-Reinforced Polymer Matrix Composites

ASTM D7905 uses the end notch flexure (ENF) test method to determine mode II fracture toughness. This method works on the principle of applying a point load to the centre of a beam in a three-point bending arrangement, with an initial mid-plane delamination located at one end of the test specimen (Figure 69b). Stable crack growth during an ENF test is only possible if

$^{a}/_{L} > 0.7$, where a is the initial delamination crack length and L is the distance from the centre of one support span to the centre of loading [53, 125]. This ratio suggests that there is only a relatively small region of stable crack growth during ENF testing when compared to ELS testing, and this length is generally considered inadequate for producing a sufficient measure of the mode II fracture toughness. ASTM D7905 recommends that the ratio $^{a}/_{L}$ be approximately equal to 0.5 but makes it clear that this produces unstable crack growth. As such, only the fracture toughness initiation values can be obtained from both the initial delamination and a pre-crack. There is only one data reduction method available for determination of the mode II fracture toughness, G_{IIC}, and that is the compliance calibration method.

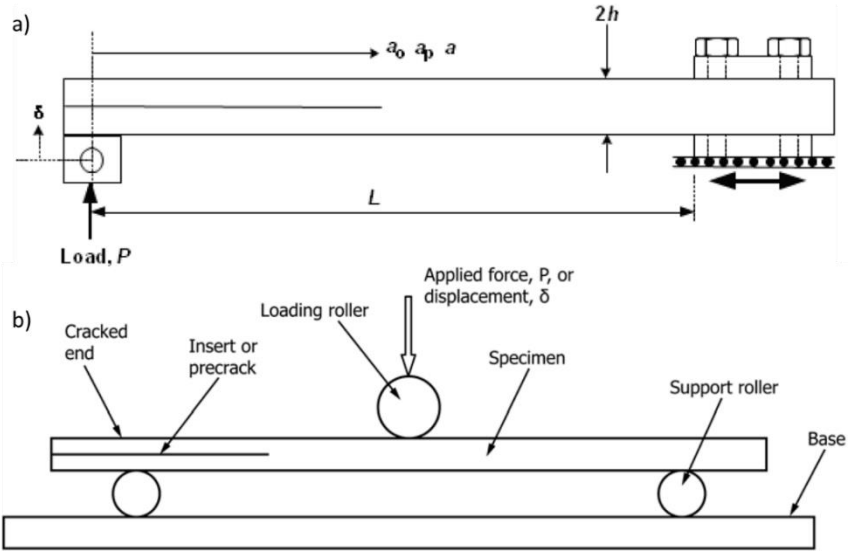

Figure 69. *Mode II loading and test setup for: a) ISO 15114 ELS [122] and; b) ASTM D7095 ENF [123]*

Fracture toughness testing of 3D composites in the literature

Given that the purpose of adding a through-thickness reinforcement to a composite preform is to improve damage tolerance and delamination resistance, it is useful to quantify its influence on interlaminar fracture toughness. Delamination resistance and fracture toughness of various 3D composites have been the subject of many studies. Many of these studies tend to use 3D woven preforms, though some have also tested composites including z-pins, tufts and stitches. The results of these investigations are discussed below and share many similarities that can be

used to provide a general overview of the performance of 3D composites with regards to delamination resistance.

Test standard limitations with 3D composites

A feature common to all fracture toughness testing discussed thus far is the requirement for an initial delamination, or starter defect, along the midplane of test specimens. This initial delamination is manufactured into composite panels specifically for the purpose of conducting fracture toughness testing. It is recommended that a non-adhesive film, typically a thin PTFE film approximately 13µm thick, is used. Once the laminate is cured, the PTFE film can be removed. This method is suitable for all layered composite materials though in the case of 3D composites slightly more preplanning is required. For z-pinned, tufted and stitched composites, the starting position of the through-thickness reinforcement can be chosen to allow a non-adhesive film to be placed along the midplane [6, 7, 24, 127]. For 3D woven composites, planning for this type of testing must be considered during the weaving stage. For a thin film insert to be used, the preform must be woven such that there is a length of material where the through-thickness reinforcement does not connect across the midplane [128]. If consideration for this type of testing is not made during weaving, it is not possible to use a film insert during laminate manufacture. It has been reported that the thickness of the starter defect influences the measurement of the fracture toughness initiation value, such that increasing the starter defect thickness increases the measured fracture toughness initiation value and the measurement scatter [129, 130]. In addition, the use of a thicker starter defects blunts the initial crack front, requiring more energy for a crack to initiate. Therefore, it is suggested that the starter defect should be as thin as possible. However, in cases where the use of film inserts are not possible, some studies have found success by cutting starter cracks along the midplane using saw blades [131, 132] (Figure 70). Unfortunately, the minimum thickness of the starter crack that can be achieved with this method is limited to that of the finest saw available. In [131], a starter crack of 0.4 mm thick was achieved using a saw, though it should be noted that this is over 30 times the recommended PTFE film thickness. Another option is to use diamond wire saws to produce the starter defect as these can be as thin as 0.13 mm, which is only 10 times the recommended film thickness. Caution should be taken when using either of these methods in order to minimise the production of any edge effects around the midplane cut. Edge effects can lead to the development of multiple crack fronts that do not follow the specimen midplane and thus have a mixed-mode failure front.

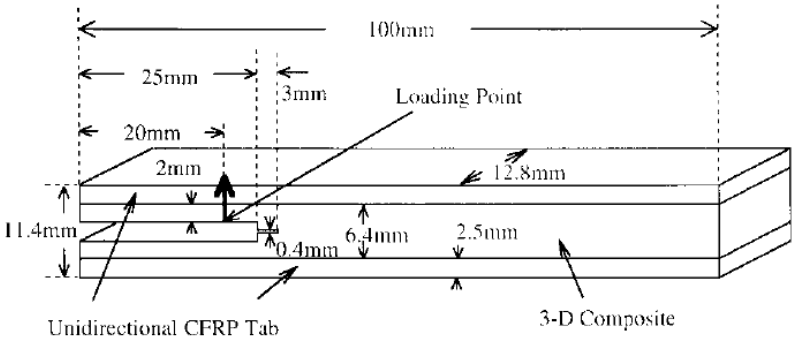

Figure 70. *Example of cut made for use as a start crack in 3D composites [131]*

Due to the improved through-thickness properties of 3D composites, premature failure of the specimens can either occur at the bond between the specimen and the loading blocks, or at the root of the starter defect through excessive bending of the loading arms. A common method to increase the potential for crack initiation and propagation, whilst also reducing the likelihood of the loading arms failing in flexure, is to attach reinforcing tabs along the entire length of the specimen. CFRP [128, 131], steel [132], and aluminium [133] reinforcement tabs have each been bonded to the surface of 3D composites to stiffen the arms and prevent failure by bending. In [133] the reinforcement and loading tabs were integrated to further reduce the potential for any bond-line failure during loading (Figure 71). In contrast, Tamuzs et al. [132] used a "comb tooth" device to apply a wedge force directly to the crack faces instead of pulling on the loading arms (see Figure 72).

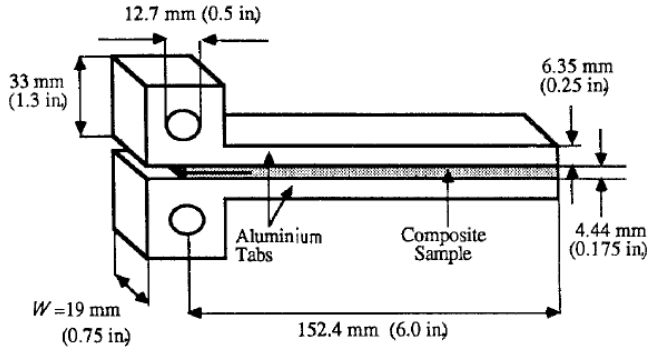

Figure 71. *Integrated reinforcement and loading tab [133]*

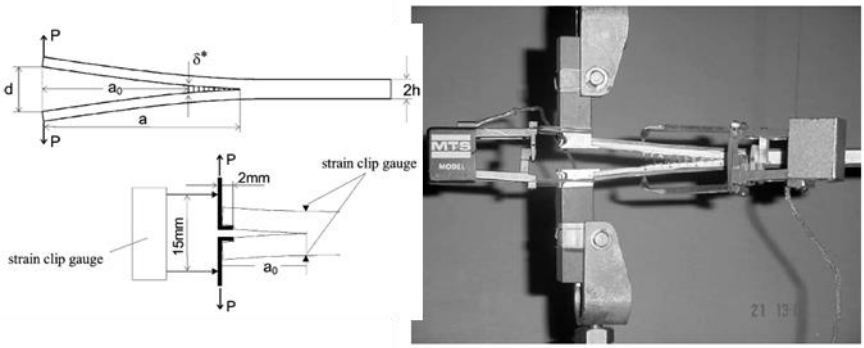

Figure 72. *Comb-tooth device used to produce mode I crack opening [132]*

In the published studies, the fracture toughness values reported were termed "apparent" with the authors noting the inadequacies associated with the analysis methods available. The analysis methods in each test standard ignore the effect of fibre bridging or treat it as a negligible effect. Although fibre bridging can occur during testing of unidirectional and 2D composites, its influence on the measurement of fracture toughness of 3D composites will be much larger due to the presence of the through-thickness reinforcement. Some studies, such as the work of Robinson and Das [134] have looked to modify data reduction methods used by test standards. In this case, modifications were proposed for the corrected beam theory (CBT) in ISO 15024 (or modified beam theory in ASTM D5528) by correcting for the development of large-scale bridging zones; here, bridging was due to the presence of z-pins. While modifications to these data reduction methods may help determine a closer representation of the fracture toughness in z-pinned [134] or tufted [18] composites, its effectiveness for use with other 3D composites is unknown and would require further study.

Note 4: The bridging effect in 3D composites occurs through stick-slip behaviour, observed as repeated loading and unloading cycles whilst the delamination crack front continues to grow [135]. The loading and unloading behaviour is the result of the crack front passing around the through-thickness reinforcements, which provides new interfaces for energy absorption thus hindering crack progression. Additional energy is required to initiate other damage mechanisms such as tow debonding and pull-out, crack branching, and fracture of the through-thickness reinforcement [133]. Since there is usually some amount of spacing between through-thickness reinforcements, a load drop and acceleration of the crack front is observed due to the lower load carrying ability of the unreinforced interface.

Variability in measuring fracture toughness values is influenced by numerous factors related to both the test specimen geometries and methods of load application (see previous section on

fracture toughness test standards). For 3D composites the through-thickness reinforcement provides an additional component to measurement variability. For instance, if a crack front initiates in a region with no through-thickness reinforcement, the initial fracture toughness will be low, increasing only when the crack front encounters regions with through-thickness reinforcement. Conversely, a crack front initiating adjacent to a through-thickness reinforcement will be much higher. As such, the potential scatter in initiation fracture toughness measurements will increase [128].

Fracture toughness testing

Test Methods

Mode I

Mode I fracture toughness tests were conducted using ISO 15024. Six mode I specimens were manufactured, each with nominal dimensions of 20 mm wide by 150 mm long (see Table 30). Half of the specimens were GFRE ORT and the other half were CFRE LTL. All specimens had the warp tows orientated along their length. This material direction was chosen to coincide with the direction of the z-binders.

Table 30. *Average dimensions of Mode I test specimens. Measurements provided as mean ± std. dev.*

Material	Length (mm)	Width (mm)	Thickness (mm)	Arm thickness* (mm)
GFRE ORT	150	19.99 ± 0.02	3.16 ± 0.02	≈ 6.68
CFRE LTL	150	20.01 ± 0.02	5.09 ± 0.03	≈ 7.64

*Arm thickness is one half of the specimen thickness and includes the thickness of the CFRE reinforcement tab used (5.1 mm)

Specimen preparation

Test specimens should be prepared following the guidance provided within ISO 15024. This includes the addition of a thin non-adhesive (PTFE) film insert and loading blocks. Since both the GFRE ORT and CFRE LTL materials used here were already in laminate form, the use of a thin PTFE film as a starter defect was not possible. For composite laminates the finest starter defect thickness achievable is approximately 0.13 mm using a diamond wire saw. This technique can be used to machine starter cracks to the required length, in this case a 60 mm long starter defect was required as per ISO 15024. Additionally, it is recommended that specimens are cut to size using a diamond saw.

Recommendation 1: In instances where a thin film cannot be used as a starter defect, such as for 3D woven fabrics or laminated composite panels, a diamond wire saw, or equivalent, should be used to produce the starter defect.

Due to the known difficulty in initiating and propagating a crack front during mode I loading of 3D composites, the bending stiffness of the loading arms for both materials was increased by applying tabs to each surface of the test specimens. Here, CFRE LTL material with the weft tows orientated along the length was chosen as tab material due to both its thickness (≈5.1 mm) and stiffness. Tabs can be attached to each surface of the test specimen using an appropriate adhesive such as 3M™ Scotch-Weld™ Structural Paste Adhesive EC-9323-2 B/A. To ensure that a good bond is achieved between the test specimen and the tabs, specimen and tab surfaces should be grit blasted.

Recommendation 2: To assist the initiation and development of the crack tip when conducting a fracture toughness test on 3D composites, increase the bending stiffness of each loading arm by attaching tabs. UD CFRP with a minimum thickness of 5 mm is preferred due to its orthotropy, though other composite material formats or metals (steel or aluminium) can be used.

Note 5: Increasing the starter defect thickness can lead to a measured increase in initiation fracture toughness due in part to blunting of the stress concentration at the tip of the front of the defect.

Note 6: Generally, during the manufacture of fracture toughness test specimens a thin PTFE film is placed between plies located either side of the midplane. Since 3D woven materials tend to have an uneven number of layers, with the number of weft layers being one greater than the number of warp layers, a warp or weft tow will sit across the midplane of the specimen.

The removal of through-thickness reinforcements can allow the insertion of a thin PTFE film. However, the film will have to be offset from the centre, i.e. placed between the central warp or weft tow layer and neighbouring weft or warp tow layer, as it is not possible to place the film through the centre of the central tow layer. Alternatively, the central tows could also be removed to allow the film to be placed along the midplane.

Caution: adjustments to the preform will likely affect the localised geometry and may lead to disturbances in the fibre architecture that extend past the length of the starter defect.

For load introduction, loading blocks (or piano hinges) can be used. These are attached to the end of test specimen with the starter defect. Loading blocks were used in this work and had a dimension of 20 x 20 x 20 mm, with an 8 mm diameter hole. The loading blocks should be grit blasted to aid the production of a good bond when attached to test specimens via the tabs.

Test setup

Testing was conducted on an Instron 4507 test frame with a 20 kN load cell. A crosshead displacement rate of 1 mm/min was used for all tests. The test setup is as shown in Figure 73 consisting of two pull rods, one attached to the load cell and the other fixed to the machine crosshead. It is recommended that alignment of the load line is checked prior to testing. This can be achieved by using a ground steel block of 20 x 20 mm cross-section with two clevis pin holes at either end. The alignment bar should have a similar length to that of the specimen thickness and loading blocks. Once suitable alignment is achieved, the locking rings on both pull rods should be tightened whilst the alignment bar is still attached to the pull rods.

Figure 73. *Mode I test setup*

Crack growth and length should be monitored using a suitable and appropriate means. Applying a matt white coating along the edges of the test specimen generally helps to enhance the visibility of the crack front during loading. To provide a scale for crack growth, self-adhering transparent rules with millimetre increments can be attached to the surface of the specimen.

These ruler measurements are generally lined up with the end of the starter defect and measure from -5 mm to +55 mm, with -5 mm to 0 mm being used to measure the pre-crack length.

Measurement of crack growth can be achieved using either a travelling microscope or camera with a magnifying lens on a travelling platform. Here, a 5MPx LaVision camera was used to capture images of crack growth during loading. A Navitar zoom lens was used to magnify the camera image so the crack tip could be more easily observed. In addition, the camera was attached to a tripod through a three-axis translation stage, so the position of the crack tip could be tracked. Images were captured at a rate of 1 Hz using the LaVision software DaVis 8.4, with each image containing timestamped load and crosshead displacement data from the Instron test machine.

The test procedure is split into two parts: initial loading and reloading. Initial loading is conducted to produce a pre-crack from the starter defect. Here, the specimen is loaded until a pre-crack length of 3 to 5 mm is achieved, upon which the test specimen is subsequently unloaded to the start position. Reloading is then undertaken until a crack length of 50 mm has been propagated from the pre-crack. While the standard suggests the load and displacement measurements should be taken every 1 to 5 mm of crack growth, image capture was used to obtain a higher number of data points and increase the resolution of crack growth measurements.

Data reduction techniques

The mode I interlaminar fracture toughness, G_{IC}, was calculated using the corrected beam theory (CBT) equation (Equation (28)). In this equation, P and δ refer to the load and crosshead/crack opening displacement, a is the total crack length, Δ is an effective crack extension to correction for arm rotation at the crack front, b is the specimen width, F is a large-displacement correction, and N is the load block correction.

$$G_{IC} = \frac{3P\delta}{2b(a + |\Delta|)} \times \frac{F}{N} \tag{28}$$

Mode II

Mode II testing was conducted using the calibrated end-loaded split (C-ELS) test method described in ISO 15114. Six mode II test specimens, three GFRE ORT and three CFRE LTL, were produced with nominal dimensions of 190 mm long by 20 mm wide, as shown in Table 31. Test specimens had the warp-direction orientated along their length.

Table 31. *Average dimensions of mode II test specimens. Measurements provided as mean ± std. dev.*

Material	Length (mm)	Width (mm)	Thickness (mm)	Arm thickness* (mm)
GFRE ORT	190	20.00 ± 0.03	3.08 ± 0.02	≈ 6.64
CFRE LTL	190	20.03 ± 0.04	5.11 ± 0.03	≈ 7.65

*Arm thickness is one half of the specimen thickness and includes the thickness of the CFRE reinforcement tab used (5.1 mm)

Specimen preparation

Specimen preparation techniques used for mode II test specimens are the same as for mode I test specimens. Therefore, for further details on recommended preparation methods, see the specimen preparation for mode I test specimens. For the load block configuration needed during mode II testing using ISO 15114, see the test setup section below.

Test setup

Testing was conducted on an Instron 4507 test machine using a 20kN load cell and the test fixture shown in Figure 74. The test fixture consists of a pull-rod fixed to the load cell and a base attached to the crosshead. The base has a clamping fixture for the test specimen in place but can slide to the required position relative to the pull-rod. For the C-ELS test method described in ISO 15114 there are three stages to testing: clamp calibration, pre-cracking, and re-loading.

Note 7: Test specimens should be clamped within the test fixture in a repeatable and reproduceable manner. One means to achieve this is by using a torque wrench to tighten all the bolts on the clamping fixture to the same torque. The chosen level of torque applied can depend on the test fixture used. ISO 15114 suggests that a bolt torque of 8 Nm is sufficient for clamping CFRP composites. For the test fixture used in this work (Figure 74), a torque of 4 Nm on each bolt was found to be adequate regardless of fibre reinforcement.

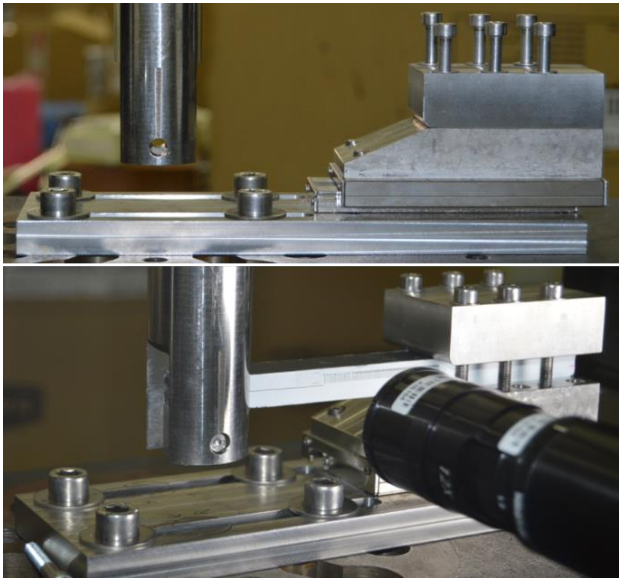

Figure 74. *Mode II End-loaded split test setup – ISO 15114*

Stage 1: Clamp calibration

This stage is used to determine the clamp correction factor and the flexural modulus of the test specimen. The correction factor accounts for the effects of beam root deflections and rotations at both the crack tip and clamping point, as well as transverse shear effects in the composite arms.

A single test specimen is loaded into the test fixture in an inverse ELS arrangement, i.e. the defect end is clamped in the fixture, while load is applied to the non-defect end. In this arrangement, a single loading block is attached to one side of the non-defect end and load is applied via the pull arm in an upward direction. Tests should be conducted at multiple free lengths, each loaded to the same load level. Only the load and crosshead displacement need to be recorded. In this work, free lengths of 110, 100, 90, 80 and 75 mm were used, with loading conducted at a rate of 1 mm/min until a load of 500 N was reached.

Note 8: During the clamp calibration stage it is noted that a load of 250 N should be applied to carbon fibre composites and 150 N to glass fibre composites. However, these values are prescribed for unidirectional composites with the recommended specimen dimensions. For other formats and non-standard test specimen dimensions, the loading can be adjusted as necessary.

Note 9: The free length is the distance between the load line, which is located through the centre of the loading pin, and the front edge of the clamping fixture

Stage 2 – Pre-cracking

This can be performed either by mode I or mode II loading at a rate of 1 mm/min until a pre-crack length of 3 to 5 mm is achieved. If mode I pre-cracking is used, then ISO 15114 suggests loading should be undertaken following the procedure outlined in ISO 15024. For pre-cracking using mode II it is recommended that a short free length is used in order to ensure stable crack growth is achieved; ISO 15114 suggests a free length equal to $^4/_3$ the length of the starter defect. In this work, mode I loading was chosen to produce the pre-crack due to limitations of the available mode II test fixture in achieving the required free length for mode II pre-cracking.

The number of loading blocks required will depend on the chosen pre-cracking mode; two blocks are used in mode I loading, while only one is needed for mode II. In both cases the loading block/s should be bonded to the defect end of the test specimen. If pre-cracking was performed in mode I, then one of the loading blocks should be removed prior to stage 3.

Stage 3 – Reloading

This stage is undertaken to determine the mode II fracture toughness during propagation of the crack front. Loading is performed in much the same way as stage 2, though the free length is set such that $^a/_L > 0.55$ and the rate of loading is reduced to 0.5 mm/min. The crack length is recorded until it is approximately 10 mm from the clamping fixture, upon which the test is terminated and the specimen is unloaded.

Note 10: The use of a slower test speed during stage 3 will enable crack growth to be monitored and recorded more effectively.

For stages 2 and 3, crack growth can be monitored using a travelling microscope or a camera system. In this work a camera was used as described in the mode I method section previously.

Data reduction techniques

ISO 15114 provides three methods for calculating the mode II fracture toughness, G_{IIC}: experimental compliance method (ECM), simple beam theory (SBT), and corrected beam theory using effective crack length (CBTE). Both ECM and SBT rely on a visual measurement of the crack length during loading, whereas CBTE uses an effective crack length calculated using the flexural modulus and clamp correction factor determined during clamp calibration loading. The G_{IIC} equations for each method are shown below in equations (29)-(31). In this work, all three methods were used for comparison.

ECM		SBT		CBTE	
$G_{IIC} = \frac{3P^2a^2m}{2b}$	(29)	$G_{IIC} = \frac{9P^2a^2}{4b^2h^3E_1}$	(30)	$G_{IIC} = \frac{9P^2{a_e}^2}{4b^2h^3E_1}$	(31)

Results and analysis

Mode I

Initial loading

Figure 75 shows the mode I load-displacement traces for both the GFRE ORT and CFRE LTL materials during initial loading. The loading responses are reasonably linear up to the point where the test was stopped. During this loading stage both materials reached a pre-crack length of approximately 5 mm. For both the GFRE ORT and CFRE LTL materials, pre-cracking was observed to initiate from the starter defect at approximately 150 N.

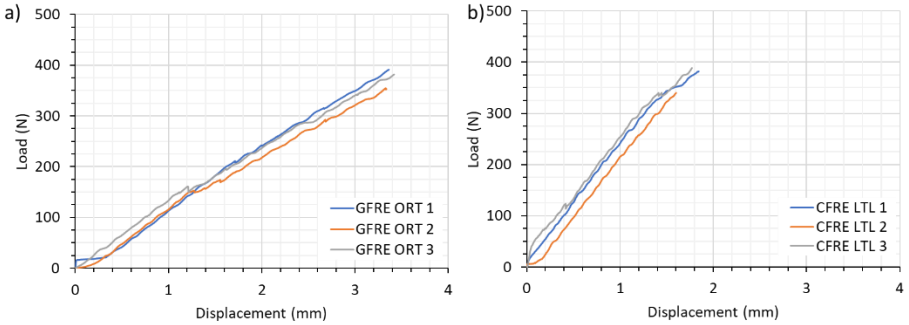

Figure 75. *Load-displacement graphs of mode I pre-cracking: a) GFRE ORT; b) CFRE LTL*

For both the GFRE ORT and CFRE LTL materials pre-cracks were observed to initiate as a single crack from the end of the starter defect. Development of the crack front depends on the material structure as indicated by the appearance of the cracks in Figure 76a and b . In Figure 76b there is clear crack branching, while no branching can be seen in Figure 76a. In Figure 76b, the crack branching observed is related to the presence of z-binders.

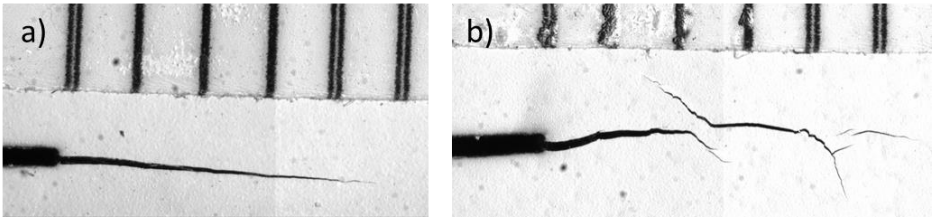

Figure 76. *Pre-crack examples during Mode I loading of two test specimens*

Reloading

The load-displacement response for both the GFRE ORT and CFRE LTL materials during the reloading stage are shown in Figure 77. In both cases, loading is initially linear but soon becomes highly nonlinear whereby multiple load drops and increases were observed. The initial nonlinearity is indicative of the early growth of the crack front from the pre-crack, whereas the load drops and increases suggest the presence of interference to the development of the crack front via stick-slip behaviour. Interference tends to appear in forms that will impede the growth of the crack front, such as fibre bridging and crack branching.

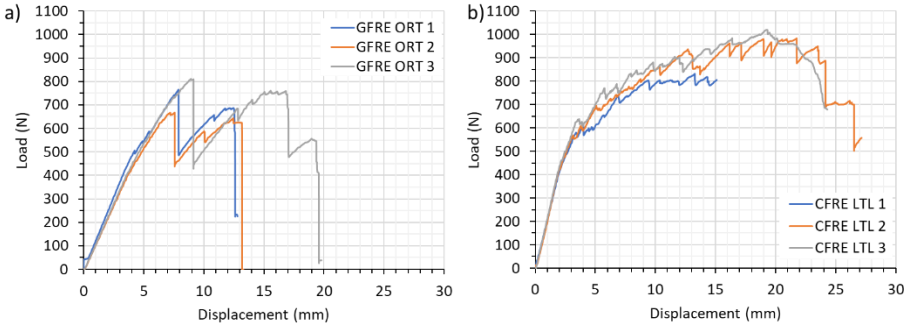

Figure 77. *Load-displacement graphs of mode I reloading: a) GFRE ORT; b) CFRE LTL*

For the GFRE ORT specimens, failure always occurred at, or near to the bond-line between the test specimen and the reinforcing tab and is responsible for the large initial load drop (Figure 77a). With the z-binder traversing the entire thickness of the material, it bridges the crack plane providing a path to the surface of the material which the crack can follow. This route is more favourable than the development of the crack front through the initial crack plane. An example of a GFRE ORT specimen failing near the bond-line can be seen in Figure 78. In this specimen, the resin layer at the surface of the specimen was torn from the fibres. Failures in this manner are invalid and it was not possible to produce a measure of G_{IC} – this will be discussed in more detail later.

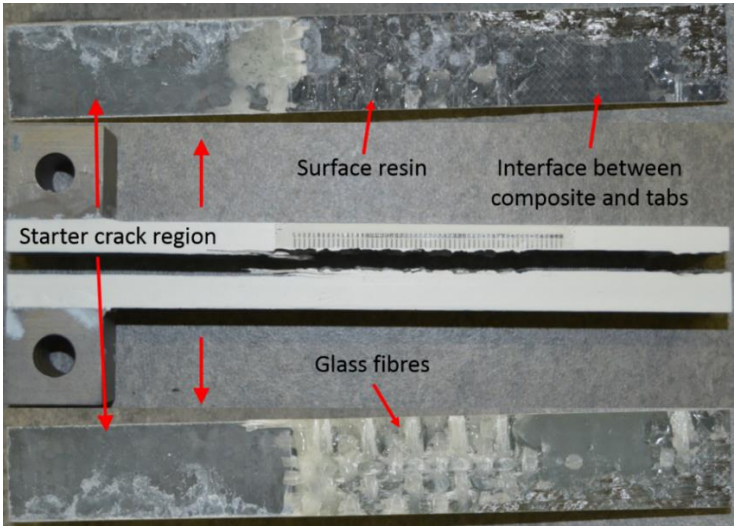

Figure 78. *Image of the failure surfaces of a Mode I loaded GFRE ORT specimen*

For all the CFRE LTL specimens, crack initiation and propagation occurred entirely within the material as intended. However, crack branching and fibre bridging around the midplane of the specimen were prevalent during loading. As for the GFRE ORT material, the z-binders in the CFRE LTL provide a path for the crack front to branch into multiple planes. As shown in Figure 79a, multiple cracks developed along the length of the material, following the various tow profiles. Due to the short through-thickness travel of the z-binder in the LTL structure, crack branching became restricted to only a few planes around the midplane of the material. In addition to crack branching, there was significant fibre bridging across the crack plane (Figure 80). Typically, fibre bridging in 3D composites is due to the through-thickness reinforcement, however in this LTL structure weft tows bridge the crack plane. Crack branching allows the weft tows to separate themselves from the surrounding material but are pinned against each crack surface by a z-binder which leads to bridging of the crack plane.

Clearly crack growth in 3D composites is complex and depends on the through-thickness reinforcement architecture, with the work shown in this Guide indicating that propagation is much more readily achievable in the CFRE LTL compared to the GFRE ORT. This influence of through-thickness reinforcement architecture has also been observed in the literature [128, 135], with other factors such as the size, spacing and total volume content of through-thickness reinforcement affecting the measured fracture toughness [6, 7, 18, 20, 21].

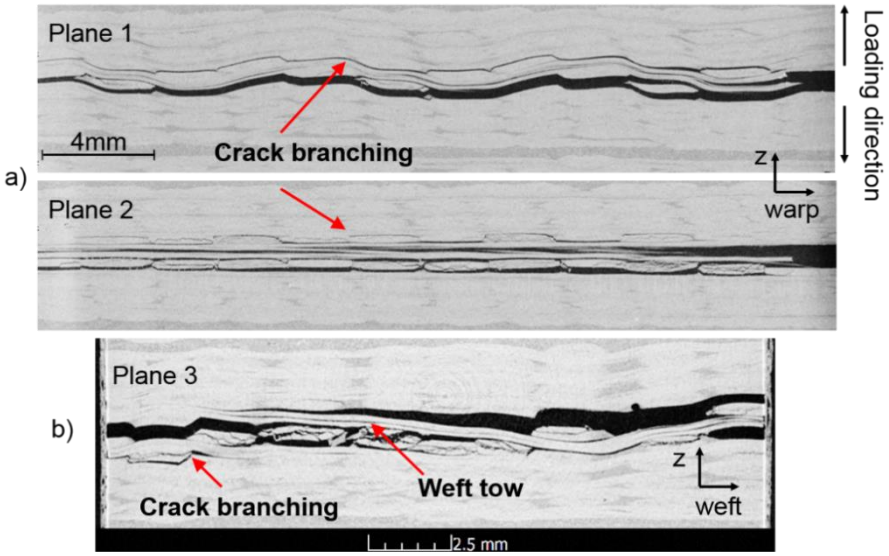

Figure 79. *XCT images of a Mode I loaded CFRE LTL specimen showing examples of: a) crack branching along the loading direction; b) crack branching and fibre bridging across the specimen width*

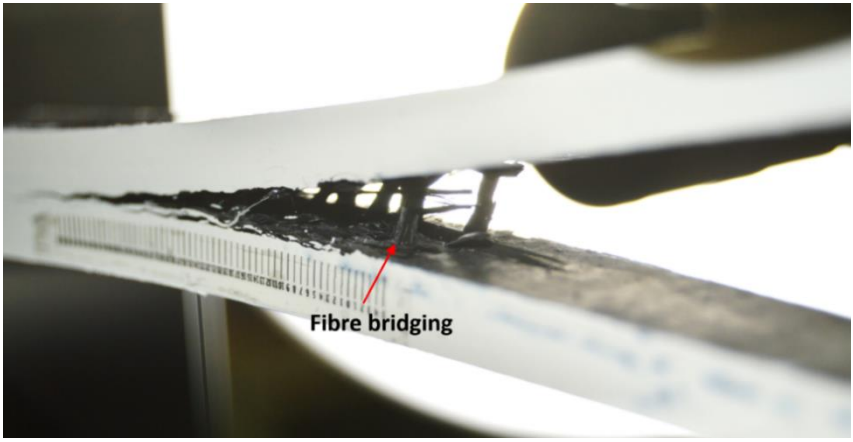

Figure 80. *Image taken during Mode I loading of a CFRE LTL specimen showing the large scale fibre bridging that develops.*

Measurement of mode I fracture toughness, G_{IC}

Due to the complexity of the loading and crack development in both the GFRE ORT and CFRE LTL it is difficult to measure an effective crack length that can be used to calculate G_{IC}. While the

data reduction techniques in ISO 15024 could be used to determined G_{IC} for crack initiation, they would not be suitable for measuring propagation G_{IC}. In the case of the GFRE ORT material, the failure mode was invalid making any measurement of G_{IC} other than initiation impossible. For the CFRE LTL, large-scale fibre bridging and crack branching occurred, which is not taken into account in any of the data reduction techniques. In addition, crack branching makes it difficult to produce an accurate measure of the crack length.

Table 32 shows the initiation G_{IC} values measured from the starter defect and calculated using the CBT method and determined using three different criteria as recommended in ISO 15024: visual observation of crack growth (VIS), the point at which the load-displacement response becomes nonlinear (NL), and at a 5% deviation in compliance (5%/MAX). For the GFRE ORT, all three measurements are very similar, whereas there is a much greater variation for the CFRE LTL. ISO 15024 suggests the NL value is usually the most conservative measurement of the initiation G_{IC}, however, for both the GFRE ORT and the CFRE LTL the VIS point is lowest. This is likely due to the image capture allowing for crack initiation to be observed earlier than live visual crack measurement allows. The initiation values for both materials are low, likely in the order of the matrix, suggesting that there is no through-thickness reinforcement present ahead of the starter defect. Despite the similarity in load required for crack initiation between both materials, the G_{IC} of the CFRE LTL from visual observation is much lower than the GFRE ORT due to the difference in flexural stiffness between each material.

Table 32. *Crack initiation values as measured from using the nonlinear (NL), visual (VIS), and 5% loss in compliance (5%/MAX) criteria suggested in ISO 15025*

		Crack length, a	Load, P	Displacement, δ	Fracture Toughness, G_{IC}
		mm	N	mm	J/m²
GFRE ORT					
Starter defect	NL	51.9 ± 0.2	166.7 ± 31.6	1.3 ± 0.3	268.8 ± 160.5
	VIS	50.4 ± 0.2	159.7 ± 17.0	1.4 ± 0.3	223.8 ± 143.9
	5%/MAX	51.9 ± 1.1	184.0 ± 53.8	1.5 ± 0.5	256.1 ± 129.1
CFRE LTL					
Starter defect	NL	57.2 ± 1.8	293.3 ± 30.6	1.3 ± 0.1	267.4 ± 53.9
	VIS	53.7 ± 2.6	143.9 ± 72.6	0.7 ± 0.2	80.4 ± 63.6
	5%/MAX	57.1 ± 1.5	337.9 ± 4.5	1.54 ± 0.1	390.9 ± 41.4

Although modifications to mode I data reduction methods have been proposed to include the influence of fibre bridging [134], they rely on the development of a single crack front along the midplane of the material. This may be easier to achieve in stitched, tufted, or z-pinned composites, but will be more difficult for 3D woven composites. It is possible to use the current methods to produce an approximate measure of G_{IC} for qualitative measurement purposes only, but this would still require the development of a single crack plane and therefore may not be easily achievable in all 3D composites. Further studies would be required to determine an acceptable data reduction method for use with 3D composites of all forms.

Recommendation 3: When testing 3D composites, do not use either of the current Mode I test standards (ASTM D5528 and ISO 15024) if any form of quantitative fracture toughness measurements are required. Testing using these methods should be limited to qualitative analyses since loading is not pure Mode I and the data reduction techniques are not adequate for these types of materials. Any data collected should be labelled as 'apparent' mode I fracture toughness.

Mode II

Pre-cracking

Figure 81a shows the mode I pre-cracking load-displacement response for both the GFRE ORT and CFRE LTL materials. As expected, loading is linear, following the same trend as observed previously. Propagation of damage during pre-cracking was also similar, with the development of multiple crack fronts developing.

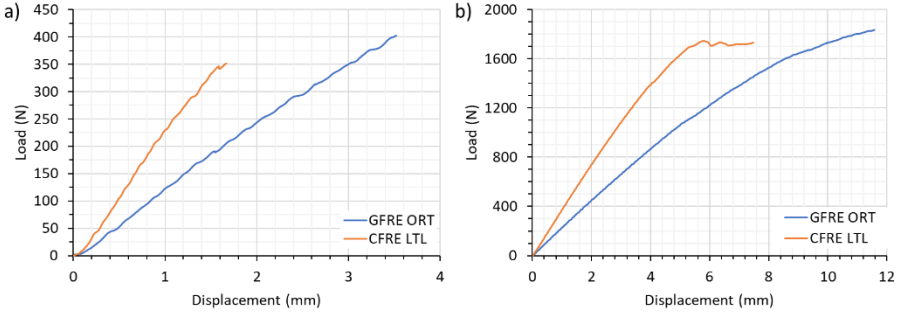

Figure 81. *Load displacement graphs for GFRE ORT and CFRE LTL materials when: a) pre-cracked under mode I, and b) reloaded under mode II loading*

Reloading

Figure 81b shows the mode II loading response for both the GFRE ORT and CFRE LTL materials. Both curves are initially linear with the GFRE ORT becoming gradually nonlinear while the CFRE LTL reaches a plateau. Crack growth in both materials was very different.

Despite the much larger crosshead displacement measurement, very little crack growth along the length of the specimen occurred during mode II loading of the GFRE ORT material, and failure occurred via flexure. Despite not growing along the length of the specimen, multiple cracks were observed to develop around the pre-crack, branching off in multiple directions and following material features. Failure in this manner is invalid and indicates the difficulty in propagating a crack front in this material architecture. Since mode II crack growth of similar architectures has been achieved in various studies [11, 18, 128, 136], it is likely crack growth can be achieved but further work would be required to determine the correct parameters.

In contrast, the CFRE LTL material more easily developed a crack front under mode II loading. Under these loading conditions very little crack branching occurred, and growth tended to follow stick-slip behaviour. The increasing load suggests the development of a bridging zone at, and behind, the crack front, whereas the flattening of the load indicates that the bridging zone is fully developed. A developed bridging zone is where the uptake of load by a section of z-binder crossing the crack front is proportional to the load lost by sections failing at the end of the bridging zone.

Measurement of mode II fracture toughness, G_{IIC}

As mentioned previously, ISO 15114 provides different methods for calculating G_{IIC}, including a method that does not require any crack length measurements to be made visually. Due to the invalid failure of the GFRE ORT material, none of these methods can be used to determine either initiation or propagation G_{IIC} and have not been included here.

For the CFRE LTL the crack propagation occurred more readily allowing for a crack length measurement to be made. However, while the crack extended along the length of the specimen, it tended to follow the profile of tows present at the edge of the specimen and therefore did not maintain a straight path. As such, the measurements of G_{IIC} shown here are based on an approximate crack length assumed to extend linearly along the specimen's length. Here, measurements of G_{IIC} were made using all three suggested methods, i.e. ECM, SBT, and CBTE, for comparison. The G_{IIC} initiation values vary depending on the data reduction method used, with measured values from ECM being the lowest and CBTE being the highest as can be seen in Figure 82. In addition, despite the increasing G_{IIC} trend, both the ECM and SBT data reduction methods produce vastly different measurements of G_{IIC}. Interestingly, the CBTE method initially produces a different G_{IIC} propagation trend, but after 10 mm of effective crack growth becomes almost identical to measurements made using the SBT method.

Recommendation 4: Mode II testing using ISO 15114 is not suitable for quantitative fracture toughness measurements of 3D composites since the data reduction techniques do not take into account the effects of crack branching or deviation from linearity. However, this test method could be used qualitatively but measurements should be labelled as 'apparent' mode II fracture toughness

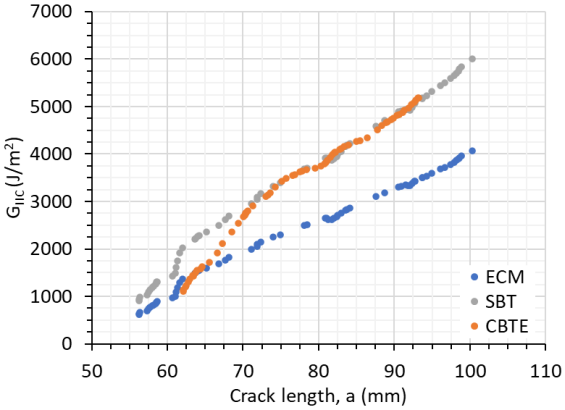

Figure 82. *Graph showing measurements of G_{IIC} plotted against crack length for the CFRE LTL material.*

Conclusions and recommendations

In this chapter fracture toughness testing was conducted according to ISO 15024 for mode I and ISO 15114 for mode II. Due to the presence of a through-thickness reinforcement in 3D composites, it can be difficult to initiate and propagate a crack front. This often leads to flexural failure of the specimen arms rather than crack propagation. However, by increasing the flexural stiffness of the beam arms it is possible to induce crack initiation and propagation. From the work presented here and literature studies, it is recommended that tabs should be applied to the specimen arms. While various materials have been used in the literature, CFRP with a thickness of at least 5 mm should be sufficient. Although UD CFRP is preferred due to its high orthotropy, other formats can be used as was the case in the work present in this GPG. It is worth noting that beam arm stiffening is not guaranteed to enable crack propagation as it is highly dependent on the 3D composite structure being tested.

While the use of a thin film insert is recommended to act as a starter defect, it is not always possible depending on the material format and its supply for testing. One recommended alternative is to use a thin diamond wire saw to produce the starter defect. This was used

successfully in the work presented here to initiate delamination cracks. Currently the thinnest diamond wire available is 0.13 mm in diameter.

The following observations were made during both mode I and mode II loading:

- GFRE ORT: Successfully initiated crack growth in mode I but unsuccessful propagation of the crack front in either mode I or mode II. In both cases crack branching near the pre-crack lead to eventual failure,

  For mode I, failure occurred at the bond-line between the reinforcement tab and the material as a result of crack branching to the surface via the z-binder,

  In mode II, the beam arm failed in flexure with almost no propagation of the mode II crack front. In addition, significant crack branching occurred around the pre-crack region.

- CFRE LTL: Successfully initiated and propagated a crack front in both mode I and mode II loading. In both cases, loading occurred following the typical stick-slip behaviour observed in other 3D composite studies as a result of the through-thickness reinforcement hindering crack growth.

  Under mode I loading, large-scale crack branching and fibre bridging were observed. Crack branching occurs readily due to the z-binder providing a path to other tow layers. In addition, the crack plane was generally not straight and tended to follow tow profiles. The combination of non-straight crack growth and crack branching makes it difficult to measure the crack length effectively.

  In mode II loading, only minor crack branching was observed. It is difficult to observe the extent of crack branching and any influence of fibre bridging during mode II loading. However, the flattening of the loading response indicates that a fully developed bridging zone formed.

The data reduction techniques suggested within both ISO 15024 and 15114 are based on linear elastic fracture mechanics. Neither of these takes into account the influence of large-scale fibre bridging or crack branching. Studies in the literature have attempted to modify these data reduction techniques, focussing on the bridging effect for z-pinned, tufted, and stitched composites since these materials tend to develop a single crack plane. These would need to be studied further, along with round-robin testing to determine their applicability to all 3D

composites. Based on the current work undertaken, the mode I or mode II data reduction techniques are not recommended for use on materials that produce large-scale crack branching or fibre bridging. However, should a single crack plane develop it may be possible to use these to produce a qualitative fracture toughness measurement, ignoring the influence of fibre bridging.

Chapter 7

Impact and Post-Impact

- Standard test methods for impact and post-impact
- Impact and post-impact of 3D composites in the literature
- Post-impact testing: CAI
- Conclusions and recommendations

Introduction

With the application of composite materials in a range of safety critical components, their ability to withstand and resist the development of damage becomes increasingly important. Understanding the damage tolerance of a composite format is critical to ensuring its safe usage during its operational life.

Many composite structures are subjected to a variety of different impact loadings, resulting in the development of damage within the material. While some impacts can produce obviously visible damage to a structure, others, such as accidental dropping of tools during maintenance procedures, can cause what is known as barely visible impact damage (BVID). Continued usage of a material with BVID can potentially lead to catastrophic failure of a component or structure if not monitored or left untreated.

Induced damage within a composite structure will lead to a reduction in the designed performance. While damage developed during standard loading conditions can somewhat be accounted for during the design stage, impact damage provides a level of unknown uncertainty with regards to the residual loading behaviour of a material. It is therefore useful to understand the effect of damage on the properties of a material or structure when subjected to various loading conditions.

Standard test methods for impact and post-impact

The effect of impact on the behaviour of a material that has been subjected to an impact load is variable and is influenced by many factors including:

- Laminate layup
- Specimen geometry
- Indenter geometry and mass
- Impact energy and force
- Damage type, size, and location
- Support or boundary conditions

Due to these influences, impact testing should be conducted to provide understanding of typical material behaviour under a set of defined conditions. There are test standards available for producing controlled levels of impact which, if required, can then be used to measure residual properties.

Impact

There are several test methods available for assessing the damage resistance of composite materials subjected to an impact event. Test standards ASTM D7136 [137] and ISO 6603 [138, 139] detail testing using drop-weight impact, while ASTM D6264 [140] uses quasi-static indentation to produce impact type damage. Drop-weight testing utilises gravity and a falling mass dropped from a predefined height to provide the intended energy of the impact strike. Conversely, quasi-static indentation allows an object to be pushed into a material at a chosen rate until a desired amount of damage is imparted or perforates both surfaces of the material. Although there is a suggested impact energy and size/shape of indenter, each standard recognises and allows user defined setups enabling flexible investigation of damage resistance. However, as stated previously, it must be realised that testing is highly dependent on several factors and thus direct comparison between different materials cannot easily be made even with similar setups.

For all test methods, specimens are placed over a cut-out in their respective test fixtures. ASTM D6264 prescribes a low test speed of 1.25 mm/min and therefore specimens do not need to be clamped down to the test fixture. In contrast, drop-weight testing requires specimens to be clamped to the fixture to avoid unintended movement of the specimen during impact. ASTM D7136 uses toggle clamps at four locations to hold the specimen in place, while ISO 6603 places the specimen between two plates, each with the same size cut-out.

Note 1: Real-life impact events typically consist of multiple strikes against an object due to rebounding of the impactor until all strike energy is absorbed. Unless multiple impacts are specifically required, drop-weight tests limit impact to a single strike by capturing the impactor when it rebounds off the material. This allows the damage developed upon impact to be more easily characterised.

Although in principal similar, there are a few differences noted between ASTM D7136 and ISO 6603:

- Specimen dimensions: ASTM D7136 – 150 mm x 100 mm and a thickness of 4-6 mm

  ISO 6603* – depends on material thickness

  (1) 60 mm square with a 2 mm thickness

  (2) 140 mm square with a 4 mm thickness

- Test fixture cut-out: ASTM D7136 – 125 mm x 75 mm

  ISO 6603 – depends on specimen dimensions

  (1) 40 mm diameter for specimen (1) above

  (2) 100 mm diameter for specimen (2) above

* the larger test specimen in ISO 6603 is generally recommended for use with fibre-reinforced composites, while the smaller size should be used for plastics.

ASTM D6264 uses specimen dimensions and a fixture cut-out similar to ISO 6603 but allows specimen thicknesses within the range suggested by ASTM D7136. Here, a test plate of 150 mm square and a cut-out of 125 mm diameter is recommended.

ISO 6603 is also split into two parts, with ISO 6603-1 using a non-instrumented drop-weight machine and ISO 6603-2 requiring instrumentation. In ISO 6603-1 only the energy based on the mass of the striker and height at which it is dropped is recorded, while ISO 6603-2 additionally records both the force throughout the duration of the test and deflection of the striker relative to test specimen. ISO 6603-2 is generally preferred if analysis of the force required to develop various failure modes is to be undertaken. ASTM D7136 also suggests using an instrumented test frame.

For many composite materials, especially those containing carbon-fibre, it is difficult to observe the damage that has developed post-impact. It is generally recommended that non-destructive evaluation (NDE), or testing (NDT), is performed on specimens to determine both the extent of damage, and the type of damage that has developed. The choice of NDE method is left to the user, though often ultrasonic C-scanning is preferred. However, not all NDE techniques are sensitive to the same damage modes and a combination of techniques may be required to properly characterise the damage state. For instance, C-scanning is not particularly sensitive to matrix cracking but can detect delamination damage, whereas micro X-ray Computed Tomography (μXCT) can see matrix cracks but can struggle to observe delamination damage depending on the image resolution.

Post-Impact: Compression-After-Impact

While it is useful to understand the damage that develops in a material during an impact strike, it is even more valuable to measure the associated knockdown in material properties under various loading conditions. Currently, the only post-impact test standards available are those which measure the residual compressive properties of specimens. The test method is known as compression-after-impact (CAI) and test procedures are detailed in both ASTM D7137 [141] and ISO 18352 [142].

ASTM D7137 focusses on the compression testing of impacted specimens, with ASTM D6264 or D7136 focusing on the impact resistance. In contrast, ISO 18352 covers impact resistance, NDE and residual compression test phases. Although ISO 18352 suggests referring to ISO 6603 for extra information on drop-weight impact testing, many components within the standard such as specimen geometry and dimensions, test fixture setup and dimensions, suggested impact energies and striker mass and size, are all much closer to those suggested in ASTM D7137.

Both test standards recommend using the same test fixture for compression testing, an example of which is shown in Figure 83. Here, the specimen is simply supported by knife edges along its longitudinal edges which restricts translational motion in the out-of-plane direction but allows rotation. The top and bottom edges of the specimen are placed between two flat surfaces and clamped to prevent out-of-plane and rotational motion. Out-of-plane motions can lead to buckling of specimens which is an unacceptable failure mode.

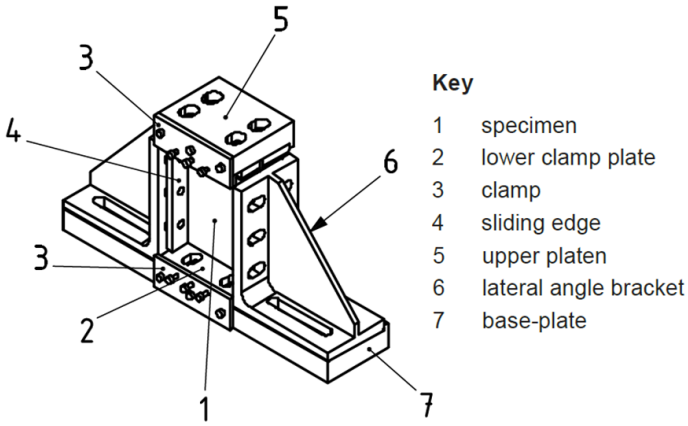

Figure 83. *Compression-after-impact (CAI) test fixture [142]*

Impact and post-impact of 3D composites in the literature

Impact testing of 3D composites is an area that has been extensively studied within the literature and is typically conducted using either indentation or drop-weight test methods [4, 5, 46, 48, 143, 144, 145, 146], though most studies do not cite the use of any test standard. One study by Potluri et al. used drop-weight testing on four different 3D woven preforms but stated that they could not follow ASTM D7136 since the test panels used were all less than 2 mm thick. Instead, a modified clamping rig developed for thin laminates was used, which clamps test specimens between two plates similar to ISO 6603. Compared to standard impact testing using ASTM

D7136, where test specimen dimensions are 150 mm x 100 mm clamped over an opening of 125 mm x 75 mm, the modified method used much smaller specimens at 89 mm x 54 mm clamped over a 40 mm diameter hole chosen to prevent excessive bending during impact.

Additional methods used in various literature studies to produce impact damage include the use of a split Hopkinson pressure bar (SHPB) [147, 148, 149, 150], which can provide a range of impact velocities, or gas guns for ballistic impacts [151, 152]; neither of these have been standardised.

Some observations noted from impact studies of 3D woven composites include:

- Fibre architecture influences – Gerlach et al. [150] noted that increasing the z-binder volume content led to a reduction in the size of the delaminated and damaged regions when impacted. This was similarly observed by Potluri et al. [48] when comparing a modified layer-to-layer, a standard layer-to-layer, an angle interlock and an orthogonal weave.
- Comparison with 2D woven composites – 3D weaves produce much smaller damage areas when impacted once [150]. Under repeated impact, Baucom et al. [143, 144] noted that 3D orthogonal weaves required twice as many impacts to perforate the material when compared to a 2D plain weave. The increased energy absorbed translated into more extensive damage in the forms of debonding/delamination of the z-binders and surface weft tows.
- Impact velocity – increasing impact velocity increases the energy absorbed [150]. At low impact velocities the dominant failure modes are debonding and delamination, with increases in impact damage showing significant levels of fibre rupture and intra-ply failure.
- Energy absorption – stacked 3D weaves absorb more energy than a single ply 3D weave of the same thickness. Suggested to be related to the number of z-binder crowns present, which are believed to be uniquely responsible for energy absorption, especially in orthogonal weaves [46].

Unlike impact testing, post-impact property investigations appear to be more limited in the literature [48, 150]. Of those reported, ASTM D7137 tends to be the favoured test standard for measuring post-impact compressive properties, despite ISO 18352 being very similar. One study by Potluri et al. [48] found that the loss of compressive strength with impact energy was similar regardless of the 3D woven format, noting that differences were mainly a function of undamaged compressive strength. Hart et al. [47], using a 3D orthogonal weave, observed no significant loss of compressive strength and modulus at any of the energies tested, attributing the reinforcement to restricting localised buckling during loading. Both studies used non-

standard specimen dimensions, with Potluri et al expressing that the reduced dimensions were due to limited thickness of the materials being tested.

In addition to CAI, Hart et al. [47] undertook flexure-after-impact (FAI) testing, noting a large reduction in the flexural strength and modulus. The FAI specimens tested were found to be more sensitive to delamination damage than CAI specimens. There are currently no test standards for FAI, and the work undertaken used ASTM D6272 (4PB).

Post-impact testing: CAI

Test Methods

CAI testing reported in this Guide was conducted according to ISO 18352.

Specimen preparation

Test specimens were cut from panels using a diamond saw. Compression specimens require uniform loading to reduce the potential for premature buckling failure. As such, specimen ends need to be both flat and parallel to each other to a high tolerance of 0.02 mm. This can be achieved through machining processes such as grinding, or if sufficiently accurate using an automated diamond saw.

For this Guide, GFRE ORT and CFRE LTL specimens were cut along both the warp- and weft-loading directions. While the thickness of the CFRE LTL is within the range recommended in ISO 18352, the GFRE ORT thickness was not. Despite this, all testing was conducted using standard length and width dimensions. Five tests were conducted per loading direction and the average dimensions are detailed in Table 33.

Table 33. *Average dimensions of CAI test specimens. Measurements provided as the mean ± std. dev.*

Loading direction	Length (mm)	Width (mm)	Thickness (mm)
GFRE ORT			
Warp	149.88 ± 0.01	100.01 ± 0.02	3.04 ± 0.04
Weft	149.88 ± 0.02	100.03 ± 0.03	3.12 ± 0.06
CFRE LTL			
Warp	149. 89 ± 0.00	100.10 ± 0.03	5.00 ± 0.02
Weft	149.89 ± 0.01	100.05 ± 0.02	5.11 ± 0.04

In addition to test specimens, an alignment plate was machined to standard test specimen dimensions, i.e. 150 x 100 x 5 mm to be used during test setup. Like the test specimens it is important that this specimen has high tolerances between edges and faces.

Test setup

Testing is split into three parts, impact, NDE and CAI.

Stage 1: Impact

Impact testing was undertaken by drop-weight using an Instron CEAST 9340 impact test frame, with the setup shown in Figure 84. The support fixture at the bottom of the test frame clamps the test specimens using toggle clamps as per the test standard recommendations. The cut-out is 125 mm x 75 mm.

A hemispherical steel impact striker with a 16 mm diameter was used to impact each test specimen. The total mass of the drop-weight load train was 5.12 kg including the mass of the hemispherical impact striker. ISO 18352 recommends that an impact energy per unit thickness of material, E_c, of $6.7\ \mathrm{J/mm}$ should be used unless otherwise agreed. Using equation (32) and (33), along with nominal thicknesses of 3 mm and 5 mm for the GFRE ORT and CFRE LTL, respectively, impact energies and impact heights are as shown in Table 34.

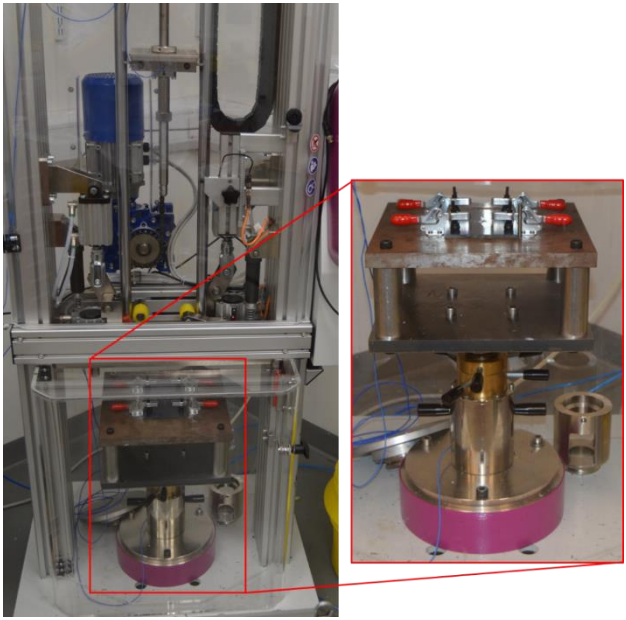

Figure 84. *Drop-weight impact testing setup*

$$E = E_c t \quad (32) \qquad h = \frac{E}{mg} \quad (33)$$

Table 34. *Impact mass, energy, and height for the GFRE ORT and CFRE LTL materials*

Material	Nominal thickness, t (mm)	Mass, m (kg)	Impact energy, E (J)	Impact height, h (mm)
GFRE ORT	3	5.123	20.1	399.9
CFRE LTL	5		33.5	666.6

Stage 2: Non-destructive evaluation (NDE)

After impact testing specimens were analysed using NDE techniques to determine the extent of the damage that had developed. Although the preferred technique is ultrasonic C-scanning, ISO 18352 does allow other NDE techniques to be used. Here one specimen of each material was scanned using both ultrasonic C-scan and flash thermography. NDE of most specimens was done using flash thermography as it was ultimately shown to produce similar amounts of damage information to ultrasonic C-scan.

Stage 3: Compression-after-impact (CAI)

The CAI testing reported in this Guide was conducted on an Instron 4507 test frame with a 200 kN load cell at a speed of 2 mm/min.

The test fixture is split into three components: a base plate, two sliding angle brackets, and a top face platen. The sliding angle brackets sit within the recess of the base plate and are pushed up against the longitudinal edges of the test specimen. Each angle bracket contains two knife edges that are used to simply support the test specimen and restrict out-of-plane motion. A pair of clamping plates are situated on the base plate between the two angle brackets to stop movement out-of-plane and rotational movement of the specimen. The top face platen also contains two clamping plates to lock against the test specimen but is not fixed to the test frame. A self-alignment plate is screwed into the load cell and then placed against the top face platen to help with general alignment of the test fixture. The setup can be seen in Figure 85.

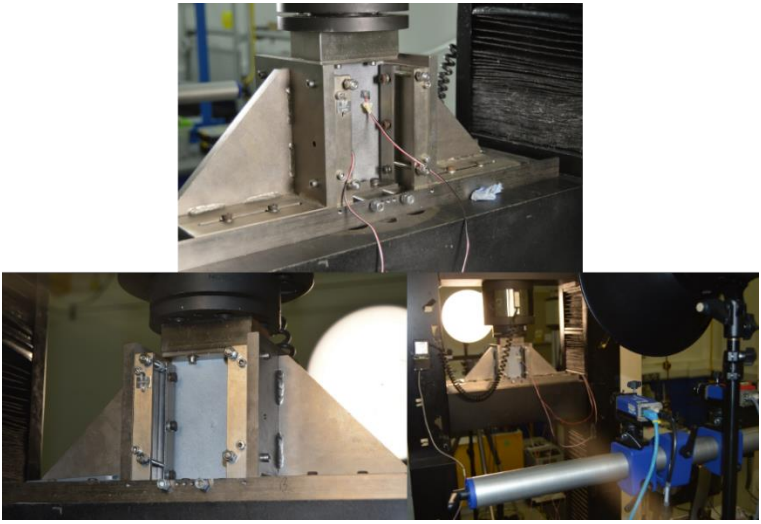

Figure 85. *CAI test setup; (top) with strain gauges; (bottom) with DIC*

For compression testing it is important to ensure that the test fixture is well aligned within the test frame in order to reduce the potential for bending/buckling during loading. Ground steel bars/plates are useful for setting up the alignment of the test fixture. In the CAI test fixture, the steel plate used for alignment should have the same dimensions as the test specimens.

Note 2: Good alignment can be achieved through fine adjustment of the knife edges and bottom clamp of the test fixture. Strain measurements can be used to determine how good the alignment is. Two strain gauges should be bonded to either face of the alignment plate, each 25 mm in from the top and one longitudinal edge. Ideally all strains will read the same value when the steel plate is loaded elastically. However, if this cannot be attained, ISO 18352 recommends that all strain gauges should measure strains within 10% of the mean. If strains lie outside of 10% of the mean strain, adjustment to the fixture should be undertaken. This can be an iterative process, but the magnitude and sign attached to the strain measurements of each gauge can provide an indication of the direction of adjustment needed.

Note 3: Once the test fixture alignment is set, only loosen the knife edges and bottom clamp on one side of the test fixture when removing a test specimen. This should ensure that alignment is maintained during testing.

ISO 18352 recommends that strain is measured using strain gauges on each test specimen during testing. Like the alignment plate, two strain gauges are required on each side of the test

specimen, 25 mm in from the top and one of the longitudinal edges. The use of these strain gauges is useful for several reasons:

- To check alignment of the test fixture with regards to the test specimen through monitoring the mean difference in strain – each gauge should be within 10% of the mean strain,
- To monitor for evidence of bending/buckling behaviour,
- To measure an average global strain during loading for calculating the residual compressive modulus and strain at failure.

In this work only one specimen of each material type was tested using strain gauges, with all other tests using DIC to monitor the strain during loading. Strain gauges with a gauge-length of 2-3 mm are typically used but due to the size of the unit cell of these materials, longer strain gauges with a 10 mm gauge-length were used. DIC was also used on specimens with strain gauges for comparison of measurements.

Back-to-back stereo DIC was used to measure strain for all tests conducted and an example of the setup can be seen in Figure 85b. Four 5Mpx resolution LaVision cameras with 50 mm fixed focal length lenses were used. LaVision DaVis 8.4 was used for image capture and processing. Full-field strain maps were produced using a subset size of 51 and a step size of 17. All specimens were sprayed mat white and speckled with mat black paint. Instead of measuring the average strain at four locations, i.e. two on each surface, average strain measured using DIC was taken as a strip across the specimen width. The strain measurements remained in the same location of the test specimen as the strain gauges, covering a length of 10 mm and a width of 50 mm.

Note 4: It is important to make sure that the specimen is fully seated and in contact with all load bearing surfaces. Load the specimen until ~ 450 N is reached and then reduce the load to ~10 N.

Note 5: Before testing a specimen, it is recommended to load it to ~10% of its expected failure load, checking the strain on each face is within 10% of the mean. This should be done for each test to make sure that the alignment remains good.

Note 6: ISO 18352 recommends that the percentage bending remain less than 10% for a test to be considered valid. However, percentage bending slightly greater that this can still be acceptable so long as buckling failures are not induced.

Calculations of the CAI strength and modulus are performed using equations (6) and (7) from the compression section of this Guide. In addition, percentage bending can be calculated using equation (8).

Results and analysis

Observed impact damage

After impact, specimens of both materials were visually inspected for damage. The translucence of the GFRE ORT material allowed the extent of damage to be easily observed, while only surface damage could be seen on the CFRE LTL.

Figure 86 and Figure 87 show examples of warp- and weft-direction impacted GFRE ORT test specimens, respectively. Most of the damage is concentrated locally around the impact site and includes only a small delaminated region. In all GFRE ORT specimens, some perforation of the bottom surface occurred as indicated by the presence of fractured tows. Damage remains localised to the impact site due to a combination of the through-thickness reinforcement providing extra surface area for energy absorption and the fracture of fibres around the impact site. Beyond this region, damage generally consists of transverse and longitudinal matrix cracks extending a short distance away from the impact site. Matrix cracks interacting with z-binders away from the impact site lead to debonding of the through-thickness portion z-binders. While not strictly necessary due to the translucency of this material, both thermography and C-scanning were also used for damage detection. Unfortunately, neither of these techniques were able to show anything beyond the location of impact, as indicated by the thermography images included in Figure 86 and Figure 87.

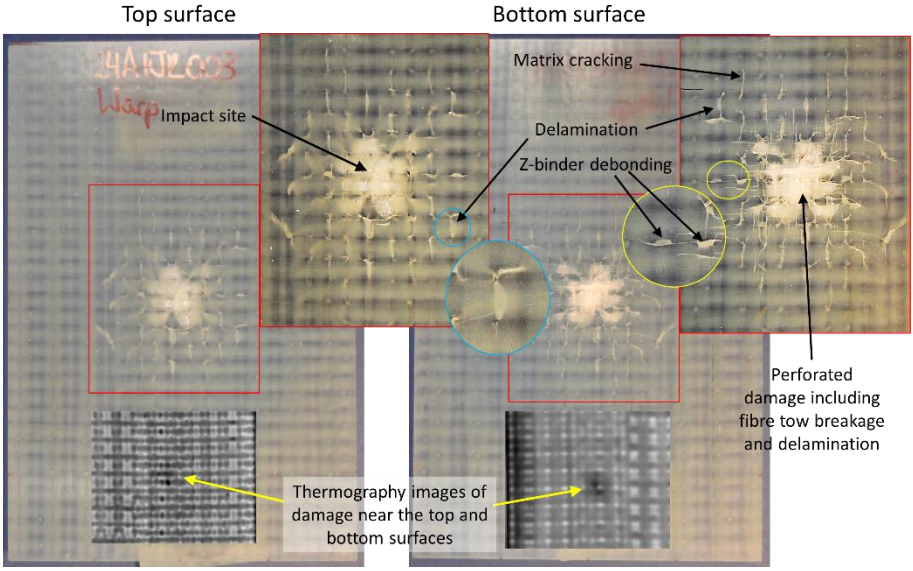

Figure 86. *Impact damage on the top and bottom surface of a GFRE ORT warp-direction CAI specimen*

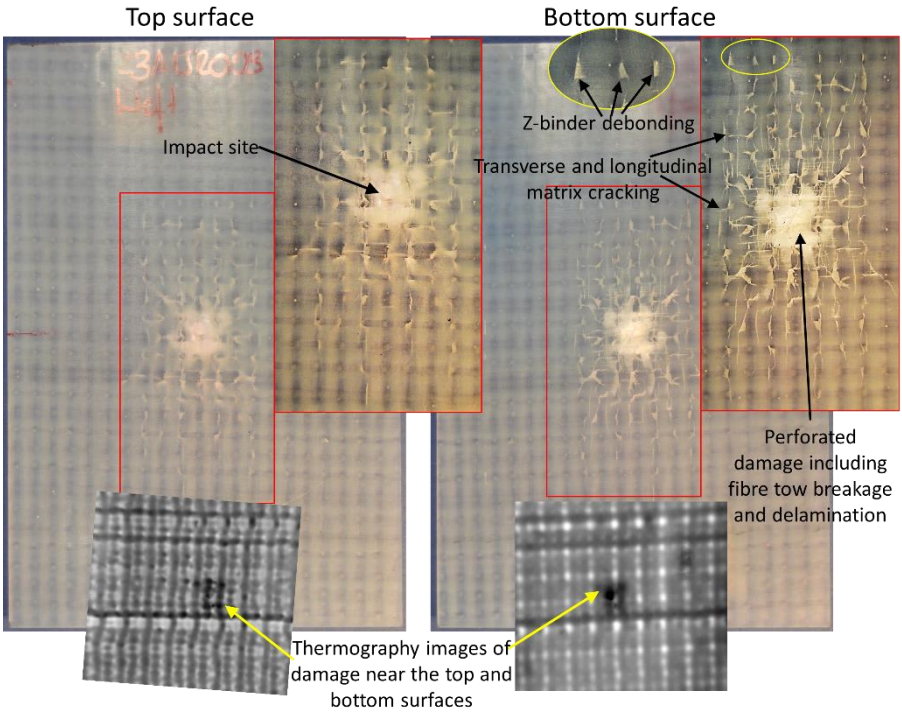

Figure 87. *Impact damage on the top and bottom surface of a GFRE ORT weft-direction CAI specimen*

Unlike the GFRE ORT material, impact of the CFRE LTL did not result in the perforation of any test specimens. Instead, only a slight bulging of the bottom surface occurred. Damage on the top surface appears as a long longitudinal crack and a shorter transverse crack extending away from the impact site. There is also clear indication of multiple matrix cracks on the bottom surface of test specimens. These matrix cracks develop through the surface weft tows, appearing as transverse and longitudinal cracks in the warp and weft specimens, respectively. Thermography shows some of the extent of damage in the CFRE LTL materials as indicated in Figure 88 and Figure 89. Damage tends to remain fairly localised around the initial impact site. As for the GFRE ORT material, restriction of damage growth in the CFRE LTL is due to the z-binders absorbing much of the impact energy.

The extent of delamination damage is greater in the CFRE LTL material. Compared to the GFRE ORT material, there are a lot more z-binders through-the-thickness in the CFRE LTL material that can absorb energy. In addition, the LTL z-binders can allow damage to travel further, reducing

the potential for fibre fracture, especially toward the underside of the material. As such, greater energy would be required to cause perforation of the bottom surface of the material.

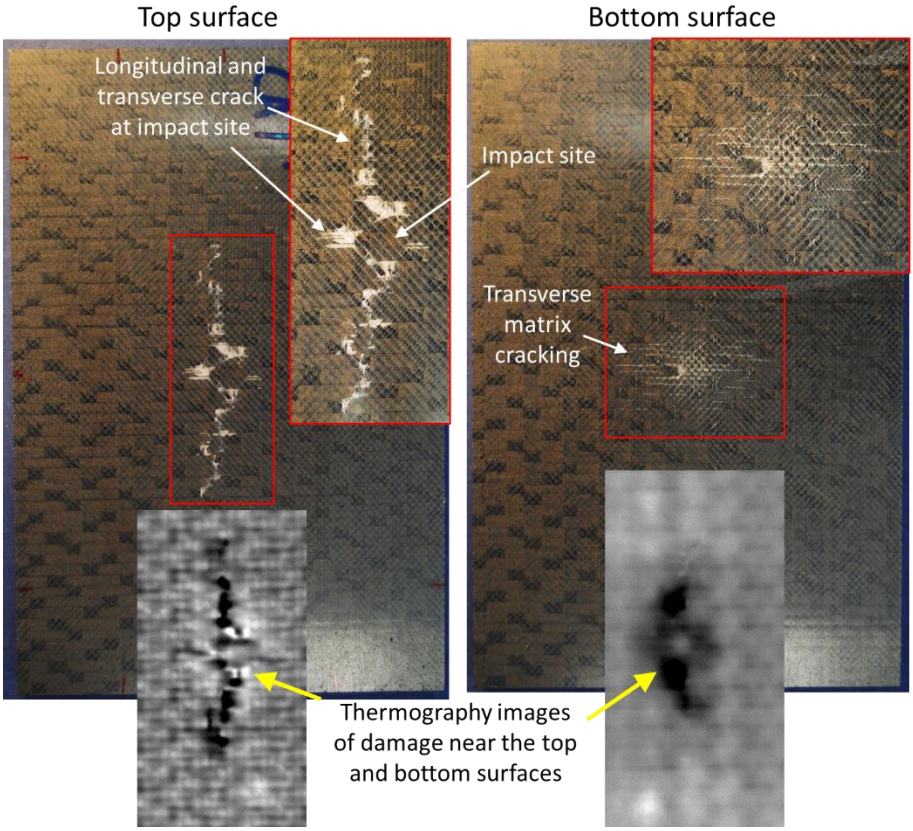

Figure 88. *Impact damage on the top and bottom surface of a CFRE LTL warp-direction CAI specimen*

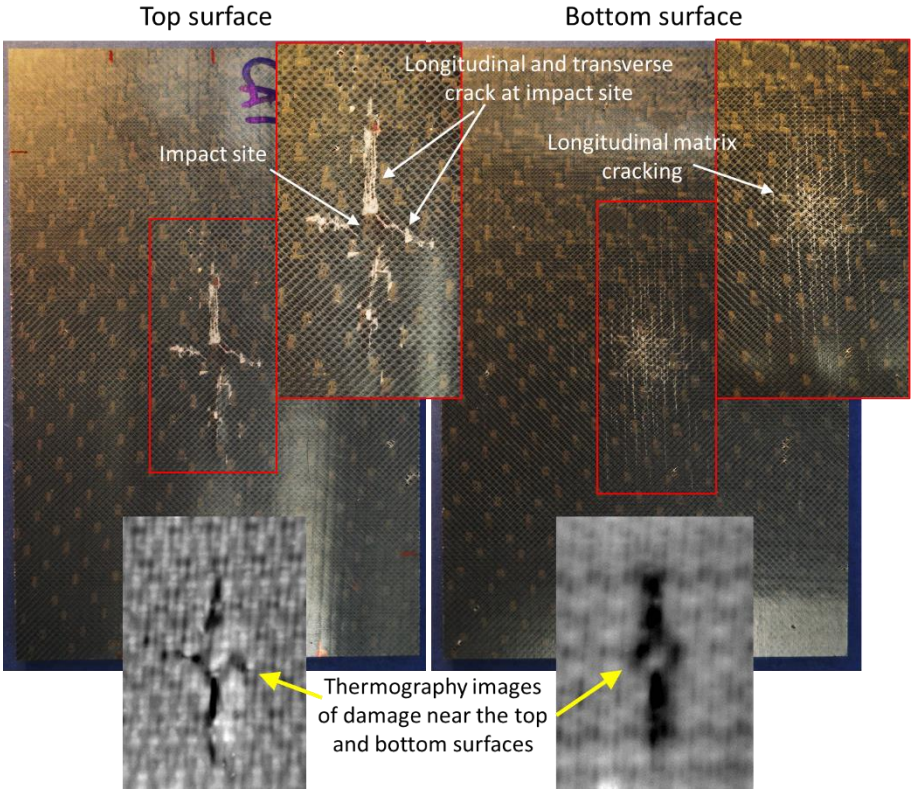

Figure 89. *Impact damage on the top and bottom surface of a CFRE LTL weft-direction CAI specimen*

Residual properties: Compression-after-impact

Under post-impact compressive loading, each material produced vastly different responses. For the GFRE ORT material, regardless of loading direction, large scale buckling occurred in all specimens tested, invalidating testing. Initial loading was linear until approximately 0.15-0.2% strain, after which the loading response became highly nonlinear until tests were stopped. Figure 90 shows an example of a full-field strain map during buckling, where the region of high strain is indicative of the bulging of the test specimen. The thickness of the GFRE ORT material is outside the range recommended in either ISO 18352 or ASTM D7137, suggesting that these dimensions are not sufficient for testing this material.

For the CFRE LTL material, all specimens regardless of loading direction failed as intended through the region of impact. No buckling occurred during loading. Unlike the GFRE ORT material, the CFRE LTL has the recommended specimen thickness for the specimen dimensions

suggested in ISO 18352 and ASTM D7137. Acceptable failures further indicates that the specimen dimensions used here are more suitable to materials of similar thickness to the CFRE LTL material and not the GFRE ORT material. Further investigation would be required to determine suitable scaling of dimensions to specimen thickness for this type of testing.

Recommendation 1: Conduct an initial impact and CAI test using the standard test dimensions. If buckling occurs or appears likely to influence the measurements, scale down the size of the test specimen. For 3D composites, the amount a test specimen should be scaled down to avoid buckling failure will be a combination of the material structure and its thickness. Since the extent of damage across a test specimen is limited by the through-thickness reinforcement, scaling down a specimen should not be an issue.

Generally, consider scaling down the test specimen dimensions of any materials with a thickness less than 4 mm (lower band suggested in ASTM D7137 and ISO 18352).

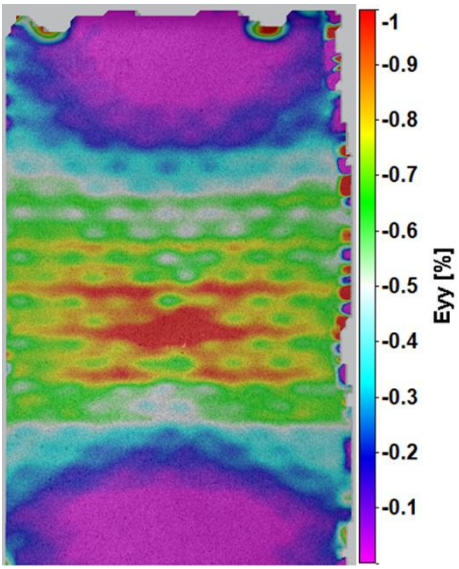

Figure 90. *Example of full-field strain map of a GFRE ORT CAI test specimen indicating bending*

Table 35 shows the residual compressive strength and modulus measured from the CAI tests for the CFRE LTL material. Compared to the undamaged compressive strength and modulus shown in Chapter 3, these impacted specimens lose almost half their strength, but the modulus remains relatively unchanged. The lack of change of modulus indicates that the localisation of damage around the impact site does not affect the stiffness of the material at a distance away from it.

Table 35. *Residual compressive strength and modulus of the CFRE LTL material loaded in compression along the warp- and weft-direction post-impact. Measurements provided as the mean ± std. dev. of five test specimens per material loading direction*

Loading direction	Residual compressive strength, σ_c (MPa)	Compressive modulus, E_c (GPa)
Warp	188.60 ± 7.39	57.13 ± 1.17
Weft	179.66 ± 5.56	58.47 ± 1.52

Conclusions and recommendations

In this chapter, CAI testing has been conducted using ISO 18352 on a GFRE ORT and CFRE LTL material. Both materials showed a localisation of damage around the impact site due to the z-binders providing extra surface area for energy absorption. For proportionally similar impact energies, the LTL structure allowed damage to spread over a greater area, while the ORT structure restricted spread causing perforation and fracture along the bottom surface of the test specimen.

Under compressive loading, the GFRE ORT material failed via buckling, regardless of loading direction. Conversely, the CFRE LTL failed acceptably through the impact region. The differences in failure between each material indicates that the recommended specimen dimensions are only suitable for the specific thicknesses suggested in ISO 18352. The standard does not provide any alternative dimensions for materials of different thicknesses, especially those thinner than recommended (5 mm ± 1 mm). As such, further work would be required to determine sufficient scaling of the test specimens for different material thicknesses. However, scaling down of the specimen dimensions should be undertaken for material with a thickness less than 4 mm.

References

[1] A. P. Mouritz, "Review of z-pinned composite laminates," *Composites: Par A,* vol. 38, pp. 2383-2397, 2007.

[2] P. Chang, A. P. Mouritz and B. N. Cox, "Properties and failure mechanisms of z-pinned laminates in monotonic and cyclic tension," *Composites: Part A,* vol. 37, pp. 1501-1513, 2006.

[3] A. P. Mouritz and P. Chang, "Tension fatigue of fibre-dominated and matrix-dominated laminates reinforced with z-pins," *International Journal of Fatigue,* vol. 32, pp. 650-658, 2010.

[4] X. Zhang, L. Hounslow and M. Grassi, "Improvement of low-velocity impact and compression-after-impact performance by z-fibre pinning," *Composites Science and Technology,* vol. 66, pp. 2785-2794, 2006.

[5] M. D. Isa, S. Feih and A. P. Mouritz, "Compression fatigue properties of z-pinned quasi-isotropic carbon/epoxy laminate with barely visible impact damage," *Composite Structures,* vol. 93, pp. 2269-2276, 2011.

[6] I. K. Partridge and D. D. R. Cartié, "Delamination resistant laminates by Z-fibre pinning: Part I manufacture and fracture performance," *Composites: Part A,* vol. 36, pp. 55-64, 2005.

[7] D. D. R. Cartié, M. Troulis and I. K. Partridge, "Delamination of Z-pinned carbon fibre reinforced laminates," *Composites Science and Technology,* vol. 66, pp. 855-861, 2006.

[8] D. D. R. Cartié, J.-M. Laffaille, I. K. Partridge and A. J. Brunner, "Fatgue delamination behaviour of unidirectional carbon fibre/epoxy laminates reinforced by Z-fibre pinning," *Engineering Fracture Mechanics,* vol. 76, pp. 2834-2845, 2009.

[9] A. P. Mouritz, "Delamination properties of z-pinned composites in hot-wet environment," *Composites: Part A,* vol. 52, pp. 134-142, 2013.

[10] K. Pingkarawat and A. P. Mouritz, "Improving the mode I delamination fatigue resistance of composites using z-pins," *Composites Science and Technology,* vol. 92, pp. 70-76, 2014.

[11] F. Pegorin, K. Pingkarawat, S. Daynes and A. P. Mouritz, "Mode II interlaminar fatigue properties of z-pinned carbon fibre reinforced epoxy composites," *Composites: Part A,* vol. 67, pp. 8-15, 2014.

[12] F. Pegorin, K. Pingkarawat, S. Daynes and A. P. Mouritz, "Influence of z-pin length on the delamination fracture toughness and fatigue resistance of pinned composites," *Composites: Part B,* vol. 78, pp. 298-307, 2015.

[13] A. P. Mouritz, "Compression properties of z-pinned composite laminates," *Composites Science and Technology,* vol. 67, pp. 3110-3120, 2007.

[14] P. Chang, A. P. Mouritz and B. N. Cox, “Flexural properties of z-pinned laminates,” *Composites: Part A,* vol. 38, pp. 244-251, 2007.

[15] A. P. Mouritz, K. H. Leong and I. Herszberg, “A review of the effect of stitching on the in-plane mechanical properties of fibre-reinforced polymer composites,” *Composites: Part A,* vol. 28A, pp. 979-991, 1997.

[16] K. Dransfield, C. Baillie and Y. W. Mai, “Improving the delamaintion resistance of CFRP by stitching - a review,” *Composites Science and Technology,* vol. 50, pp. 305-317, 1994.

[17] J. Wittig, “Recent development in the robotic stitiching technology for textile structural composites,” *Journal of Textile and Apparel, Technology and Management,* vol. 2, no. 1, 2001.

[18] J. W. G. Treiber, “Perfomance of tufted carbon fibre/epoxy composites,” *Phd Thesis, Cranfield University,* 2011.

[19] G. Dell'Anno, J. W. G. Treiber and I. K. Partridge, “Manufacturing of composite parts reinforced through-thickness by tufting,” *Robotics and Computer-Integrated Manufacturing,* vol. 37, pp. 262-272, 2016.

[20] D. M. Lombetti, “Tufting of complex composite structures,” *Phd Thesis, Cranfield University,* 2015.

[21] G. Dell'Anno, “Effect of tufting on the mechanical behaviour of carbon fabric/epoxy composites,” *Phd Thesis, Cranfield University,* 2007.

[22] M. Colin de Verdiere, A. A. Skordos, M. May and A. C. Walton, “Influence of loading rate on the delamination response of untufted and tufted carbon epoxy non crimp fabric composites: Mode I,” *Engineering Fracture Mechanics,* vol. 96, pp. 11-25, 2012.

[23] M. Colin de Verdiere, A. A. Skordos, A. C. Walton and M. May, “Influence of loading rate on the delamination response of untufted and tufted carbon epoxy non-crimp fabric composites/Mode II,” *Engineering Fracture Mechanics,* vol. 96, pp. 1-10, 2012.

[24] C. Osmiani, G. Mohammed, J. W. G. Treiber, G. Allegri and I. K. Partridge, “Exploring the influence of micro-structure on the mechanical properties and crack bridging mechanisms of fibrous tufts,” *Composites: Part A,* vol. 91, pp. 409-419, 2016.

[25] C. Scarponi, A. M. Perillo, L. Cutillo and C. Foglio, “Advanced TTT composite materials for aeronautical purposes: Compression after impact (CAI) behaviour,” *Composites: Part B,* vol. 38, pp. 258-264, 2007.

[26] A. Henao, R. Guzman de Villoria, J. Cuartero, M. Carrera, J. Picon and A. Miravete, “Enhanced Impact Energy Absorption Characteristics of Sandwich Composites through Tufting,” *Mechanics of Advanced Materials and Structures,* vol. 22, pp. 1016-1023, 2015.

[27] P. Deconinck, J. Capelle, V. Bouchart, P. Chevier and F. Ravailler, “Delamination propagation analysis in tufted carbon fibre-reinforced plastic composites subjected to high-velocity impact,” *Journal of Reinforced Plastics & Composites,* vol. 33, no. 14, pp. 1353-1363, 2014.

[28] A. T. Martins, Z. Aboura, W. Harizi, A. Laksimi and K. Khellil, “Analysis of the impact and compression after impact behavior of tufted laminated composites,” *Composite Structures,* vol. 184, pp. 352-361, 2018.

[29] G. Dell'Anno, D. D. R. Cartie, I. K. Partridge and A. Rezai, “Exploring mechanical balance in tufted carbon fabric/epoxy composites,” *Composites: Part A,* vol. 38, pp. 2366-2373, 2007.

[30] V. Koissin, J. Kustermans, S. V. Lomov, I. Verpoest, B. Van Den Broucke and V. Witzel, “Structurally stitched NCF preforms: Quasi-static response,” *Composites Science and Technology,* vol. 69, pp. 2701-2710, 2009.

[31] V. Koissin, J. Kustermans, S. V. Lomov, I. Verpoest, H. Nakai, T. Kurashiki, K. Hamada, Y. Momoji and M. Zako, “Structurally stitched woven preforms: experimental characterisation, geometrical modelling, and FE analysis,” *Plastics, Rubber and Composites,* vol. 38, pp. 98-105, 2009.

[32] M. Amirul Islam, “3D woven fabrics, structures, and methods of manufacture,” in *Woven Textiles: Principles, Technologies and Applications*, 2nd ed., Elsevier, 2020, pp. 329-391.

[33] M. Y. Matveev, V. Koncherry, L. P. Brown, S. S. Roy, P. Potluri and A. C. Long, “Meso-scale optimisation of 3D composites and novel preforming technologies,” in *22nd International Conference on Composite Materials*, Melbourne, 2019.

[34] M. N. Saleh, A. Yudhanto, P. Potluri, G. Lubineau and C. Soutis, “Characterising the loading direction sensitivity of 3D woven composites: Effect of z-binder architecture,” *Composites: Part A,* vol. 90, pp. 577-588, 2016.

[35] A. Bogdanovich and M. Mohamed, “Three-Dimensional Reinforcements for Composites,” *SAMPE Journal,* vol. 45, no. 6, Nov/Dec 2009.

[36] L. Lee, S. Rudov-Clar, A. Mouritz, M. Bannister and I. Herszberg, “Effect of weaving damage on the tensile properties of three-dimensional woven composites,” *Composite Structures,* vol. 57, pp. 405-413, 2002.

[37] S. Rudov-Clark, A. P. Mouritz, L. Lee and M. Bannister, “Fibre damage in the manufacture of advanced three-dimensional woven composites,” *Composites: Part A,* vol. 34, pp. 963-970, 2003.

[38] B. Lee, K. Leong and I. Herszberg, “Effect of Weaving on the Tensile Properties of Carbon Fibre Tows and Woven Composites,” *Journal of Reinforced Plastics and Composites,* vol. 20, pp. 652-670, 2001.

[39] E. Archer, S. Buchanan, A. T. McIlhagger and J. P. Quinn, “The effect of 3D weaving and consolidation on carbon fibre tows, fabrics and compoistes,” *Journal of Reinforced Plastics and Composites,* vol. 29, no. 20, pp. 3162-3170, 2010.

[40] M. H. Mohamed and A. E. Bogdanovich, “Comparative analysis of different 3D weaving processes, machines and products,” in *17th International Conference on Composite Materials*, Edinburgh, 2009.

[41] Erginer Seramik, “KOMPOZİT,” [Online]. Available: https://www.erginer.com.tr/kompozit/.

[42] S. V. Lomov, A. E. Bogdanovich, D. S. Ivanov, D. Mungalov, M. Karahan and I. Verpoest, "A comparative study of tensile properties of non-crimp 3D orthogonal weave and multi-layer plain weave E-glass composites. Part 1: Materials, methods and principal results," *Composites: Part A,* vol. 40, pp. 1134-1143, 2009.

[43] S. Dai, P. R. Cunningham, S. Marshall and C. Silva, "Influence of fibre architecture on the tensile, compressive and flexural behaviour of 3D woven composites," *Composites: Part A,* vol. 69, pp. 195-207, 2015.

[44] M. Dahale, G. Neale, R. Lupicini, L. Cascone, C. McGarrigle, J. Kelly, E. Archer, E. Harkin-Jones and A. McIlhagger, "Effect of weave parameters on the mechanical properties of 3D woven glass composites," *Composite Structures,* vol. 223, 2019.

[45] A. P. Mouritz, C. Baini and I. Herszberg, "Mode I interlaminar fracture toughness properties of advanced fibreglass composites," *Composites: Part A,* vol. 30, pp. 859-870, 1999.

[46] J. N. Baucom and M. A. Zikry, "Evolution of Failure Mechanisms in 2D and 3D woven composites systems under quasi-static perforation," *Journal of Composites Materials,* vol. 37, pp. 1651-1674, 2003.

[47] K. R. Hart, P. X. L. Chia, L. E. Sheridan, E. D. Wetzel, N. R. Sottos and S. R. White, "Comparison of Compression-After-Impact and Flexure-After-Impact protocols for 2D and 3D woven fiber-reinforced composites," *Composites: Part A,* vol. 101, pp. 471-479, 2017.

[48] P. Potluri, P. Hogg, M. Arshad, D. Jetavat and P. Jamshidi, "Influence of Fibre Architecture on Impact Damage Tolerance in 3D Woven Composites," *Applied Composite Materials,* vol. 19, pp. 799-812, 2012.

[49] ASTM International, "ASTM D638 - 14 Standard Test Method for Tensile Properties of Plastics," West Conshohocken, PA, 2014.

[50] ASTM International, "ASTM D5083 - 17 Standard Test Method for Tensile Properties of Reinforced Thermosetting Plastics Using Straight-Sided Specimens," West Conshohocken, PA, 2017.

[51] ASTM International, "ASTM D3039/D3039M - 14 Standard Test Method for Tensile Properties of Polymer Matrix Composite Materials," West Conshohocken, PA, 2014.

[52] British Standards Institution, "BS EN ISO 527-1:2012 Plastics - Determination of tensile properties Part 1: General principles," BSI, 2012.

[53] J. M. Hodgkinson, Mechanical Testing of Advanced Fibre Composites, Woodhead Publishing, 2000.

[54] British Standards Institution, "BS EN ISO 527-4: 1997 Plastics - Determination of tensile properties - Part 4: Test conditions for isotropic and orthotropic fibre-reinforced plastic composites," BSI, 1997.

[55] D. O. Adams and D. F. Adams, "DOT/FAA/AR-02/106: Tabbing Guide for Composite Test Specimens," National Technical Information Service (NTIS), Springfield, Virginia, 2002.

[56] A. Davis, A. Foreman, R. Shaw and G. Sims, “Measurement Good Practice Guide No. 38 - Fibre Reinforced Plastic Composites - Machining of Composites and Specimen Preparation,” NPL, Teddington, UK, 2001.

[57] ASTM International, “ASTM D5766/D5766M - 11 Standard Test Method for Open-Hole Tensile Strength of Polymer Matrix Laminates,” Wst Conshohocken, PA, 2011.

[58] R. Munoz, V. Martinez, F. Sket, C. Gonzalez and J. Llorca, “Mechanical behaviour and failure micromechanisms of hybrid 3D woven composites in tension,” *Composites: Part A,* vol. 59, pp. 93-104, 2014.

[59] B. K. Behera and B. P. Dash, “Mechanical behavior of 3D woven composites,” *Materials and Design,* vol. 67, pp. 261-271, 2015.

[60] K. C. Warren, R. A. Lopez-Anido and J. Goering, “Experimental investigation of three-dimensional woven composites,” *Composites: Part A,* vol. 73, pp. 242-259, 2015.

[61] M. N. Saleh, G. Lubinau, P. Potluri, P. J. Withers and C. Soutis, “Micro-mechanics based damage mechanics for 3D orthogonal woven composites: Experiment and numerical modelling,” *Composite Structures,* vol. 156, pp. 115-124, 2016.

[62] A. E. Bogdanovich, M. Karahan, S. V. Lomov and I. Verpoest, “Quasi-static tensile behavior and damage of carbon/epoxy composite reinforced with 3D non-crimp orthogonal woven fabric,” *Mechanics of Materials,* vol. 62, pp. 14-31, 2013.

[63] S. V. Lomov, M. Karahan, A. E. Bogdanovich and I. Verpoest, “Monitoring of acoustic damage during tensile loading of 3D woven carbon/epoxy composites,” *Textile Research Journal,* vol. 84, no. 13, pp. 1373-1384, 2014.

[64] N. Castaneda, B. Wisner, J. Cuadra, S. Amini and A. Kontsos, “Investigation of the z-binder role in progressive damage of 3D woven composites,” *Composites: Part A,* vol. 98, pp. 76-89, 2017.

[65] B. N. Cox, M. S. Dadkhah, W. L. Morris and J. G. Flintoff, “Failure mechanisms of 3D woven composites in tension, compression, and bending,” *Acta Metallurgica et Materialia,* vol. 42, no. 12, pp. 3967-3984, 1994.

[66] B. N. Cox, M. S. Dadkhah and W. L. Morris, “On the tensile failure of 3D woven composites,” *Composites: Part A,* vol. 27A, pp. 447-458, 1995.

[67] K. H. Leong, B. Lee, I. Herszberg and M. K. Bannister, “The effect of binder path on the tensile properties and failure of multilayer woven CFRP composites,” *Composites Science and Technology,* vol. 60, pp. 149-156, 2000.

[68] P. Tan, L. Tong, G. P. Steven and T. Ishikawa, “Behavior of 3D orthogonal woven CFRP composites. Part I. Experimental investigation,” *Composites: Part A,* vol. 31, pp. 259-271, 2000.

[69] D. S. Ivanov, S. V. Lomov, A. E. Bogdanovich, M. Karahan and I. Verpoest, “A comparative study of tensile properties of non-crimp 3D orthogonal and multi-layer plain weave E-glass composites. Part 2: Comprehensive experimental results,” *Composites: Part A,* vol. 40, pp. 1144-1157, 2009.

[70] P. J. Callus, A. P. Mouritz, M. K. Bannister and K. H. Leong, “Tensile properties and failure mechanisms of 3D woven GRP composites,” *Composites: Part A,* vol. 30, pp. 1277-1287, 1999.

[71] S. Dai, P. R. Cunningham, S. Marshall and C. Silva, “Open hole quasi-static and fatigue characterisation of 3D woven composites,” *Compostie Structures,* vol. 131, pp. 765-774, 2015.

[72] M. Pankow, B. Justusson, M. Riosbaas, A. M. Waas and C. F. Yen, “Effect of fiber architecture on tensile fracture of 3D woven textile composites,” *Composite Structures,* vol. 225, 2019.

[73] International Digital Image Correlation Society (iDICs), “A Good Practices Guide for Digital Image Correlation,” 2018.

[74] J. P. Quinn, A. T. McIlhagger and R. McIlhagger, “Examination of the failure of 3D woven composites,” *Composites: Part A,* vol. 39, pp. 273-283, 2008.

[75] ASTM International, “ASTM D695 - 15 Standard Test Method for Compressive Properties of Rigid Plastics,” West Conshohoken, PA, 2015.

[76] Wyoming Test Fixtures Inc., [Online]. Available: https://wyomingtestfixtures.com/.

[77] The Boeing Company, “Boeing Specification Support Standard BSS 7260: Advanced Composite Compression Tests,” Seattle, WA, 1988.

[78] British Standards Institution, “BS EN 2850:2017 Aerospace series - Carbon fibre thermosetting resin - Unidirectional laminates - Compression test parallel to fibre direction,” BSI, 2017.

[79] ASTM International, “ASTM D3410/D3410M - 16 Standard Test Method for Compressive Properties of Polymer Matrix Composite Materials with Unsupported Gage Section by Shear Loading,” West Conshohocken, PA, 2016.

[80] ASTM International, “ASTM D6641/D6641M - 16 Standard Test Method for Compressive Properties of Polymer Matrix Composite Materials Using a Combined Loading Compression (CLC) Test Fixture,” West Conshohocken, PA, 2016.

[81] D. Adams, “The Combined Loading Compression (CLC) test method,” 2011. [Online]. Available: https://www.compositesworld.com/articles/the-combined-loading-compression-clc-test-method.

[82] ASTM International, “ASTM D8066/8066M - 17 Standard Practice Unnotched Compression Testing of Polymer Matrix Composite Laminates,” 2017.

[83] ASTM International, “ASTM D6484/D6484M - 14 Standard Test Method for Open-Hole Compressive Strength of Polymer Composite Laminates,” West Conshohocken, PA, 2014.

[84] British Standards Institution, “BS EN ISO 14126:1999 Fibre-reinforced plastic composites - Determination of compressive properties in the in-plane direction,” BSI, 1999.

[85] British Standards Institution, “BS ISO 12817:2013 Fibre-reinforced plastic composites - Determination of open-hole compression strength,” BSI, 2013.

[86] B. N. Cox, M. S. Dadkhah, R. V. Inman, W. L. Morris and J. Zupon, “Mechanisms of compressive failure in 3D composites,” *Acta Metallurgica et Materialia,* vol. 40, no. 12, pp. 3285-3298, 1992.

[87] M. S. Dadkhah, B. N. Cox and W. L. Morris, “Compression-compression fatigue of 3D woven composites,” *Acta Metallurgica et Materialia,* vol. 43, no. 12, pp. 4235-4245, 1995.

[88] British Standards Institution, “BS EN ISO 14125:1998+A1:2011 Fibre-reinforced plastic composites - Determination of flexural properties,” BSI, 1998.

[89] ASTM International, “ASTM D7264/D7264M - 15 Standard Test Method for Flexural Properties of Polymer Matrix Composite Materials,” West Conshohocken, PA, 2015.

[90] ASTM International, “ASTM D790 - 15 Standard Test Methods for Flexural Properties of Unreinforced and Reinforced Plastics and Electrical Insulating Materials,” West Conshohocken, PA, 2015.

[91] ASTM International, “ASTM D6272 - 17 Standard Test Method for Flexural Properties of Unreinforced and Reinforced Plastics and Electrical Insulating Materials by Four-Point Bending,” West Conshohocken, PA, 2017.

[92] X. Gao, N. Tao, X. Yang, C. Wang and F. Xu, “Quasi-static three-point bending and fatigue behavior of 3-D orthogonal woven composites,” *Composites: Part B,* vol. 159, pp. 173-183, 2019.

[93] W. S. Kuo, K. T. H., K. B. Cheng and K. Y. Hsieh, “Flexural behavior of three-axis woven carbon/carbon composites,” *Journal of Materials Science,* vol. 36, pp. 2743-2752, 2001.

[94] R. Umer, H. Alhussein, J. Zhou and W. J. Cantwell, “The mechanical properties of 3D woven composites,” *Journal of Composite Materials,* pp. 1-14, 2016.

[95] D. Zhang, A. M. Waas, M. Pankow, C. F. Yen and S. Ghiorse, “Flexural Behavior of a Layer-to-Layer Orthogonal Interlocked Three-Dimensional Textile Composites,” *Journal of Engineering Materials and Technology,* vol. 134, 2012.

[96] D. Zhang, A. M. Waas and C. F. Yen, “Progressive damage and failure response of hybrid 3D textile composites subjected to flexural loading, part I: Experimental studies,” *International Journal of Solids and Structures,* Vols. 75-76, pp. 309-320, 2015.

[97] D. Zhang, M. Sun, X. Liu, X. Xiao and K. Qian, “Off-axis bending behaviors and failure characterization of 3D woven composites,” *Composite Structures,* vol. 208, pp. 45-55, 2019.

[98] ASTM International, “ASTM D3518/D3518M - 13 Standard Test Method for In-Plane Shear Response of Polymer Matrix Composite Materials by Tensile Test of a ±45° Laminate,” West Conshohocken, PA, 2013.

[99] British Standards Institution, “BS EN ISO 14129:1998 Fibre-reinforced plastic composites - Determination of the in-plane shear stress-shear strain response, including the in-plane shear modulus and strength by the ±45° tension test method,” BSI, 1998.

[100] ASTM International, “ASTM D5379/D5379M - 12 Standard Test Method for Shear Properties of Composite Materials by the V-notched Beam Method,” West Conshohocken, PA, 2012.

[101] ASTM International, “ASTM D7078/D7078M - 12 Standard Test Method for Shear Properties of Composite Materials by V-Notched Rail Shear Method,” West Conshohocken, PA, 2012.

[102] Instron®, [Online]. Available: https://www.instron.co.uk/en-gb.

[103] D. O. Adams, J. M. Moriarty, A. M. Gallegos and D. F. Adams, “DOT/FAA/AR-03/63 Development and Evaluation of the V-notched Rail Shear Test for Composite Laminates,” National Technical Information Service (NTIS), Springfield, Virginia, 2003.

[104] D. O. Adams, J. M. Moriarty, A. M. Gallegos and D. F. Adams, “The V-notched Rail Shear Test,” *Journal of Composite Materials,* vol. 41, no. 3, pp. 281-297, 2007.

[105] British Standards Institution, “BS EN ISO 14130:1998 Fibre-reinforced plastic composites - Determination of apparent interlaminar shear strength by short-beam method,” BSI, 1998.

[106] ASTM International, “ASTM D2344/D2344M - 16 Standard Test Method for Short-Beam Strength of Polymer Matrix Composite Materials and Their Laminates,” West Conshohocken, PA, 2016.

[107] British Standards Institution, “BS ISO 19927:2018 Fibre-reinforced plastic composites - Determination of interlaminar strength and modulus by double beam shear test,” BSI, 2018.

[108] G. Zhou, P. H. Nash, J. Whitaker and N. Jones, “Double beam shear (DBS) as a new test method for determining interlaminar shear properties of composite laminates,” in *16th European Conference on Composite Materials (ECCM16)*, Seville, Spain, 2014.

[109] ASTM International, “ASTM D3846 - 08 (Reapproved 2015) Standard Test Method for In-Plane Shear Strength of Reinforced Plastics,” West Conshohocken, PA, 2015.

[110] P. Dadras and J. S. McDowell, “Analytical and experimental evaluation of double-notch shear specimens of orthotropic materials,” *Experimental Mechanics,* vol. 30, pp. 184-189, 1990.

[111] W. R. Broughton, M. R. L. Gower, M. J. Lodeiro and R. M. Shaw, “MATC(MN)06 Through-Thickness Testing of Polymer Matrix Composites,” National Physical Laboratory (NPL), London, 2001.

[112] R. M. Shaw and G. D. Sims, “Round-robin validation exercise for the determination of through-thickness shear strength in compression,” National Physical Laboratory (NPL), London, 2003.

[113] British Standards Institute, “BS EN ISO 15310:2005 - Reinforced plastics - Determination of the in-plane shear modulus by the plate twist method,” BSI, 2005.

[114] L. Qin, Z. Zhang, X. Li, X. Yang, Z. Feng, Y. Wang, H. Miao, L. He and X. Gong, “Full-field analysis of shear test on 3D orthogonal woven C/C composites,” *Composites: Part A,* vol. 43, pp. 310-316, 2012.

[115] G. Weissenbach, D. Brown and L. Limmer, “In-plane Shear Measurements of Textule Composites with Large Unit Cells using the Plate Twist Test,” *Polymers & Polymer Composites,* vol. 10, no. 7, pp. 511-520, 2002.

[116] S. Buchanan, E. Archer, D. Townsend, S. Jenkins, A. T. McIlhagger and J. P. Quinn, “Determination of in-plane shear modulus of 3D woven composites with large repeat unit cells,” *Plastics, Rubber and Composites,* vol. 41, no. 4/5, pp. 194-198, 2012.

[117] A. C. Garg, “Delamination - A Damage Mode in Composite Structures,” *Engineering Fracture Mechanics,* vol. 29, no. 5, pp. 557-584, 1988.

[118] I. S. Raju and T. K. O'Brien, “Fracture mechanics concepts, stress fields, strain energy release rates, delamination initiation and growth criteria,” in *Delamination behaviour of composites*, Cambridge, England, Woodhead Publishing Limited, 2008, pp. 3-27.

[119] L. Tong, A. Mouritz and M. Bannister, 3D Fibre Reinforced Polymer Composites, Oxford: Elsevier Science Ltd., 2002.

[120] Bristish Stanards Institution, “BS ISO 15024:2001 Fibre-reinforced plastic composites - Determination of mode I interlaminar fracture toughness, Gic, for unidirectionally reinforced materials,” BSI, 2001.

[121] ASTM International, “ASTM D5528 - 13 Standard Test Method for Mode I Interlaminar Fracture Toughness of Unidirectional Fibre-Reinforced Polymer Matrix Composites,” West Conshohocken, PA, 2013.

[122] British Standards Institution, “BS ISO 15114:2014 Fibre-reinforced plastic composites - Determination of the mode II fracture resistance for unidirectionally reinforced materials using the calibrated end-loaded split (C-ELS) test and an effective crack length approach,” BSI, 2014.

[123] ASTM International, “ASTM D7905/D7905M - 14 Standard Test Method for Determination of the Mode II Interlaminar Fracture Toughness of Unidirectional Fibre-Reinforced Polymer Matrix Composites,” West Conshohocken, PA, 2014.

[124] ASTM International, “ASTM D6671/D6671M - 13 Standard Test Method for Mix Mode I-Mode II Interlaminar Fracture Toughness of Unidirectional Fibre Reinforced Polymer Matrix Composites,” West Conshohocken, PA, 2013.

[125] P. Davis, B. R. K. Blackman and A. J. Brunner, “Mode II Delamination,” in *Fracture Mechanics Testing Methods for Polymers, Adhesives and Composites: ESIS Publication 28*, D. R. Moore, A. Pavan and J. G. Williams, Eds., Elsevier Science Ltd., 2001, pp. 307-316.

[126] B. R. K. Blackman, A. J. Brunner and J. G. Williams, “Mode II fracture testing of composites: a new look at an old problem,” *Engineering Fracture Mechanics,* vol. 73, pp. 2443-2455, 2006.

[127] M. C. de Verdiere, A. A. Skordos, A. C. Walton and M. May, “Influence of loading rate on the delamination response of untufted and tufted carbon epoxy non-crimp fabric composites/Mode II,” *Engineering Fracture Mechanics,* vol. 96, pp. 1-10, 2012.

[128] D. T. Fishpool, A. Rezai, D. Baker, S. L. Ogin and P. A. Smith, “Interlaminar toughness characterisation of 3D woven carbon fibre composites,” *Plastics, Rubber and Composites,* vol. 42, no. 3, pp. 108-115, 2013.

[129] P. Davies, W. Cantwell and H. H. Kausch, “Measurement of Initiation Values of Gic in IM6/PEEK Composites,” *Composites Science and Technology,* vol. 35, pp. 301-313, 1989.

[130] P. Davies, C. Moulin and H. H. Kausch, “Measurement of Gic and Giic in Carbon/Epoxy Composites,” *Composites Science and Technology,* vol. 39, pp. 193-205, 1990.

[131] Y. Tanzawa, N. Watanabe and T. Ishikawa, “Interlaminar fracture toughness of 3-D orthogonal interloced fabric composites,” *Composites Science and Technology,* vol. 59, pp. 1261-1270, 1999.

[132] V. Tamuzs, S. Tarasovs and U. Vilks, “Delamination properties of translaminar-reinforced composites,” *Composites Science and Technology,* vol. 63, pp. 1423-1431, 2003.

[133] V. A. Guenon, T.-W. Chou and J. W. Gillespie-Jr, “Toughness properties of a three-dimensional carbon-epoxy composites,” *Journal of Materials Science,* vol. 24, pp. 4168-4175, 1989.

[134] P. Robinson and S. Das, “Mode I DCB testing of composite laminates reinforced with z-direction pins:a simple model for the investigation of data reduction strategies,” *Engineering Fracture Mechanics,* vol. 71, pp. 345-364, 2004.

[135] G. Stegchuster, K. Pingkarawat, B. Wendland and A. P. Mouritz, “Experimental determination of the mode I delamination fracture and fatigue properties of thin 3D woven composites,” *Composites: Part A,* vol. 84, pp. 308-315, 2016.

[136] M. Pankow, A. Salvi, A. M. Waas, C. F. Yen and S. Ghiorse, “Resistance to delamination of 3D woven textile composites evaluated using End Notch Flexure (ENF) tests: Experimental results,” *Composites: Part A,* vol. 42, pp. 1463-1476, 2011.

[137] ASTM International, “ASTM D7136/D7136M - 15 Standard Test Method for Measuring the Damage Resistance of a Fiber-Reinforced Polymer Matrix Composite to a Drop-Weight Impact Event,” West Conshohocken, PA, 2015.

[138] British Standards Institution, “BS EN ISO 6603-1:2000 Plastics - Determination of puncture impact behaviour of rigid plastics - Part 1: Non-instrumented impact testing,” BSI, 2000.

[139] British Standards Institution, “BS EN ISO 6603-2:2000 Plastics - Determination of puncture impact behaviour of rigid plastics - Part 2: Instrumented puncture testing,” BSI, 2000.

[140] ASTM International, “ASTM D6264/D6264M - 12 Standard Test Method for Measuring the Damage Resistance of a Fiber-Reinforced Polymer-Matrix Composite to a Concentrated Quasi-Static Indentation Force,” West Conshohocken, PA, 2012.

[141] ASTM International, “ASTM D7137/D7137M - 12 Standard Test Method for Compressive Residual strength Properties of Damaged Polymer Matrix Composite Plates,” West Conshohocken, PA, 2012.

[142] British Standards Institution, "BS ISO 18352:2009 Carbon-fibre-reinforced plastics - Determination of compression-after-impact properties at a specified impact-energy level," BSI, 2009.

[143] J. N. Baucom and M. A. Zikry, "Low-velocity impact damage progression in woven E-glass composite systems," *Composites: Part A,* vol. 36, pp. 658-664, 2005.

[144] J. N. Baucom, M. A. Zikry and A. M. Rajendran, "Low-velocity impact damage accumulation in woven S2-glass composite systems," *Composite Science and Technology,* vol. 66, pp. 1229-1238, 2006.

[145] R. Seltzer, C. Gonzalez, R. Munoz, J. Llorca and T. Blanco-Varela, "X-ray microtomography analysis of the damage micromechanisms in 3D woven composites under low-velocity impact," *Composites: Part A,* vol. 45, pp. 49-60, 2013.

[146] K. R. Hart, P. X. L. Chia, L. E. Sheridan, E. D. Wetzel, N. R. Sottos and S. R. White, "Mechanisms and characterization of impact damage in 2D and 3D woven fiber-reinforced composites," *Composites: Part A,* vol. 101, pp. 432-443, 2017.

[147] Y. Luo, L. Lv, B. Sun, Y. Qiu and B. Gu, "Transverse impact behaviour and energy absorption of three-dimensional orthogonal hybrid woven composites," *Composite Structures,* vol. 81, pp. 202-209, 2007.

[148] A. Hao, B. Sun, Y. Qiu and B. Gu, "Dynamic properties of 3-D orthogonal woven composite T-beam under transverse impact," *Composites: Part A,* vol. 39, pp. 1073-1082, 2008.

[149] C. Ji, B. Sun, Y. Qiu and B. Gu, "Impact damage of 3D orthogonal woven composite circular plates," *Applied Composite Materials,* vol. 14, pp. 343-362, 2007.

[150] R. Gerlach, C. R. Siviour, J. Wiegand and N. Petrinic, "In-plane and through-thickness properties, failure modes, damage and delamination in 3D woven carbon fibre composites subjected to impact loading," *Composites Sciecne and Technology,* vol. 72, pp. 397-411, 2012.

[151] T. R. Walter, G. Subhash, B. V. Sankar and C. F. Yen, "Monotonic and cyclic short beam shear response of 3D woven composites," *Composite Science and Technology,* vol. 70, pp. 2190-2197, 2010.

[152] R. Munoz, F. Martinez-Hergueta, F. Galvez, C. Gonzalez and J. Llorca, "Ballistic performance of hybrid 3D woven composites: Experiments and simulations," *Composite Structure,* vol. 127, pp. 141-151, 2015.

[153] M. Colin de Verdiere, A. K. Pickett, A. A. Skordos and V. Witzel, "Evaluation of the mechanical and damage behaviour of tufted non crimped fabric composites using full field measurements," *Composites Science and Technology,* vol. 69, pp. 131-138, 2009.